

SEQUENCE SPECIFIC NUCLEIC ACID SENSING BY PYRROLIDINYL PEPTIDE NUCLEIC ACID
AND NANOMATERIALS



A Thesis Submitted in Partial Fulfillment of the Requirements
for the Degree of Master of Science in Chemistry
Department of Chemistry
Faculty of Science
Chulalongkorn University
Academic Year 2018
Copyright of Chulalongkorn University

การตรวจลำดับเบสอย่างจำเพาะของกรดนิวคลีอิกโดยใช้พีริโรลิดีนิลเพปไทด์นิวคลีอิกแอซิดและวัสดุ
ระดับนาโนเมตร



วิทยานิพนธ์นี้เป็นส่วนหนึ่งของการศึกษาตามหลักสูตรปริญญาวิทยาศาสตรมหาบัณฑิต
สาขาวิชาเคมี ภาควิชาเคมี
คณะวิทยาศาสตร์ จุฬาลงกรณ์มหาวิทยาลัย
ปีการศึกษา 2561
ลิขสิทธิ์ของจุฬาลงกรณ์มหาวิทยาลัย

Thesis Title SEQUENCE SPECIFIC NUCLEIC ACID SENSING BY PYRROLI
DINYL PEPTIDE NUCLEIC ACID AND NANOMATERIALS
By Mr. Kriangsak Faikhruea
Field of Study Chemistry
Thesis Advisor Professor Tirayut Vilaivan, Ph.D.

Accepted by the Faculty of Science, Chulalongkorn University in Partial
Fulfillment of the Requirement for the Master of Science

..... Dean of the Faculty of Science
(Professor POLKIT SANGVANICH, Ph.D.)

THESIS COMMITTEE

..... Chairman
(Associate Professor Vudhichai Parasuk, Ph.D.)

..... Thesis Advisor
(Professor Tirayut Vilaivan, Ph.D.)

..... Examiner
(Associate Professor Sumrit Wacharasindhu, Ph.D.)

..... Examiner
(Assistant Professor Numpon Insin, Ph.D.)

..... External Examiner
(Assistant Professor Boonjira Rutnakornpituk, Ph.D.)

เกรียงศักดิ์ ฝ่ายเครือ : การตรวจลำดับเบสอย่างจำเพาะของกรดนิวคลีอิกโดยใช้พีร์โรลิดินิลเพปไทด์นิวคลีอิกแอซิดและวัสดุระดับนาโนเมตร. (

SEQUENCE SPECIFIC NUCLEIC ACID SENSING BY PYRROLIDINYL PEPTIDE NUCLEIC ACID AND NANOMATERIALS) อ.ที่ปรึกษาหลัก : ศ. ดร.ธีรยุทธ วิไลวัลย์

งานวิจัยนี้ได้พัฒนาการตรวจวัดกรดนิวคลีอิกด้วยเทคนิคฟลูออเรสเซนซ์และการเปลี่ยนสีโดยใช้พีร์โรลิดินิลเพปไทด์นิวคลีอิกแอซิดเป็นโพรบร่วมกับวัสดุระดับนาโนเมตรได้แก่ แกรฟีนออกไซด์, ไรติวซ์แกรฟีนออกไซด์, อนุภาคระดับนาโนเมตรของทองและเงิน โดยพีเอ็นพีเอโพรบถูกดัดแปรโครงสร้างให้มีประจุบวกเป็นจำนวนมากด้วยกรดอะมิโนไลซีนเพื่อเพิ่มประสิทธิภาพการดูดซับของโพรบบนวัสดุระดับนาโนเมตรชนิดต่างๆ ในการตรวจวัดแบบฟลูออเรสเซนซ์ การดัดแปรนี้จะเพิ่มประสิทธิภาพของการดับสัญญาณฟลูออเรสเซนซ์ให้ได้สัญญาณพื้นหลังที่ต่ำ อีกทั้งสัญญาณฟลูออเรสเซนซ์ยังสามารถคืนกลับมาได้หลังจากเติมดีเอ็นเอหรืออาร์เอ็นเอเป้าหมาย นอกจากนี้การดูดซับของพีเอ็นพีเอโพรบบนอนุภาคระดับนาโนเมตรของทองสามารถเหนี่ยวนำให้เกิดการเกาะกลุ่มของอนุภาคทอง ส่งผลให้สีของสารละลายเปลี่ยนจากสีแดงเป็นสีม่วงนอกเหนือไปจากการดับแสงฟลูออเรสเซนซ์อีกด้วย แต่หากให้พีเอ็นพีเอโพรบจับยึดกับดีเอ็นเอ/อาร์เอ็นเอเป้าหมายก่อนการผสมกับอนุภาคระดับนาโนเมตรของทอง จะไม่เกิดการเปลี่ยนแปลงสีและสัญญาณฟลูออเรสเซนซ์ ดังนั้นจึงสามารถบ่งชี้การมีอยู่ของดีเอ็นเอ/อาร์เอ็นเอเป้าหมายที่มีลำดับเบสเป็นคู่สมกับโพรบได้โดยการสังเกตสีด้วยตาเปล่า ซึ่งทุกวิธีการตรวจวัดในงานนี้มีความจำเพาะและสามารถบอกความแตกต่างระหว่างดีเอ็นเอ/อาร์เอ็นเอเป้าหมายที่เป็นคู่สมและมีลำดับเบสแตกต่างกันเพียงหนึ่งตำแหน่งได้ อีกทั้งยังมีขีดจำกัดการตรวจวัดที่ความเข้มข้นต่ำกว่าระดับนาโนโมลาร์ ซึ่งหลักการตรวจวัดกรดนิวคลีอิกที่พัฒนาขึ้นในงานนี้ สามารถวิเคราะห์ตัวอย่างได้ไม่ซับซ้อน รวดเร็ว ต้นทุนต่ำ มีความไวและตรวจวัดอย่างจำเพาะทั้งดีเอ็นเอและอาร์เอ็นเอเป้าหมาย อีกทั้งยังสามารถใช้ตรวจวัดดีเอ็นเอที่มาจากตัวอย่างจริงได้อีกด้วย

สาขาวิชา เคมี
ปีการศึกษา 2561

ลายมือชื่อนิสิต
ลายมือชื่อ อ.ที่ปรึกษาหลัก

5871916723 : MAJOR CHEMISTRY

KEYWORD: PNA, acpcPNA, DNA, RNA, NANOMATERIALS, SENSOR, NANOPARTICLE

Kriangsak Faikhruea :

SEQUENCE SPECIFIC NUCLEIC ACID SENSING BY PYRROLIDINYL PEPTIDE NUCLEIC ACID AND NANOMATERIALS. Advisor: Prof. Tirayut Vilaivan, Ph.D.

In this work, fluorescence and colorimetric nucleic acid sensing platforms based on pyrrolidinyl peptide nucleic acid (acpcPNA) probe and nanomaterials including graphene oxide (GO), reduced graphene oxide (rGO), gold nanoparticles (AuNPs), and silver nanoparticles (AgNPs) were developed. The acpcPNA probe was modified by multiple lysine residues to provide positive charges which enhanced the adsorption of the probe to various types of nanomaterials. In fluorescence detection mode, this results in higher quenching efficiency, resulting in lower background signal. Recovery of the quenched fluorescence signal was achieved upon hybridization with the complementary DNA/RNA target due to the displacement of the probe from the nanomaterials surface. When gold nanoparticles were employed as the nanomaterials, adsorption of acpcPNA probe caused a distinct red-to-purple color change in addition to the fluorescence quenching. No color and fluorescence change was observed if the PNA probe was previously hybridized with DNA/RNA targets, therefore the presence of complementary DNA or RNA targets could be visually observed. In all cases, single mismatch specificity and low detection limits in the sub-nanomolar levels were achieved. This nucleic acid detection platform therefore offers a simple, rapid, cost-effective, sensitive, and selective detection of DNA and RNA targets, and has been applied to the detection of real DNA samples.

Field of Study: Chemistry

Student's Signature

Academic Year: 2018

Advisor's Signature

ACKNOWLEDGEMENTS

Firstly, I would like to express my sincere gratitude to my beloved advisor Professor Dr. Tirayut Vilaivan for his patience, motivation, being influential on my skill, and immense support. His guidance and encouragement helped me to crystallize my thought which improve my systematic and critical thinking to do research. Beside my advisor, I am also appreciated my thesis committee: Associate Professor Dr.Vudhichai Parasuk, Associate Professor Dr. Sumrit Wacharasindhu, Assistant Professor Dr. Numpon Insin, and Assistant Professor Dr. Boonjira Rutnakornpituk, for their insightful comments and suggestions. I also thank to members of TV research group for stimulating discussion, friendship and supports throughout my entire study. This special thanks for special people, my mother, father, brother, and my Leia who always give me colossal love that encouraged me to graduate my master.

Kriangsak Faikhruea

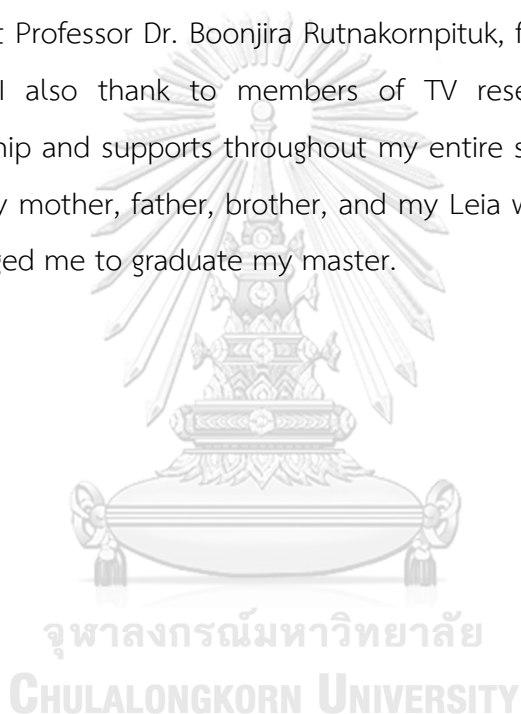


TABLE OF CONTENTS

	Page
ABSTRACT (THAI).....	iii
ABSTRACT (ENGLISH).....	iv
ACKNOWLEDGEMENTS	v
TABLE OF CONTENTS.....	vi
LIST OF FIGURES	x
LIST OF TABLES.....	xvii
LIST OF ABBREVIATIONS	xviii
CHAPTER I INTRODUCTION.....	1
1.1 Nucleic acid sensors.....	1
1.2 Backgrounds of fluorescence nucleic acid sensors based on nanomaterials and labelled DNA probes.....	2
1.3 Backgrounds of colorimetric nucleic acid sensors based on metal nanoparticles and DNA probes.....	11
1.4 Peptide nucleic acid.....	16
1.4.1 History of peptide nucleic acid and properties.....	16
1.4.2 Conformational constrained PNAs and their novel features	17
1.5 Combination of PNA probes and nanomaterials for nucleic acid sensing.....	19
1.6 Rationale and objective of this study.....	24
CHAPTER II EXPERIMENTAL SECTION.....	25
2.1 Materials.....	25
2.2 Synthesis of acpcPNA	26
2.2.1 AcpcPNA monomer synthesis	26

2.2.2 Solid phase peptide synthesis	27
2.3 Synthesis of nanomaterials	28
2.3.1 Synthesis of 12 nm citrate-capped gold nanoparticles (citrate-AuNPs)	28
2.3.2 Synthesis of 40 nm citrate-capped gold nanoparticles	29
2.3.3 Synthesis of silver nanoparticles (AgNPs).....	29
2.3.4 Synthesis of reduced graphene oxide (rGO).....	30
2.4 Fluorescence experiments	30
2.4.1 Fluorescence quenching experiments	30
2.4.2 Fluorescent discrimination.....	31
i) PNA+Quencher+DNA.....	31
ii) PNA+DNA+Quencher	31
2.5 Colorimetric assay	32
2.5.1 Naked-eyes detection of gold nanoparticles	32
2.5.2 UV-visible measurement	32
i) Selectivity.....	32
ii) Sensitivity	33
2.6 LAMP-amplification of <i>S. aureus</i> carrying staphylococcal enterotoxin A (SEA) gene 33	
CHAPTER III RESULTS AND DISCUSSION.....	35
3.1 Synthesis and characterization of acpcPNA oligomers.....	35
3.2 Synthesis and characterization of nanomaterials.....	37
3.2.1 Citrate-capped gold nanoparticles (citrate-AuNPs) (12 nm).....	37
3.2.2 Citrate-capped gold nanoparticles (40 nm).....	38
3.2.3 Silver nanoparticles (AgNPs)	39

3.2.4 Reduced graphene oxide (rGO).....	39
3.3 Fluorescence quenching efficiency	40
3.3.1 Type of quencher	40
3.3.2 Charge effect.....	43
3.3.3 Salt effect	47
3.4 Fluorescence assay for DNA detection.....	49
3.4.1 Comparison of PNAlys1 and PNAlys5 probes	49
3.4.2 Comparison of target mixing order	50
3.4.3 Kinetics of the signal restoration of PNA probes.....	53
3.4.4 Application to various quenchers.....	55
3.4.5 Sensitivity.....	57
3.4.6 Application for the detection of real DNA samples	59
3.4.7 Effect of non-specific DNA from (poly-adenine).....	61
3.4.8 Comparison with aegPNA probe	62
3.5 Fluorescence assay for detection of MicroRNA21	63
3.5.1 Kinetics.....	63
3.5.2 Variation of detection matrices.....	64
3.5.2.1 Effect of protein matrix (BSA).....	64
3.5.2.2 Effect of salt	65
3.5.3 Limit of RNA detection	67
3.5.4 Comparison to other probe/nanomaterial platforms	68
i) DNA sensing on graphene oxide	68
ii) DNA sensing on gold nanoparticles.....	70
3.6 Colorimetric assay for nucleic acid detection employing gold nanoparticles ...	71

3.6.1 Buffer variation	72
3.6.2 Effect of charge on the acpcPNA probe	73
3.6.3 Colorimetric detection of nucleic acids	76
i) Short DNA oligonucleotide target	76
ii) Long-chain DNA target.....	79
iii) Detection of real DNA sample.....	80
iv) MicroRNA21 target.....	81
3.6.4 Sensitivity of the colorimetric assay	82
3.6.5 Dual-mode detection.....	85
3.6.6 Comparison to other colorimetric DNA detection employing gold nanoparticles.....	88
CHAPTER IV CONCLUSION.....	89
REFERENCES	91
APPENDIX.....	100
VITA.....	107

LIST OF FIGURES

	Page
Figure 1.1 Representation of the target-induced fluorescence change of the ssDNA-FAM-GO complex according to Lu and co-workers ²⁰	3
Figure 1.2 GO-based multicolor DNA analysis by He and co-workers ¹⁹	4
Figure 1.3 Fluorescence assays based on DNA-GO (i) and snapshots from MD simulation (ii) ¹⁹	4
Figure 1.4 FAM-labelled DNA adsorption and desorption on GO studied by Wu and co-workers ²³	5
Figure 1.5 Sequence-dependence DNA adsorption on and displacement from graphene oxide (GO) by Liu and co-workers ²⁴	6
Figure 1.6 Graphene oxide nanopatform for noncoding RNA detection in formalin-fixed paraffin embedded (FFPE) tissue specimens ²⁷	6
Figure 1.7 Illustration of DNA-GO covalent sensor developed by Huang and co-workers ²⁹	7
Figure 1.8 A molecular-beacon type DNA sensor based on fluorophore-tagged, hairpin oligonucleotide functionalized gold nanoparticles ³³	8
Figure 1.9 Label free DNA detection based on gold nanoparticles and rhodamine B ³⁴	9
Figure 1.10 Localized Surface Plasmon Resonance (LSPR).....	11
Figure 1.11 Colorimetric DNA-detection methods using DNA-modified gold nanoparticle ³⁹	12
Figure 1.12 The aggregation of silver (a) and gold nanoparticles (b) for colorimetric detection of DNA (c)	12
Figure 1.13 The colorimetric method for differentiating between single- and double-stranded DNA oligonucleotides ⁴¹	13

Figure 1.14 AuNPs solutions in the presence of hairpin ssDNAs (A) and hairpin DNAs (B) with different lengths of ssDNA sticky ends ⁴²	14
Figure 1.15 Highly sensitive colorimetric detection of DNA by the use of gold nanoparticles and hybridization chain reaction amplification ⁴³	15
Figure 1.16 Repeating units of the DNA and aegPNA structure (A) and aegPNA-DNA antiparallel duplex according to Watson-Crick base-pairing (B).....	17
Figure 1.17 Repeating units of pyrrolidinyl PNA and acpcPNA structure (A) and acpcPNA-DNA duplex in antiparallel according to Watson-Crick base-pairing (B).....	18
Figure 1.18 Fluorescence assay for DNA detection using DNA, PNA, and PCNA ⁵⁸	20
Figure 1.19 Fluorescent DNA detection based on the GO platform by using PNA as the probe by Guo and co-workers ⁵⁹	21
Figure 1.20 A miRNA sensor based on PNA and GO platform by Ryoo and co-workers ⁶⁰	22
Figure 1.21 A strategy of colorimetric DNA detection based-on gold nanoparticles and label-free PNA by Su and co-worker ⁶³	23
Figure 1.22 PNA-AuNP colorimetric detection assay for BVDV-RNA detection by Askaravi and co-workers ⁶⁴	23
Figure 2.1 Structures of pyrrolidinyl PNA monomers and acpc spacer for solid phase peptide synthesis.....	26
Figure 3.1 TEM-image (scale bar is 20 nm) (A) and UV-vis spectra of 12 nm citrate-coated gold nanoparticle (citrate-AuNPs) (B).....	37
Figure 3.2 TEM image (scale bar 200 nm) (A) and comparison of UV-vis spectra of 12 and 40 nm gold nanoparticles (AuNPs) (B).....	38
Figure 3.3 TEM-image (scale bar is 20 nm) (A) and UV-vis spectra of citrate-capped silver nanoparticle (citrate-AgNPs) (B).....	39

Figure 3.4 ζ -potential of graphene oxide (top) and reduced graphene oxide (bottom)	40
Figure 3.5 Fluorescence quenching of labeled oligonucleotides by nanomaterials...	41
Figure 3.6 Fluorescence quenching of fluorescein-labeled DNA (A) and PNA-Lys (B) using various nanomaterials; graphene oxide (GO), reduced graphene oxide (rGO), gold nanoparticles (AuNPs), and silvernanoparticles (AgNPs). Conditions: 0.1 μ M FAM-PNA/DNA in 10 mM Tris-HCl buffer (pH 7.4), fluorescence measurement; λ_{ex} 460 nm, PMT 940 V	43
Figure 3.7 Fluorescence quenching of fluorescein-labeled acpcPNA and DNA probe by graphene oxide (GO). Conditions: 0.1 μ M FAM-PNA/DNA in 10 mM Tris-HCl buffer (pH 7.4), fluorescence measurement; λ_{ex} 460 nm, PMT 940 V.....	44
Figure 3.8 Kinetic profiles of fluorescence quenching of positively charged labeled acpcPNA with graphene oxide (GO). Conditions: 0.1 μ M FAM-PNA, 0.5 μ g/mL of GO in 10 mM Tris-HCl buffer (pH 7.4), fluorescence measurement; λ_{ex} 460 nm, PMT 940 V	46
Figure 3.9 Fluorescence quenching of FAM-PNALys ₅ using various nanomaterials: graphene oxide (GO), reduced graphene oxide (rGO), gold nanoparticles 12 and 40 nm (AuNPs), and silver nanoparticles (AgNPs). Conditions: 0.1 μ M FAM-PNALys ₅ in 10 mM Tris-HCl buffer (pH 7.4), fluorescence measurement; λ_{ex} 460 nm, PMT 940 V....	47
Figure 3.10 Quenching efficiencies of FAM-labeled DNA and PNALys ₅ with graphene oxide (GO) at various of NaCl concentrations. Conditions: 0.1 μ M FAM-PNA/DNA, 1.0 μ g/mL of GO in 10 mM Tris-HCl buffer (pH 7.4), fluorescence measurement; λ_{ex} 460 nm, PMT 940 V	48
Figure 3.11 Distinguishing fluorescent signal for DNA detection using FAM-labeled PNALys and PNALys ₅ probes with graphene oxide (GO). Conditions: 0.1 μ M FAM-PNA, 0.12 μ M DNA (1.2 equiv), 0.5 μ g/mL of GO in 10 mM Tris-HCl buffer (pH 7.4), fluorescence measurement; λ_{ex} 460 nm, PMT 940 V.....	50

Figure 3.12 Fluorogenic assays for DNA detection with different mixing recognition, PNA+DNA+GO (A), and PNA+GO+DNA (B).....	52
Figure 3.13 Brightness (i) and F/F_0 (ii) obtained from different order of mixing of PNA (FAM-PNALys ₅), DNA and quencher (GO). Conditions: 0.1 μ M FAM-PNA, 0.12 μ M DNA (1.2 equiv), 0.5 μ g/mL of GO in 10 mM Tris-HCl buffer (pH 7.4), fluorescence measurement; λ_{ex} 460 nm, PMT 940 V.....	52
Figure 3.14 Kinetic profiles of fluorescence recovery (i) and relative fluorescence signal (F/F_0) (ii) using FAM-PNALys with graphene oxide (GO). Conditions: 0.1 μ M FAM-PNALys, 0.12 μ M DNA (1.2 equiv) in 10 mM Tris-HCl buffer (pH 7.4), fluorescence measurement; λ_{ex} 460 nm, PMT 940 V.....	54
Figure 3.15 Kinetic profiles of fluorescence recovery (i) and relative fluorescence signal (F/F_0) (ii) using FAM-PNALys ₅ with graphene oxide (GO). Conditions: 0.1 μ M FAM-PNALys ₅ , 0.12 μ M DNA (1.2 equiv), 0.5 μ g/mL of GO in 10 mM Tris-HCl buffer (pH 7.4), fluorescence measurement; λ_{ex} 460 nm, PMT 940 V.....	55
Figure 3.16 Fluorescence discrimination for DNA sequence detection using FAM-PNALys ₅ using various nanomaterials as quencher: graphene oxide (A), reduced graphene oxide (B), gold nanoparticles (C), and silver nanoparticles (D) Conditions: 0.1 μ M FAM-PNA, 0.12 μ M DNA (1.2 equiv), 0.5 μ g/mL of nanomaterial in 10 mM Tris-HCl buffer (pH 7.4), fluorescence measurement; λ_{ex} 460 nm, PMT 940 V.....	56
Figure 3.17 Calibration curves for DNA detection by FAM-PNALys and FAM-PNALys ₅ using graphene oxide (GO) (PNA+GO+DNA). Conditions: 0.1 μ M FAM-PNA, 0.5 μ g/mL of GO in 10 mM Tris-HCl buffer (pH 7.4), fluorescence measurement; λ_{ex} 460 nm, PMT 940 V.....	58
Figure 3.18 Calibration curves of DNA detection by FAM-PNALys ₅ using citrate-capped gold nanoparticles (12 and 40 nm AuNPs) (PNA+AuNPs+DNA). Conditions: 0.1 μ M FAM-PNALys ₅ , 0.5 μ g/mL of AuNPs in 10 mM Tris-HCl buffer (pH 7.4), fluorescence measurement; λ_{ex} 460 nm, PMT 940 V.....	59
Figure 3.19 Detection process for DNA real sample	60

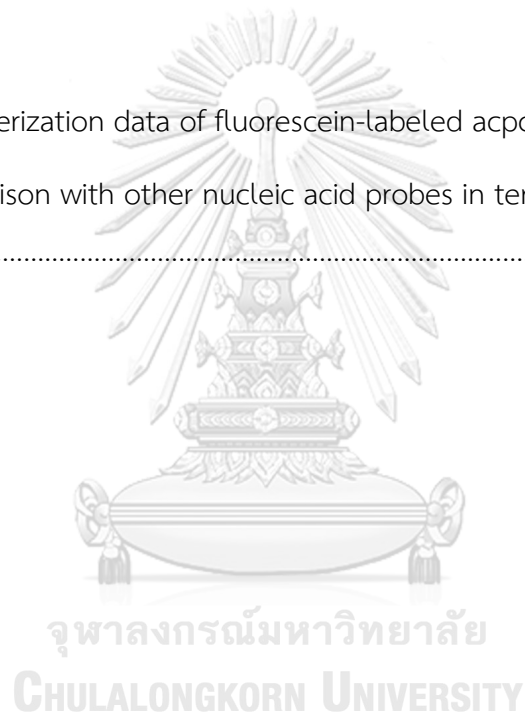
Figure 3.20 Fluorescence assay of LAMP-amplified DNA from real samples using graphene oxide (GO) (A) and 12 nm gold nanoparticles (AuNPs) (B). Conditions: 0.1 μM FAM-seaPNA in 10 mM Tris-HCl buffer (pH 7.4), fluorescence measurement; λ_{ex} 460 nm, PMT 940 V.....	60
Figure 3.21 Non-specific fluorescence increase of nucleic acid probe in presence of poly-dA as a non-specific competitor. Conditions: 0.1 μM FAM-PNALys ₅ in 10 mM Tris-HCl buffer (pH 7.4), fluorescence measurement; λ_{ex} 460 nm, PMT 940 V.....	61
Figure 3.22 Kinetic profiles of fluorescence recovery for miRNA21 detection (PNA+quencher+miRNA21). Conditions: 0.1 μM FAM-PNA21, 1.2 equiv miRNA21, 0.5 $\mu\text{g/mL}$ of quencher in 10 mM Tris-HCl buffer (pH 7.4), fluorescence measurement; λ_{ex} 460 nm, PMT 940 V.....	64
Figure 3.23 Kinetic profiles of fluorescence recovery for miRNA21 detection in 0.01% BSA solution. Conditions: 0.1 μM FAM-PNA21, 1.2 equiv miRNA21 in 10 mM Tris-HCl buffer (pH 7.4), fluorescence measurement; λ_{ex} 460 nm, PMT 940 V.....	65
Figure 3.24 Fluorescence recovery for miRNA21 detection in various NaCl solutions. Conditions: 0.1 μM FAM-PNA21, 1.2 equiv miRNA21 in 10 mM Tris-HCl buffer (pH 7.4), fluorescence measurement; λ_{ex} 460 nm, PMT 940 V.....	66
Figure 3.25 Calibration curves of miRNA21 detection by FAM-PNA21 using GO and AuNPs as quencher (PNA+quencher+DNA). Conditions: 0.1 μM FAM-PNA21, 0.5 $\mu\text{g/mL}$ of quencher in 10 mM Tris-HCl buffer (pH 7.4), fluorescence measurement; λ_{ex} 460 nm, PMT 940 V.....	67
Figure 3.26 Induced-aggregation of citrate-coated gold nanoparticles by positively charged modified acpcPNA.....	71
Figure 3.27 Colorimetry of DNA detection using citrate-coated gold nanoparticles...	72
Figure 3.28 Aggregation of citrate gold nanoparticles in various buffer systems Conditions: 200 $\mu\text{g/mL}$ of citrate-gold nanoparticles (AuNPs (12 nm)) in 10 mM of phosphate buffer (pH 7.0).....	73

- Figure 3.29** Aggregation of citrate gold nanoparticles in various concentrations of labeled-acpcPNAs. Conditions: 200 $\mu\text{g}/\text{mL}$ of citrate-gold nanoparticles (AuNPs (12 nm)) in 10 mM of phosphate buffer (pH 7.0) 74
- Figure 3.30** Optimization of FAM-PNALys₅ concentration in gold nanoparticles. Conditions: 50 mg/mL of citrate-gold nanoparticles (AuNPs (12 nm)) in 10 mM of phosphate buffer (pH 7.0)..... 75
- Figure 3.31** Optimization of NaCl concentration that does not precipitate 50 $\mu\text{g}/\text{mL}$ of gold nanoparticles (AuNPs (12 nm)) 75
- Figure 3.32** UV-visible spectra of colorimetric DNA detection using PNALys₅ and gold nanoparticles (AuNPs (12 nm)). Conditions: 0.1 μM of FAM-PNALys₅, 0.12 μM (1.2 equiv) DNA, 50 $\mu\text{g}/\text{mL}$ of citrate-gold nanoparticles (AuNPs) in 10 mM of phosphate buffer (pH 7.0) 76
- Figure 3.33** Comparison of colorimetric detection of short-chain-DNA using FAM-PNALys₅ with and without addition of NaCl. Conditions: 0.1 μM of FAM-PNALys₅, 0.12 μM (1.2 equiv) DNA, 50 $\mu\text{g}/\text{mL}$ of citrate-gold nanoparticles (AuNPs (12 nm)), 50 mM NaCl in 10 mM of phosphate buffer (pH 7.0) 77
- Figure 3.34** UV-visible spectrum (A) and naked-eyes colorimetric detection (B) of short-chain-DNA using FAM-PNALys₅ with gold nanoparticles (40 nm). Conditions: 0.1 μM of FAM-PNALys₅, 0.12 μM (1.2 equiv) DNA, 50 $\mu\text{g}/\text{mL}$ of citrate-gold nanoparticles (AuNPs (40 nm)) in 10 mM of phosphate buffer (pH 7.0)..... 78
- Figure 3.35** Comparison of colorimetric detection of long-chain-DNA using FAM-PNALys₅ between with and without addition of NaCl. Conditions: 0.1 μM of FAM-PNALys₅, 0.12 μM (1.2 equiv) DNA, 50 $\mu\text{g}/\text{mL}$ of citrate-gold nanoparticles (AuNPs (12 nm)), 50 mM NaCl in 10 mM of phosphate buffer (pH 7.0)..... 80
- Figure 3.36** Colorimetric assay for detection of DNA real sample at different FAM-seaPNA concentrations. Conditions: 50 $\mu\text{g}/\text{mL}$ of citrate-gold nanoparticles (AuNPs (12 nm)), in 10 mM of phosphate buffer (pH 7.0) 81

Figure 3.37 Colorimetric detection of for miRNA21 using FAM-PNA21 and 12 nm gold nanoparticles. Conditions: 0.1 μM of FAM-PNA21, 0.12 μM (1.2 equiv) miRNA21, 0.25 mM of citrate-gold nanoparticles (AuNPs (12 nm)) in 10 mM phosphate buffer (pH 7.0).....	82
Figure 3.38 Calibration curves for colorimetric DNA detection (i), and RNA detection (ii) using 12 nm gold nanoparticles and FAM-PNALys ₅ as a probe. Conditions: 0.1 μM of FAM-PNALys ₅ , 20 $\mu\text{g/mL}$ of citrate-gold nanoparticles (AuNPs (12 nm)) in 10 mM of phosphate buffer (pH 7.0).....	83
Figure 3.39 Calibration curve for colorimetric DNA detection using 40 nm gold nanoparticles and FAM-PNALys ₅ as a probe. Conditions: 0.1 μM of FAM-PNALys ₅ , 20 $\mu\text{g/mL}$ of citrate-gold nanoparticles (AuNPs (12 nm)) in 10 mM of phosphate buffer (pH 7.0).....	84
Figure 3.40 The principle of dual-mode detection using citrate-coated gold nanoparticles	85
Figure 3.41 Dual-mode detection of DNA using FAM-PNALys ₅ and citrate-gold nanoparticles (AuNPs) with 12 nm (A) and 40 nm (B). Conditions: 1 μM of FAM-PNALys ₅ , 1.2 μM (1.2 equiv) DNA, 50 $\mu\text{g/mL}$ of citrate-gold nanoparticles (AuNPs (12 nm)) in 10 mM of phosphate buffer (pH 7.0)	87
Figure A1 Mass spectrum (A) and chromatogram (B) of FAM-PNALys.....	101
Figure A2 Mass spectrum (A) and chromatogram (B) of FAM-PNALys ₃	102
Figure A3 Mass spectrum (A) and chromatogram (B) of FAM-PNALys ₅	103
Figure A4 Mass spectrum (A) and chromatogram (B) of FAM-PNAGlu.....	104
Figure A5 Mass spectrum (A) and chromatogram (B) of FAM-PNA21	105
Figure A6 Mass spectrum (A) and chromatogram (B) of FAM-seaPNA.....	106

LIST OF TABLES

	Page
Table 1.1 Performance of fluorescent DNA sensors	10
Table 1.2 Nanotechnology based-on PNA for biosensor	19
Table 2.1 Sequences of oligonucleotides employed in this study	25
Table 2.2 Sequence of primers used for preparation of DNA samples by LAMP	34
Table 3.1 Characterization data of fluorescein-labeled acpCNAs	36
Table 3.2 Comparison with other nucleic acid probes in term of specificity, sensitivity and limitation	69



LIST OF ABBREVIATIONS

μL	microliter
μg	microgram
μmol	micromole
mM	millimolar
μM	micromolar
nM	nanomolar
pM	picomolar
nm	nanometer
GO	graphene oxide
rGO	reduced graphene oxide
AuNPs	gold nanoparticles
AgNPs	silver nanoparticles
DNA	deoxyrinonucleic acid
miRNA	micro-ribonucleic acid
PNA	peptide nucleic acid
PCR	polymerase chain reaction
FAM	5/6-carboxyfluorescein
Lys	Lysine
Glu	Glutamic acid
BSA	bovine serum albumin
TEM	transmission electron microscope
DMF	<i>N,N'</i> -dimethylformamide
DBU	1,8-diazabicyclo[5.4.0]undec-7-ene
DIEA	diisopropylazodicarboxylate
HOAt	1-Hydroxy-7-azabenzotriazole
HATU	1-[Bis(dimethylamino)methylene]-1H-1,2,3-triazolo[4,5-b]pyridinium 3-oxide hexafluorophosphate
Ac ₂ O	acetic anhydride

Fmoc	9-fluorenylmethoxycarbonyl
Pfp	pentafluorophenyl
MALDI-TOF	matrix-assisted laser desorption/ionization-time of flight
HPLC	high performance liquid chromatography
equiv	equivalent
HEPES	4-(2-hydroxyethyl)-1-piperazineethanesulfonic acid
Tris-HCl	2-amino-2-(hydroxymethyl)-1,3-propanediol hydrochloride



CHAPTER I

INTRODUCTION

1.1 Nucleic acid sensors

Sensors are devices that are responsive to physical or chemical stimulant and generate detectable signals.¹ A sensor contains at least two parts: target recognition module, which can be a chemical or biological receptor that specifically recognizes the target, and signal transduction module which is responsible for converting the recognition event into detectable signals. Single-strand DNAs and RNAs can bind to their complementary strand specifically and are widely utilized for nucleic acid detection. Detection of specific sequences of DNAs and RNAs play critical roles in the field of food analysis,² forensic science³ and clinical diagnosis.^{4, 5} While the sequencing technology nowadays becomes more accessible, it is still quite costly, requires sophisticated instruments and generates more data than necessary for general purposes. Thus, a number of DNAs/RNAs sensors have been developed to achieve low detection limit, high specificity, fast response time and long shelf life. Various detection methods have been proposed including, but not limited to, electrochemistry,⁶ enzymatic assay,⁷ fluorescence technique,^{8, 9} and visual detection.^{10, 11} Although many of these DNA/RNA sensors have been commercialized, they still required complicated procedures, expensive instruments and specialists. These issues challenge many researchers to develop rapid, simple, low-cost, and more effective methods for DNA sequence analysis. In this work, a new nucleic acid sensor based on a new probe called pyrrolidinyl peptide nucleic acid as recognition module and nanomaterials that exhibit several beneficial aspects such as high surface area, unique electronic and optical properties, and biocompatibility as signal transduction module is proposed.^{12, 13}

1.2 Backgrounds of fluorescence nucleic acid sensors based on nanomaterials and labelled DNA probes

With the aforementioned unique advantages, nanomaterials have been extensively employed in the design of rapid, simple, and cost-effective sensors in recent years. Recent attentions have been focused on the nanomaterial-based biosensors that involve interactions between nanomaterials and biomolecules either by covalent or non-covalent interactions. Fluorescence-labelled DNA probes can be used for sensing purposes such as in real-time polymerase chain reaction (PCR) or intra cellular imaging.¹⁴⁻¹⁶ The probe can be labelled with a "dumb" label that always give fluorescence regardless of its hybridization status, in such case phase separation between the free and target-bound probe, for example by solid phase hybridization to immobilized target followed by washing to remove the excess probe, is required in order to make sure that the signal is the result of probe-target binding. On the other hand, a "smart" probe can be designed so that the fluorescence signal can change according to the presence or absence of the target. A classic example of such probe is called "molecular beacon" which was designed to have a terminal fluorophore-quencher pair that can interact via the formation of stem-loop structure in the absence of target.^{14, 15} The interaction between the fluorophore-quencher via static quenching or the distance-dependent Förster resonance energy transfer (FRET) caused to probe to exhibit low fluorescence in the absence of the target. Binding of the target opens up the stem and the fluorophore-quencher pair dissociates, resulting in the increased fluorescence signal. Recently, traditional quenchers which are mostly organic dyes has been replaced with much more effective nanomaterials-based quenchers such as carbon nanomaterials and metallic nanoparticles which resulted in better signal-to-noise ratio.¹⁷

Graphene oxide (GO), a carbon-based nanomaterial that is related to graphene, but with highly oxidized surface, has been widely used in many applications because of its unique electronic and thermal properties.¹⁸ The high water-solubility of GO makes it more useful than graphene in biosensing applications. GO is known to non-covalently interact more strongly with single stranded DNA

(ssDNA) than double stranded DNA (dsDNA). Various applications have utilized this fact together with the universal fluorescence quenching ability of GO.^{12, 19} Physisorption of fluorescently-labelled DNA and GO was firstly reported in 2009 by Lu and co-workers.²⁰ Single-strand DNA was adsorbed on GO surface via π - π stacking, hydrogen bonding, hydrophobic interaction and its fluorescence was quenched due to FRET process.²¹ Importantly, the signal could be recovered upon hybridization with complementary target as shown in **Figure 1.1**. The selectivity for human thrombin was reported for single-base mismatch discrimination. In term of sensitivity, 2.0 nM of detection limit was reported, which is approximately ten-fold lower than that of the regular dye-quencher.²²

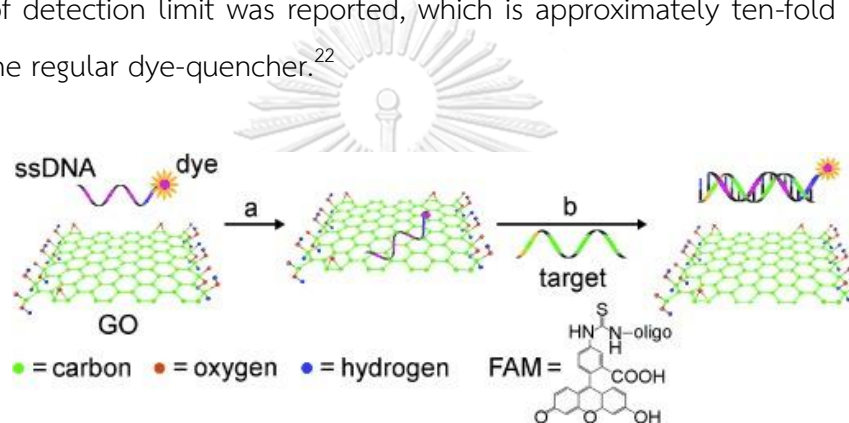


Figure 1.1 Representation of the target-induced fluorescence change of the ssDNA-FAM-GO complex according to Lu and co-workers²⁰

Physisorption of dye-labelled DNA by nanomaterials served as a basis of simple, rapid, high sensitive and selective detection in many DNA/RNA sensors. In 2010, He and co-workers developed a GO-based multicolor fluorescent DNA nanoprobe.¹⁹ Because of extraordinarily high quenching efficiency, GO simultaneously quenched multiple DNA probes with different dyes. The signal could be recovered selectively by specific DNA target corresponding to each probe with single-base mismatch specificity. In term of sensitivity, the detection limit was reported to be as low as 100 pM for DNA detection.

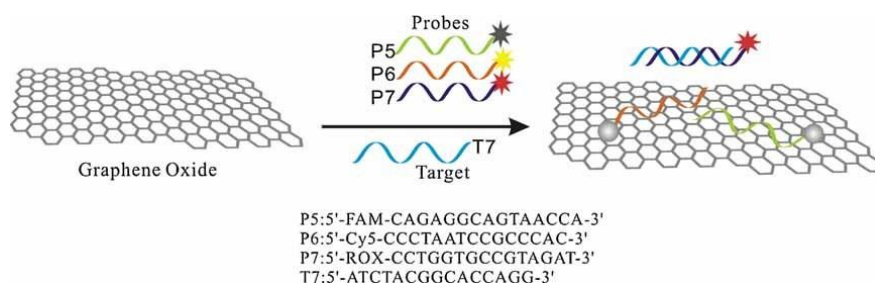


Figure 1.2 GO-based multicolor DNA analysis by He and co-workers¹⁹

Besides, the mixing order was also examined, pre- (probe+target+quencher) and post-mixing strategy (probe+quencher+target). The kinetic of fluorescence recovery of post-mixing was slower than pre-mixing method, implied that GO possesses significantly different adsorption affinity for ssDNA and dsDNA. For insights of the interaction, molecular dynamic (MD) simulation was confirmed that nucleobases were directly adsorbed at GO. In contrast, dsDNA could not be stably adsorbed on GO surface and remained helical structure because of shielding of dense negative charge backbone.

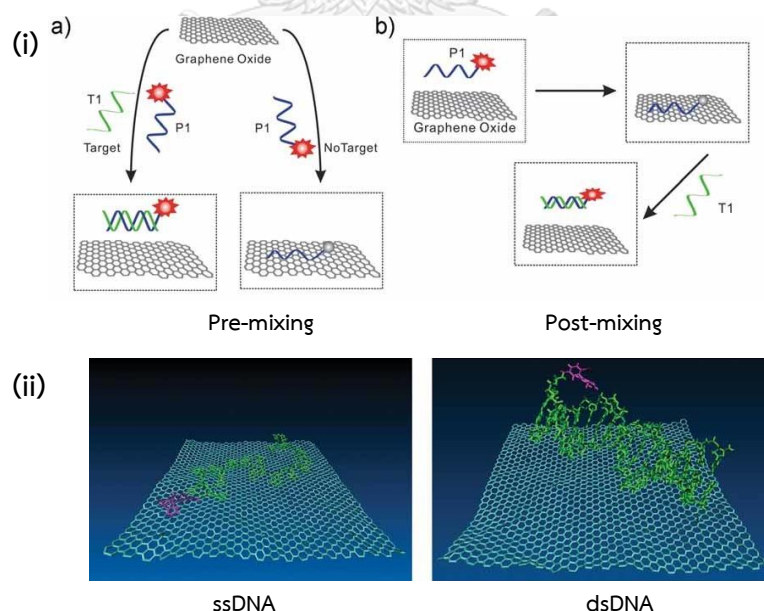


Figure 1.3 Fluorescence assays based on DNA-GO (i) and snapshots from MD simulation (ii)¹⁹

In 2011, Wu and co-workers reported several factors that affect DNA adsorption/desorption.²³ Shorter DNAs adsorbed more rapidly and tightly to GO surface, and the DNA adsorption favoured low pH and high ionic strength (high salt concentration). However, the DNA adsorption was lower at high temperature and may lead to false positive results.

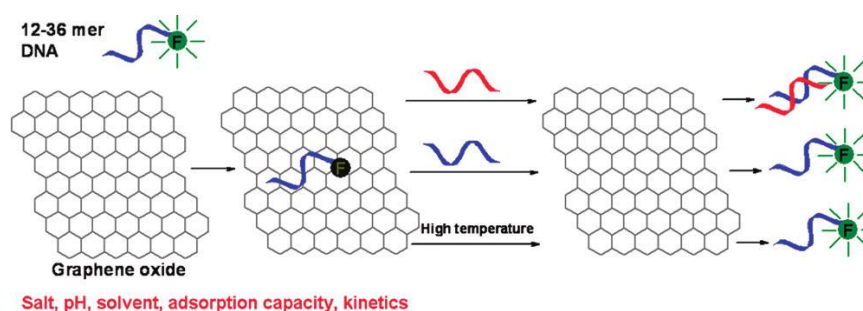


Figure 1.4 FAM-labelled DNA adsorption and desorption on GO studied by Wu and co-workers²³

Moreover, the mechanism of DNA-GO sensing was studied and non-specific displacement was also reported by Liu and co-workers in 2013.²⁴ From the report, the quenched probe was displaced and facilitated from GO surface by DNA homopolymer especially for poly-adenine base sequence because the purines (A and G) could interact more strongly with GO surface than pyrimidines (C and T).^{25, 26} Thus, the use of A-rich of DNA sequence could have problems from small restoration and large non-specific displacement.

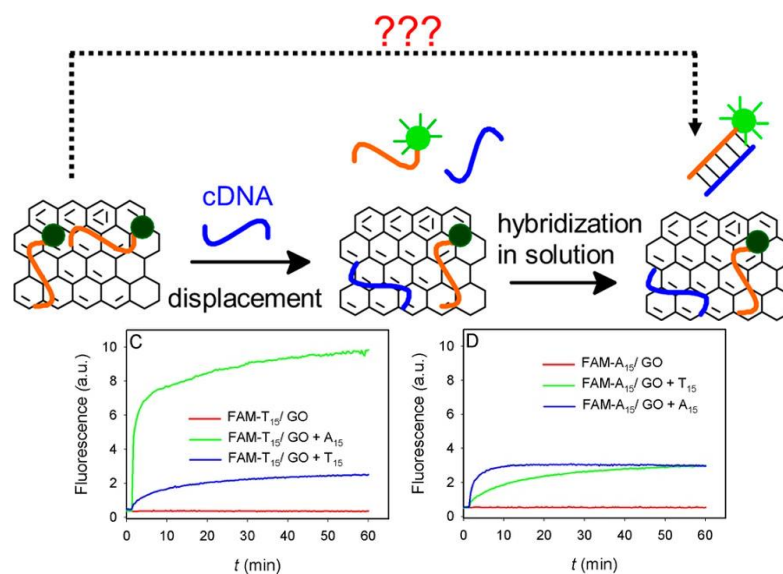


Figure 1.5 Sequence-dependence DNA adsorption on and displacement from graphene oxide (GO) by Liu and co-workers²⁴

GO also acts as DNA delivery vehicle and this can be used for in situ detection based on turn-on fluorescence strategy. For example, Hwang and co-workers developed GO-quenching-based fluorescence to detect RNA in tissue.²⁷

Graphene-quenching of fluorescence in situ hybridization (G-FISH)

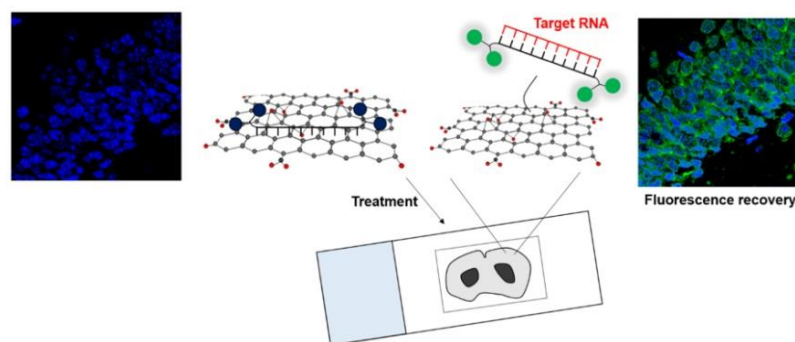


Figure 1.6 Graphene oxide nanoplatform for noncoding RNA detection in formalin-fixed paraffin embedded (FFPE) tissue specimens²⁷

Generally, the negatively-charged GO surface interfered with the adsorption of negatively charged DNA due to the electrostatic repulsion between the negatively charged functional groups on the GO surface and the phosphate backbone of DNA. This results in slow and incomplete quenching. In addition, non-covalent labelled DNA-GO could not resist high temperature and high salt concentration.^{23, 24} These drawbacks challenge researchers to apply other nucleic acid probes in which the charge repulsion is reduced or by covalently immobilized the probe onto the GO surface.

In 2012, a covalent GO-DNA probe was reported by Huang and co-workers.^{28, 29} The fluorescence-labelled DNA was immobilized to GO via amide linkages as shown in **Figure 1.7**. In contrast to the non-covalent DNA-GO sensors, the covalent sensor is highly resistant to nonspecific probe displacement with sub-nanomolar range of detection limit and high signal-to-noise ratio. Furthermore, the sensor was easily separated, protected DNA and facilitated DNA delivery in cells. However, the quenching efficiency is length-dependent and being low for long-chain DNA probes. Moreover, multiple steps are required for the immobilization.

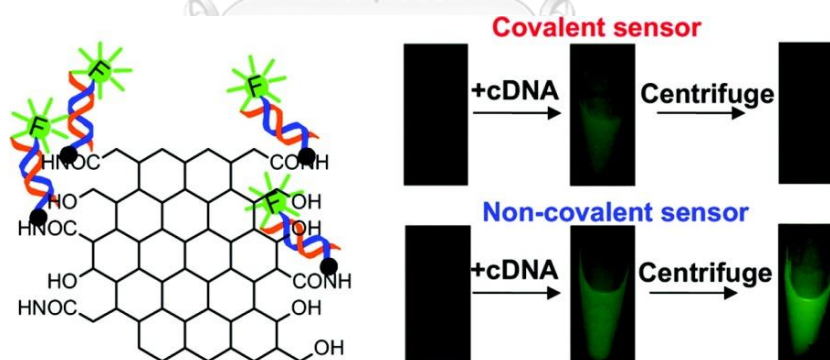


Figure 1.7 Illustration of DNA-GO covalent sensor developed by Huang and co-workers²⁹

Another important class of nanoquencher is metallic nanoparticles, i.e. gold nanoparticles (AuNPs) and silver nanoparticles (AgNPs). Metallic-nanoparticles-based DNA conjugates have been extensively utilized for analysis of various biological targets ranging from biomolecules³⁰ to pathogenic microorganism.³¹ Traditionally, nucleic acid probes are modified with an alkyl thiol group to facilitate their attachment onto the nanoparticles surface.³² Suitable-designed dye-labelled DNA can be effectively quenched by gold nanoparticles similar to GO or organic quencher, and the signal was restored upon hybridization with the DNA target as shown in **Figure 1.8**

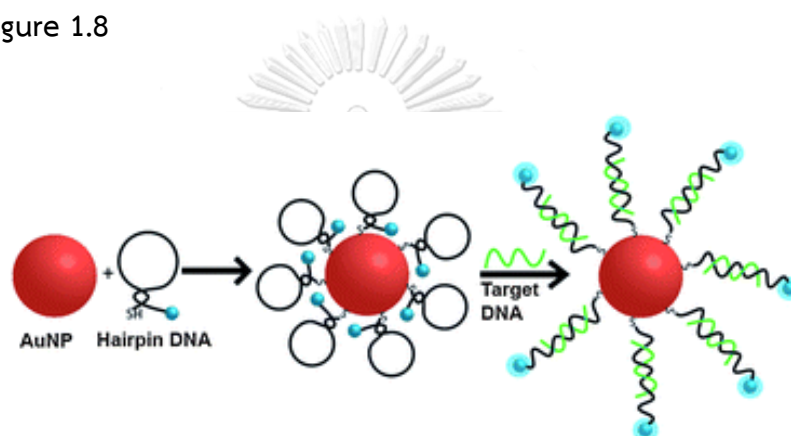


Figure 1.8 A molecular-beacon type DNA sensor based on fluorophore-tagged, hairpin oligonucleotide functionalized gold nanoparticles³³

The molecular beacon based on gold nanoparticles quencher have been used as fluorescence sensing platform for various biological analyses *in vitro*. The low cytotoxicity also makes it useful for *in vivo* sensing applications.³³ For an example, live cell imaging of mRNA using hairpin DNA-functionalized AuNPs was achieved by Jayagopal and co-workers.¹⁶ Due to high target signal-to-background ratio, the detection of mRNA enabled real-time analysis of mRNA transport and processing in living cells.

Covalent immobilization of the probe, or pre-attachment of the fluorescence label required more manipulation steps that reduced practicability of the sensor. In an interesting example, Zhang and co-workers developed a DNA detection method using unmodified AuNPs and rhodamine B.³⁴ This assay relied on two properties, one was the different absorption ability between ssDNA and dsDNA by AuNPs, and

another was different quenching ability between aggregated and dispersed AuNPs as shown in **Figure 1.9**. AuNPs was stabilized by adsorption of single-strand DNA and they resisted to aggregation induced by addition of high concentrations of salt. Consequently, stabilized AuNPs can effectively quench rhodamine B and the fluorescence signal was low. On the other hand, dsDNA could not protect AuNPs from aggregation in the presence of salt, and the quenching efficiency of rhodamine B by aggregated AuNPs was much lower than the dispersed AuNPs, leading to fluorescence increase.

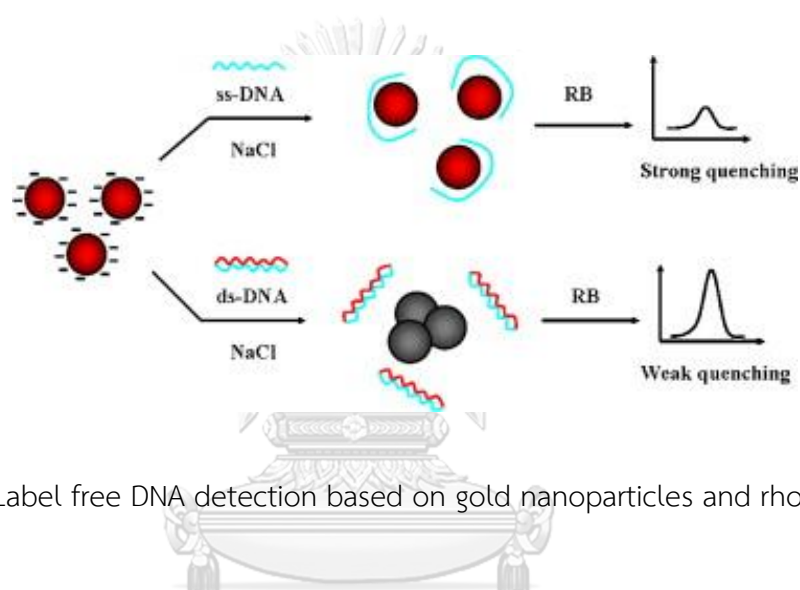


Figure 1.9 Label free DNA detection based on gold nanoparticles and rhodamine B³⁴

The comparison of performances of selected nanomaterials-based DNA sensing platforms with covalent and non-covalent probe immobilization are summarized in **Table 1.1**.

Table 1.1 Performance of fluorescent DNA sensors

Type	Sensitivity	Assay time	Probe synthesis
Molecular beacon ¹⁴	nM	Rapid (min)	Dual labeling
GO-DNA-dye conjugates ²⁹	nM	Slow (~1 h)	Dual labeling
GO-based DNA detection (premixing) ²⁰	~10 nM	Slow (0.5 h)	Single labeling
GO-based DNA detection (postmixing) ¹⁹	100 pM	Rapid (min)	Single labeling
AuNP-DNA-dye conjugates (stem loop probe) ³⁵	nM	Rapid (min)	Dual labeling
AuNP-DNA-dye conjugates (linear probe) ³⁶	No report	Slow (~1 h)	Dual labeling
Unmodified AuNP-based DNA detection ³⁴	pM	Rapid (min)	Single labeling

1.3 Backgrounds of colorimetric nucleic acid sensors based on metal nanoparticles and DNA probes

In addition to being an effective quencher, gold nanoparticles also exhibit an important size-dependent optical property, known as localized surface plasmon resonance (LSPR). LSPR is a phenomenon occurring on metal nanoparticle with size comparable or smaller than the wavelength of light. The resonant oscillation of the electron is stimulated by incident light near the surface, and the maximum optical absorption of the particles occurred at the plasmon resonant frequency.³⁷ The degree of oscillation depends on electron cloud, which conforms to particle size and direction (shape) as shown in **Figure 1.10**.

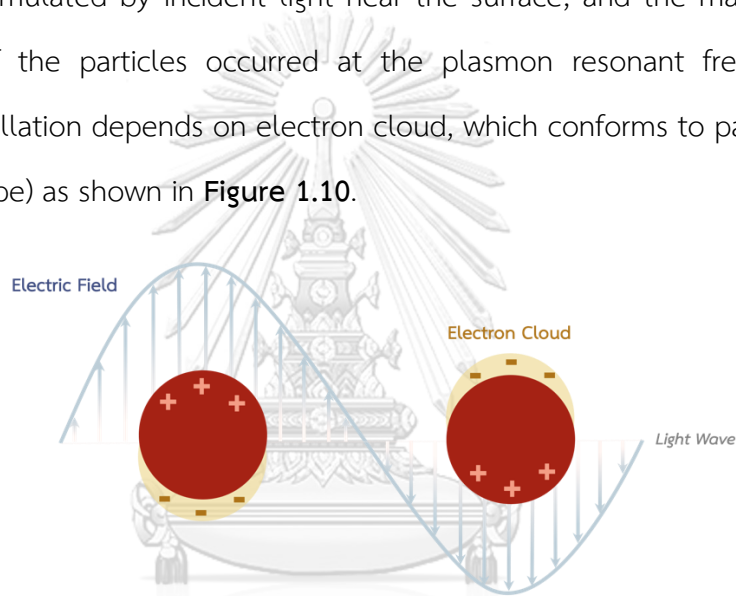


Figure 1.10 Localized Surface Plasmon Resonance (LSPR)

CHULALONGKORN UNIVERSITY

In 1996, Mirkin and co-workers reported that reversible macroscopic aggregation of DNA-conjugated AuNPs could form upon target hybridization, resulting in a distinctive color change from red to purple as shown in **Figure 1.11**.³⁸ The color change provided a simple and inexpensive means for nucleic acid detection. Besides, the colorimetric method provides sufficient specificity to accurately distinguish single-base mismatched from complementary DNA targets.

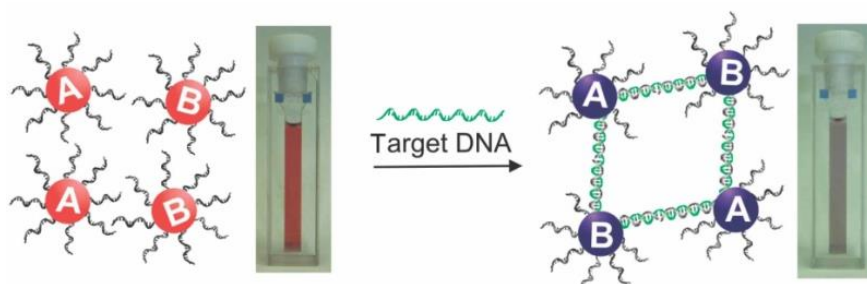


Figure 1.11 Colorimetric DNA-detection methods using DNA-modified gold nanoparticle³⁹

Multiplexed colorimetric detection was developed to detect Kaposi's sarcoma-associated herpesvirus (KHSV) and *Bartonella* (BA) DNA by Mancuso and co-workers.⁴⁰ The different DNA probes were functionalized on different metal nanoparticles, KHSV probe for gold nanoparticles and BA probe for silver nanoparticles. Due to the presence of target, gold and silver nanoparticle microscopic aggregation are tuned for each target to develop a multi-color sensor (**Figure 1.12**). The multiplexed colorimetry could be investigated KHSV and confounding DNA (BA DNA) in one-pot detection system in presence of 1-2 nM of targets.

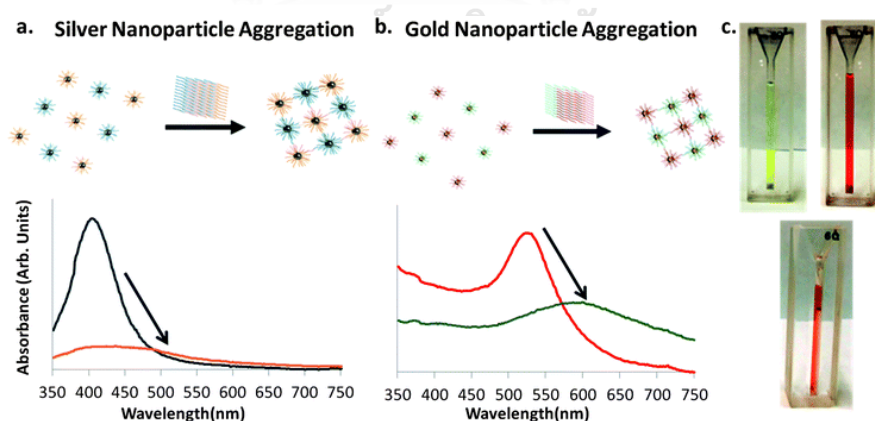


Figure 1.12 The aggregation of silver (a) and gold nanoparticles (b) for colorimetric detection of DNA (c)

Rothberg and Li subsequently reported a label-free colorimetric detection method that does not require the probe immobilization onto the nanoparticles.⁴¹ Single-strand DNA bound to gold surface, and stabilized the AuNPs towards salt-induced aggregation. In contrast, dsDNA did not readily bind and led to aggregation of AuNPs in salt solution as shown in **Figure 1.13**, resulting in a color change from red to purple. In the procedure, the DNA probe and the target were introduced to the AuNPs followed by salt addition. The color changes from red to purple color upon salt addition indicated the presence of target. The sensitivity of this label-free sensing for visual detection was at the level of 100 fmol of target and was close to the use of DNA-conjugated nanoparticles.

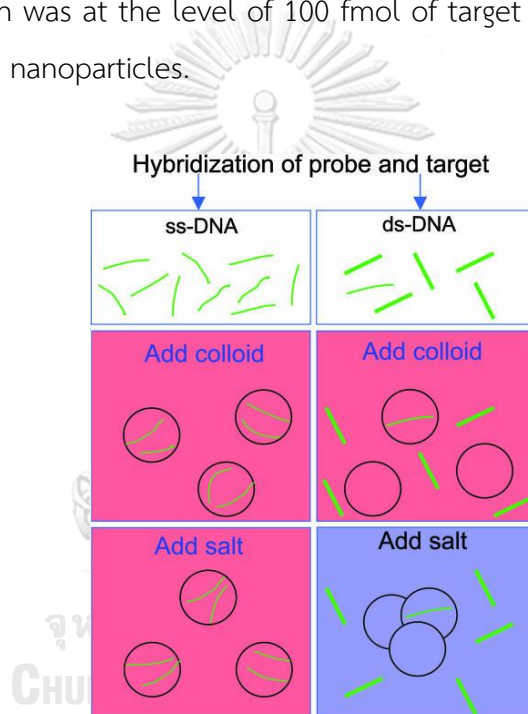


Figure 1.13 The colorimetric method for differentiating between single- and double-stranded DNA oligonucleotides⁴¹

The adsorption of ssDNA on gold nanoparticles is length dependent - being more efficient with short DNA sequences. In 2016 He and co-workers showed that single-strand DNA in the form of hairpin with sticky end could be adsorbed on the gold surface and gave an inverse blue-to-red color variation with the increase of sticky end length when the length is within a certain range.⁴² The principle was applied for AuNPs-based colorimetric DNA assay with picomolar sensitivity and high specificity.

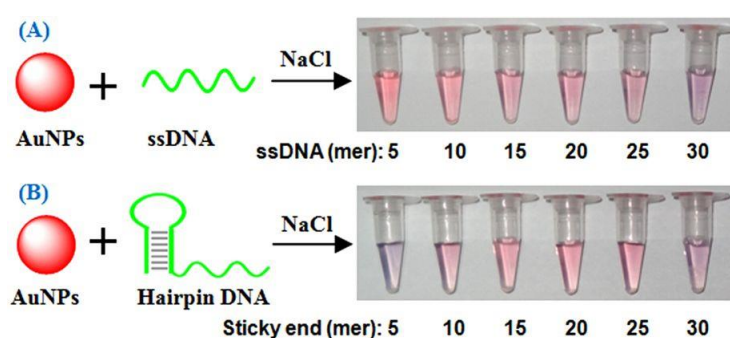


Figure 1.14 AuNPs solutions in the presence of hairpin ssDNAs (A) and hairpin DNAs (B) with different lengths of ssDNA sticky ends⁴²

The unmodified gold nanoparticles could be adapted for enzyme-free colorimetric detection and hybridization chain reaction (HCR) amplification developed by Liu in 2013.⁴³ Hairpin DNA probes with single-strand sticky end could stabilize gold surface and prevent salt-induced aggregation. When the formation of double-strand DNA polymer by HCR was performed, the sticky-end stabilization on AuNPs surface was lost and AuNPs undergo aggregation in salt solution as shown in **Figure 1.15**.

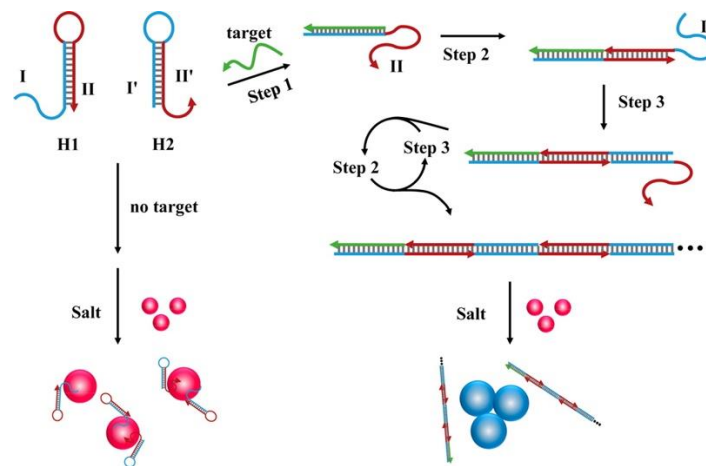


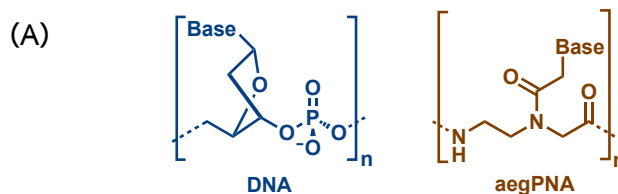
Figure 1.15 Highly sensitive colorimetric detection of DNA by the use of gold nanoparticles and hybridization chain reaction amplification⁴³



1.4 Peptide nucleic acid

1.4.1 History of peptide nucleic acid and properties

Peptide nucleic acid (PNA) is nucleic acid mimic which the pentose sugar and the phosphate backbone were replaced by a synthetic polypeptide, leading to a new uncharged backbone. The PNA prototype which consists of *N*-(2-aminoethyl)glycine unit as its backbone, now known as aegPNA (**Figure 1.16A**), was proposed by Nielsen and co-workers in 1991.^{44, 45} Despite their distinct chemical structures and functionalities, the orientation and distance between the nucleobases and the backbone in PNA is similar to that of natural nucleic acids. Therefore, aegPNA can bind to DNA or RNA following the Watson-Crick base-pairing rules with high specificity (**Figure 1.16B**). In fact, the mismatch discrimination ability of PNA is even better than DNA or RNA. Due to absence of negative charges on the backbone, electrostatic repulsion of aegPNA-DNA duplexes is absent, and this is reflected by a much higher thermal stability of the PNA-DNA and PNA-RNA duplexes over regular DNA-DNA or DNA-RNA duplexes especially under low ionic strength environment. Furthermore, the unnatural backbone of PNA exhibits excellent biological and chemical stability, for example, it shows complete resistant to various proteases or nucleases. Consequently, the strong DNA/RNA binding affinity and ability to specifically discriminate between fully matched and single-base mismatched nucleic acid target makes PNA useful alternative for traditional nucleic acid as a probe for sensing applications.



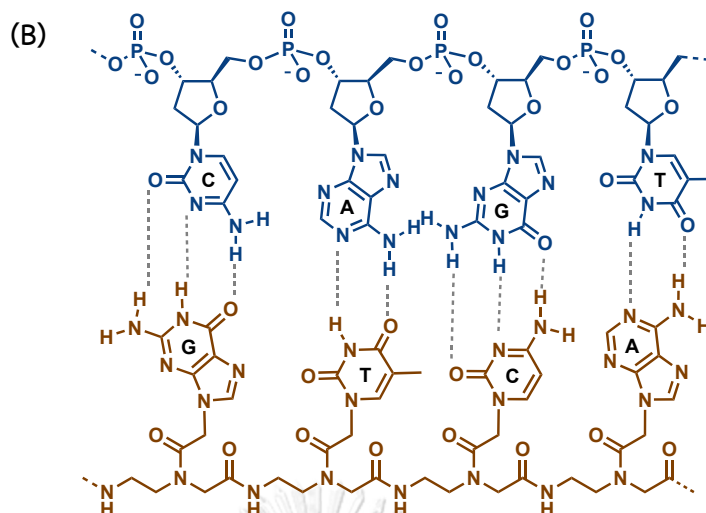


Figure 1.16 Repeating units of the DNA and aegPNA structure (A) and aegPNA-DNA antiparallel duplex according to Watson-Crick base-pairing (B)

1.4.2 Conformational constrained PNAs and their novel features

Over past few decades, various PNA systems have been developed in order to improve the properties, i.e. binding affinity and specificity, of the first generation PNA (aegPNA). One of the most successful concepts is the introduction of conformational constraint into the PNA backbone to reduce the entropy change during the formation of PNA-DNA duplex. Based on this idea, the pyrrolidinyl PNA which consisted with 2-amino-1-cyclopentacarboxylic acid (ACPC) and nucleobase-modified proline backbone as shown in **Figure 1.17A** was proposed by Vilaivan and co-workers since the year 2005.⁴⁶⁻⁴⁹ The conformationally rigid acpcPNAs show higher thermal stability compared to aegPNA. In addition, acpcPNA exhibited excellent specificity as shown by the large decrease in thermal stability in mismatched hybrids in comparison with fully matched hybrids. Importantly, the specificity of acpcPNA is considerably higher than aegPNA and the more recently reported state-of-the-art γ PNA.⁴⁶ In addition, only binding in antiparallel direction was observed in acpcPNA-DNA duplex as shown in **Figure 1.17B**, whereas both of parallel and anti-parallel bindings can occur in aegPNA-DNA hybrids. The several advantages of PNA, including

the higher thermal stability over DNA-DNA and DNA-RNA or RNA-RNA duplexes, the electrostatically neutral backbone and the enzyme resistance, suggests its potential uses for DNA sensing applications.

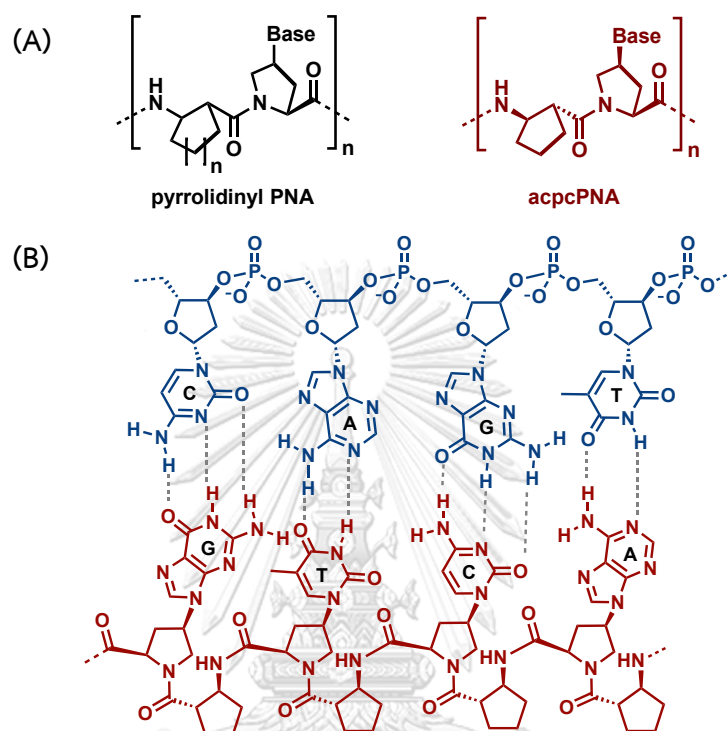


Figure 1.17 Repeating units of pyrrolidinyl PNA and acpcPNA structure (A) and acpcPNA-DNA duplex in antiparallel according to Watson-Crick base-pairing (B)

1.5 Combination of PNA probes and nanomaterials for nucleic acid sensing

There are several reports that utilized PNA as a probe that can generate fluorescence signal upon binding to the correct targets.⁵⁰ There are several possible strategies to achieve this, but this section will focus on the use of fluorescent-labelled PNA probe and a nanomaterial as external fluorescent quencher/FRET partners. In general, nanomaterials have been used as quenchers or FRET partners with fluorescent dye-labelled PNA probes. Thus, PNA is widely adapted to use as turn-on fluorescence probe with various nanomaterials by both of *in vivo* and *in vitro* detection. Some examples of PNA-nanomaterials combination for sensing purposes or other applications are exemplified in **Table 1.2**.

Table 1.2 Nanotechnology based-on PNA for biosensor

Nanoparticles	Application	Detection
Poly (lactic co-glycolic acids) (PLGA) ⁵¹	Gene editing	- Fluorescence technique (<i>in vivo</i> detection)
Mesoporous silica nanoparticles ⁵²	Antisense	- PNA-surface Immobilization
Zeolite-L-nanocrystals ⁵³	Delivery vehicle	
Cobalt ferrite core/metallic shell ⁵⁴	PNA/DNA based biosensors	
Cationic shell cross-linked nanoparticles ^{55, 56}	mRNA imaging	- Fluorescence technique (<i>in vivo</i> detection) - Non-immobilization of PNA
Gold nanoparticles ⁵	RNA detection	- Colorimetry* (<i>in vitro</i> detection) - Non-immobilization of PNA

From the examples, there are two possibilities to combine PNA and nanomaterials-covalent and non-covalent immobilization. PNA-conjugated nanomaterial is a strategy that can increase the capacity of PNA on the surface and assists fluorescence quenching process. However, additional step is required for covalent immobilization. On the other hand, the uncharged backbone of PNA provide unique means for the interaction between the PNA or PNA-DNA duplex and the nanomaterials. For example, electrostatic interaction between cationic shell nanoparticles and PNA-DNA duplex can promote high nucleic acid adsorption without the need for immobilization.^{55, 56} Thus, the non-covalent interaction between PNA and nanomaterials serves as a simplest strategy for development of PNA-based biosensors.

As an example, graphene oxide (GO), which is known to interact with single-stranded DNA by π - π interaction and hydrogen bonding⁵⁷ and has been widely used with dye-labelled DNA for fluorescent-based DNA-RNA sensing,^{19, 20} has also been used with PNA probes by Kotikam and co-workers in 2012.⁵⁸ The interaction of DNA, aegPNA, and polycarbamate nucleic acid (PCNA) oligomers were compared. Modified DNA backbone as D-PCNA with chirality and uncharged was better as a probe for DNA detection than natural DNA or aegDNA. This is because uncharged backbone support adsorption of the probe on GO surface and chirality of modified backbone affected the kinetics of the PNA-DNA binding.

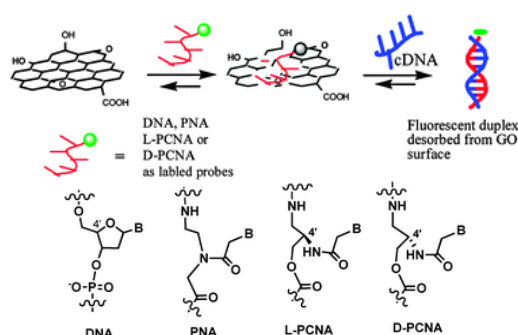


Figure 1.18 Fluorescence assay for DNA detection using DNA, PNA, and PCNA⁵⁸

In 2013, Guo and co-workers⁵⁹ developed a combination of PNA and GO overcame many problems with GO-DNA systems. The main problem of using GO with DNA probe was the non-specific nature of the interaction between ssDNA and GO sheet, which caused competitive displacement of adsorbed DNA probes by non-target ssDNA and therefore false positive may result.^{24, 57}

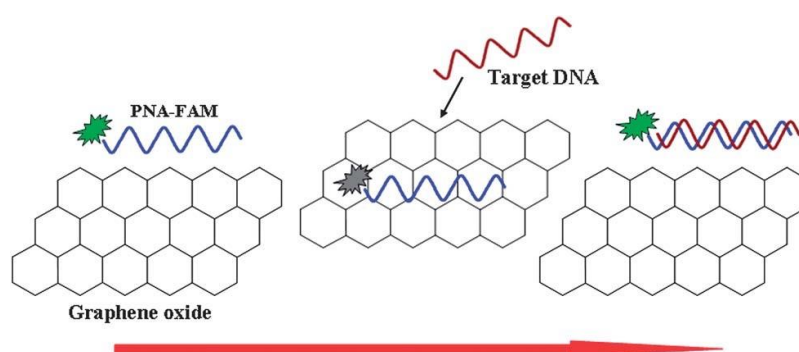


Figure 1.19 Fluorescent DNA detection based on the GO platform by using PNA as the probe by Guo and co-workers⁵⁹

When PNA probes were utilized instead of DNA, hydrophobic backbone of PNA probe enhanced the interaction with GO and therefore the non-specific displacement by non-target DNA was less likely.⁵⁸ Moreover, the stronger interactions between GO and PNA also give rise to stronger quenching effects compared with DNA probes. As a result, lower background fluorescence is achieved with PNA probes. In addition, when PNA-DNA duplexes were not readily adsorbed by GO sheets similar to DNA-DNA duplexes,^{19, 58} and the fluorescence increase upon target hybridization was enhanced. From the advantages above, many researchers studied and developed nucleic acids sensing using PNA probes and GO. In 2013, Ryoo and co-workers⁶⁰ developed PNA-GO complex for miRNA sensing. The system showed less toxicity compared with traditional polyethyleneimine (PEI)-grafted GO and oligonucleotide system, while showing high selectivity and specificity toward miRNA with very low background signal and can be used for miRNA monitoring in living cells (Figure 1.20).

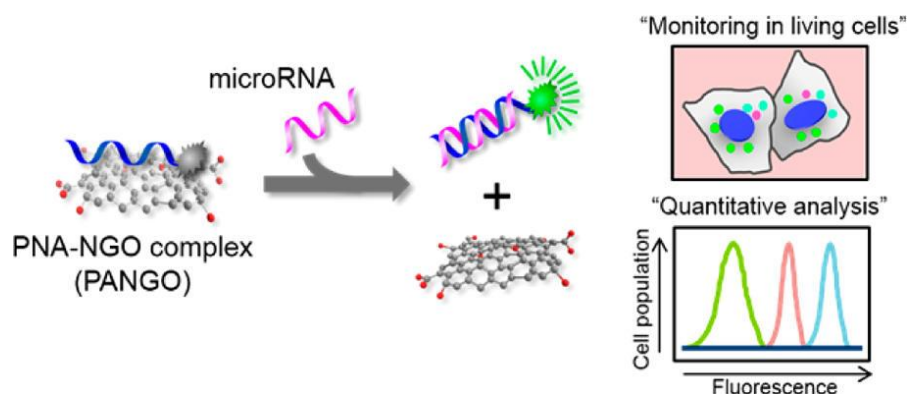


Figure 1.20 A miRNA sensor based on PNA and GO platform by Ryoo and co-workers⁶⁰

Gold nanoparticles (AuNPs) have also been extensively used in biosensor development due to their unique optical properties including distance/shape-dependent color and fluorescence quenching ability for dye-labelled probe.^{34, 61} In 2004, Li and co-worker found that citrate-coated AuNPs undergo different electrostatic reaction against single- and double-strand DNA for induced-aggregation by salt.⁴¹ This property can be applied for other label-free nucleic acid probes. In case of PNA, fluorescence method has been limited. However, in colorimetric detection mode, the surface plasmon resonance (SPR) properties of gold nanoparticles that cause obvious color change have been utilized in combination with PNA probe for label-free detection of DNA by Su and co-workers.^{62, 63} Only single stranded PNA caused color change of AuNPs and its hybridization status could be discriminated from the color. In the presence of free PNA, the color was changed to blue or purple because PNA molecules induce aggregation of the metallic nanoparticles due to the removal of charge repulsion of the citrate anion-coated particles via PNA adsorption. When complementary target DNA was added, the negatively charged PNA-DNA duplexes could not be adsorbed onto the negatively charge surface of the nanoparticles. Hence, no particles aggregation occurred and the color remained red.

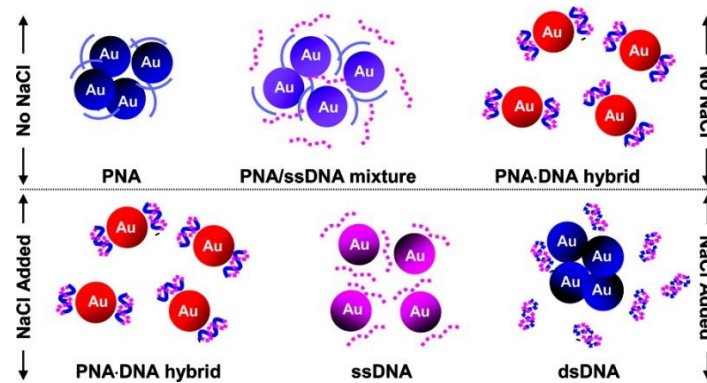


Figure 1.21 A strategy of colorimetric DNA detection based on gold nanoparticles and label-free PNA by Su and co-worker⁶³

This rapid, label-free colorimetric assay based on PNA-AuNPs has been used to detect and quantify nucleic acids in a simple, reliable, time- and cost-effective fashion. For instance, a viral RNA detection was developed in 2013 by Joshi and co-workers.⁵ Real-time PCR samples could be quantified by simple spectrophotometer with high accuracy and precision. Another example is the application in the detection of bovine viral diarrhea virus (BVDV)-RNA developed by Askaravi and co-workers⁶⁴ in 2017. Combination of PNA and unmodified-AuNPs could serve as a rapid visual detection and enzyme-free assays which was applicable for clinical laboratories.

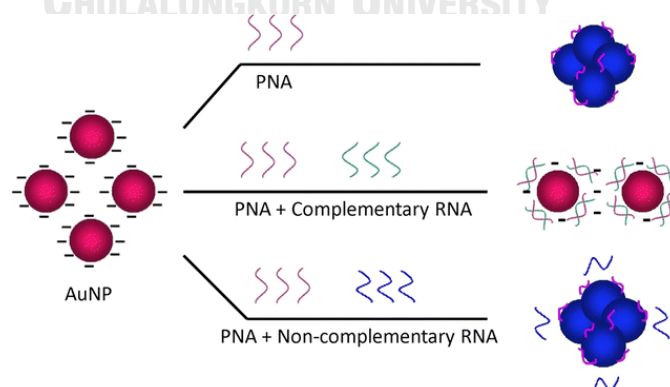


Figure 1.22 PNA-AuNP colorimetric detection assay for BVDV-RNA detection by Askaravi and co-workers⁶⁴

In all of these PNA-nanomaterials DNA/RNA sensors, only aegPNA have been studied. In view of the better performance of acpcPNA in terms of binding affinity and specificity compared to both aegPNA and DNA probes traditionally used, it is possible that the performance of the sensor could be further improved.

1.6 Rationale and objective of this study

This work aims to develop new fluorescence/colorimetric nucleic acid sensing platforms that are simple, rapid, specific and cost-effective that employ a combination of acpcPNA as the nucleic acid probe and nanomaterials, including graphene oxide (GO), reduced graphene oxide (rGO), gold nanoparticles (AuNPs), and silver nanoparticles (AgNPs) as signal transducer. In both sensing platforms, the interaction between the acpcPNA probe and the nanomaterials will be first optimized. Based on the knowledge that these nanomaterials bear multiple negative charges on the surface, it was proposed that increasing the number of positive charges on the acpcPNA probe should increase the strength of the electrostatic interaction between the PNA probe and the nanomaterials. This should result in stronger fluorescence quenching (for fluorescence assay) or better aggregation (for colorimetric assay), which in turns should improve the signal-to-noise ratio by reducing the background signal. Moreover, the use of acpcPNA probe should lead to improvement of selectivity and sensitivity of the detection compared to traditionally used aegPNA and DNA probes. Once the proof-of-concept experiments works, parameters that affect the signal will be studied and the detection conditions will be optimized. Finally, the linearity range and limits of detection, including applications to the detection of real DNA samples will be demonstrated.

CHAPTER II

EXPERIMENTAL SECTION

2.1 Materials

All chemicals used in this study were of analytical grade and were used as received without further purification. Anhydrous *N,N'*-dimethylformamide ($H_2O \leq 0.01\%$) for solid phase peptide synthesis was purchased from RCI Labscan and dried over activated 4 Å molecular sieves before use. The solid support for peptide synthesis (TengaGel S-RAM resin (0.24 mmol/g)) was obtained from Fluka. 5/6-Carboxyfluorescein succinimidyl ester (FAM-NHS) was purchased from Thermo Scientific Co., Ltd. Graphene oxide nanocolloids (NGO, 2.0 mg/mL in H_2O) and hydrogen tetrachloroaurate (III) trihydrate were obtained from Sigma-Aldrich. Tri-sodium citrate pentahydrate was from Honeywell Riedel-De Haën®. Hydrazine hydrate solution (70-79%) was from Tokyo Chemical Industry. All oligonucleotides used in this study were purchased from Pacific Science and the sequences were summarized in **Table 2.1**. MilliQ water was obtained from Millipore ultrapure water system with Millipak® 40 filter unit 0.22 µm. The nuclease-free water was purchased from Invitrogen.

Table 2.1 Sequences of oligonucleotides employed in this study

Name	Sequence
comDNA	AGT GAT CTA C
smDNA	AGT GCT CTA C
DNA (A12)	AAA AAA AAA AAA
FAM-DNA	FAM-GTA GAT CAC T
miRNA21	UAG CUU AUC AGA CUG AUG UUG A
ncRNA	UAG UUG UGA CGU ACA

2.2 Synthesis of acpcPNA

2.2.1 AcpcPNA monomer synthesis

The Fmoc-protected Pfp-activated pyrrolidiny PNA monomers (Fmoc- A^{Bz} -OPfp, Fmoc- C^{Bz} -OPfp and Fmoc-T-Opfp) or free acid monomer (Fmoc-G-OH) (all with 2'*R*,4'*R* configuration) and Pfp-activated fmoc-(1*S*,2*S*)-2-amino-1-cyclohexane carboxylic acid spacer (**Figure 2.1**) for PNAs synthesis were synthesized in house by Vilaivan and co-workers following a previously reported protocol.⁴⁸

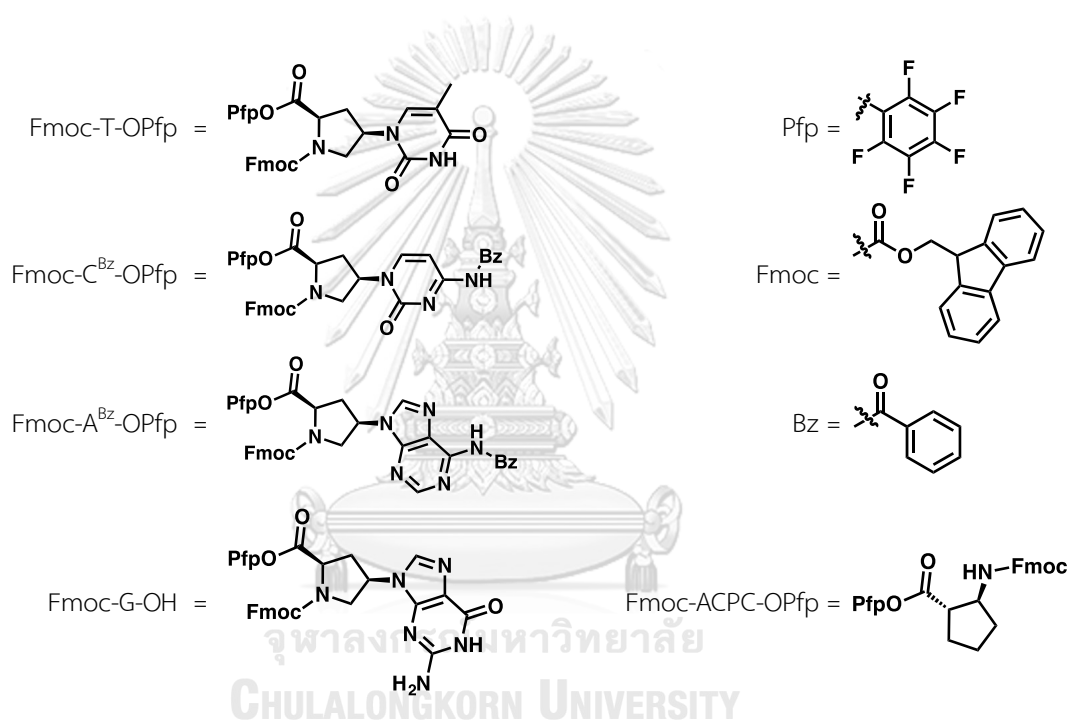


Figure 2.1 Structures of pyrrolidiny PNA monomers and acpc spacer for solid phase peptide synthesis

2.2.2 Solid phase peptide synthesis

AcpcPNAs were synthesized on TengaGel S-RAM resin by solid phase peptide synthesis at 1.5 μmol scale employing stepwise coupling of Fmoc-protected pyrrolidinyl PNA monomers and acpc spacer shown in **Figure 2.1**.⁶⁵ In brief, a synthesis cycle consists of three successive steps: deprotection, coupling and capping. In the deprotection step, the *N*-terminal Fmoc group on the resin was firstly removed (100 μL of 20% piperidine and 2% DBU in DMF, 5 minutes) to expose the *N*-terminal amino group. Next, in the coupling step, the Pfp-activated fmoc-protected amino acids, PNA monomers or acpc spacer were directly coupled to the resin (4 equiv Fmoc-L-Lys(Boc)-OPfp or Pfp-activated monomer or spacer, 4 equiv HOAt, 4 equiv DIEA in DMF, single coupling, 40 min for Fmoc-T-OPfp, 30 min for other monomers). For Fmoc-G-OH, the monomer was pre-activated by treatment with HATU/DIEA prior to the coupling (4 equiv G monomer, 4 equiv HATU, 8 equiv DIEA in DMF, single coupling 40 min). Finally, the capping step, any unreacted free amino groups on the resin were capped by acetylation with acetic anhydride (5 μL of Ac_2O and 7% of DIEA in 30 μL DMF). The deprotection-coupling-capping cycle process was repeatedly performed until the desired sequence was obtained, with exhaustive washing with DMF between each step. 5/6-Carboxyfluorescein succinimidyl ester (FAM-NHS) was attached onto the N-terminus of the obtained sequence (4 equiv FAM-NHS, 8 equiv DIEA in 30 μL DMF, 3 days) after the final Fmoc-deprotection. The residual *N*-terminal amino group was capped by acetylation. Subsequently, the exocyclic amino protecting groups of the nucleobases were removed (1:1 aqueous ammonia solution:1,4-dioxane, 65 $^\circ\text{C}$, overnight), followed by washing with methanol and dried. Lastly, the resins were treated with trifluoroacetic acid (TFA) (500 μL x 3) to cleave the PNA from the solid support. The TFA was removed under a stream of nitrogen gas and the residue containing crude PNA was re-precipitated from diethyl ether. The crude PNA was purified by reverse phase HPLC on a Waters 600 HPLC system using C-18 column (4.6 x 50 mm). The sample elution was carried out using a gradient of water (A) and methanol (B) consisting of 0.1% TFA (monitored by UV absorbance at 260 nm, 10% B for 5 minutes then linear gradient to 90% B

over 60 minutes, flow rate 0.5 mL/min). Each collected fraction was analyzed by MALDI-TOF mass spectrometry (Microflex, Bruker Daltonics) and the fractions containing the correct PNA sequence were combined and lyophilized to give the purified PNA. Purity of the PNA was confirmed by HPLC analysis (10% B for 5 minutes then linear gradient to 90% B over 35 minutes, flow rate 0.5 mL/min). Concentrations of the PNA were determined by calculation from absorbance at 260 nm as determined by UV-visible spectrophotometry using the molar extinction coefficients (ϵ_{260}) provided by the in-house web-based software developed by Vilaivan (<http://www.chemistry.sc.chula.ac.th/pna>).

2.3 Synthesis of nanomaterials

2.3.1 Synthesis of 12 nm citrate-capped gold nanoparticles (citrate-AuNPs)

The 12 nm citrate-capped of gold nanoparticles (citrate-AuNPs) were synthesized through citrate-reduction method (also known as Turkevich method).⁶⁶ A solution of hydrogen tetrachloroaurate (III) (200 $\mu\text{g/mL}$, 50 mL) was heated to boiling in a clean 250 mL Erlenmeyer flask. Next, the aqueous solution of tri-sodium citrate (40 mM, 1 mL) was rapidly added. The solution was continuously stirred until a ruby-red solution was obtained. The mixture was cooled to room temperature and stored at 4-8 $^{\circ}\text{C}$ for long-term use. The concentration of the stock solution was calculated from the HAuCl_4 concentration used as 200 $\mu\text{g/mL}$. The morphology of the synthesized gold nanoparticles was characterized by Transmission Electron Microscope (TEM) (TEM-2100 at Scientific and Technological Research Equipment Centre (STREC), Thailand) and UV-visible spectroscopy (Cary 100, Varian). The surface charge was determined on a Malvern NanoZSP Zetasizer.

2.3.2 Synthesis of 40 nm citrate-capped gold nanoparticles

The 40 nm citrate AuNPs was synthesized by a two-step seed-mediated method.⁶⁷ The 12 nm citrate-AuNPs seed particles (200 $\mu\text{g/mL}$, 0.5 mL) were prepared as described in section 2.3.1 was mixed with tri-sodium citrate solution (0.2 mM, 50 mL). The mixture was heated to boiling and a solution of hydrogen tetrachloroaurate (III) (20 mg/mL, 250 μL) was added in 25 μL aliquots every 15 minutes. After the final addition, the mixture was continuously stirred for 15 minutes. Next, the solution was cooled down to room temperature and stored at 4-8 $^{\circ}\text{C}$. The final concentration was calculated from HAuCl_4 concentration of growth solution as 100 $\mu\text{g/mL}$. Particle size was determined by UV-visible spectrophotometry and transmission electron microscope (TEM).

2.3.3 Synthesis of silver nanoparticles (AgNPs)

The silver nanoparticles were synthesized by the same procedure as gold nanoparticles (AuNPs).⁶⁸ An aqueous solution of silver nitrate (170 $\mu\text{g/mL}$, 18 mL) was heated to boiling state. Subsequently, tri-sodium citrate solution (10 mM, 2 mL) was introduced rapidly. The mixture was continuously stirred until a yellow color solution was observed. The solution was cooled to room temperature before keeping at 4 $^{\circ}\text{C}$ for long-term using. The synthesized AgNPs was characterized by UV-visible spectrophotometry and the morphology was identified by using transmission electron microscope (TEM).

2.3.4 Synthesis of reduced graphene oxide (rGO)

Reduced graphene oxide (rGO) was synthesized by hydrazine reduction of graphene oxide.⁶⁹ Firstly, the graphene oxide nanocolloids (NGO, 2 mg/mL, 5 mL) was dispersed in water to give a homogeneous suspension (10 mL of final volume). The pH of the suspension was adjusted to 10 by addition of aqueous ammonia solution. Next, hydrazine hydrate solution (79%, 20 μ L) was added. The mixture was heated at 80 $^{\circ}$ C for 1 day. The black precipitate was filtered and washed with methanol before drying. The dried precipitate was redispersed in MilliQ water (0.2 mg/mL of final concentration). The surface charge of black suspension was determined on a Malvern NanoZSP Zetasizer.

2.4 Fluorescence experiments

2.4.1 Fluorescence quenching experiments

All of fluorescence signals were monitored by Cary Eclipse Fluorescence Spectrophotometer (Varian) with excitation wavelength of 460 nm, slit width 5 nm and photomultiplier tube (PMT) detector setting at 940 V. For fluorescence quenching experiments, suspensions of the nanomaterials at the specified concentration were mixed with the fluorescein-labeled PNA or DNA probes (0.1 μ M, in 10 mM Tris-HCl buffer pH 7.4, 1.0 mL). After 30 min incubation, the fluorescence spectra were collected, and the emission at 525 nm was used to calculate the percentage brightness as shown by **Equation 2.1** and **2.2**, respectively.

$$\text{Brightness (\%)} = \frac{\text{Emission}_{\text{sample}} \times 100}{\text{Emission}_{\text{ssPNA}}}$$

Equation 2.1 Calculation of percentage brightness of quenched PNA/DNA probes

$$\text{Quenching (\%)} = \left(\frac{\text{Emission}_{\text{ssPNA}} - \text{Emission}_{\text{sample}}}{\text{Emission}_{\text{ssPNA}}} \right) \times 100$$

Equation 2.2 Calculation of percentage quenching of fluorescein-labeled probes

2.4.2 Fluorescent discrimination

i) PNA+Quencher+DNA

The fluorescein-labeled acpcPNA probe (0.1 μM in 10 mM Tris-HCl buffer (pH 7.4), 1.0 mL) was quenched by incubation with the nanomaterials as described in section 2.4.1. The nucleic acid target (DNA or RNA) (0.12 μM , 1.2 equiv) was added to the quenched PNA or DNA probe. The fluorescence emission at 525 nm was measured as described above every 10 min for 1 h. The relative fluorescence restoration (F/F_0) was calculated by **Equation 2.3**.

$$\frac{F}{F_0} = \frac{\text{Emission}_{\text{After adding target}}}{\text{Emission}_{\text{Before adding target}}}$$

Equation 2.3 Calculation of fluorescence restoration of quenched PNA/DNA probes

ii) PNA+DNA+Quencher

The fluorescein-label acpcPNA probe (0.1 μM in 10 mM Tris-HCl buffer pH 7.4), 1.0 mL) was mixed with the nucleic acid target (0.12 μM , 1.2 equiv) and then incubated for 15 min before addition of quencher. After this, the fluorescence emission at 525 nm was measured every 10 min within 1 h.

2.5 Colorimetric assay

2.5.1 Naked-eyes detection of gold nanoparticles

The PNA probe (0.5 μM) was mixed with the nucleic acid target (0.6 μM , 1.2 equiv) in 10 mM sodium phosphate buffer pH 7.0 (total volume = 15 μL) in a PCR tube (size 200 μL) and incubated for 15 minutes at room temperature. The citrate-AuNPs solution (200 $\mu\text{g}/\text{mL}$, 5 μL) was added and the solution was mixed thoroughly by vortex mixing. The color was observed under white light and the photographs were taken by Canon EOS M (18-55 mm, f 3.5-5.6) using ISO100, f5.6, shutter speed 1/20. The fluorescence light was observed under black light at 356 nm and the photographs were taken using ISO100, f5.6, shutter speed 0"8. The image analysis was recognized by ImageJ software. The plotting profile of white light photograph was analyzed using gray scale image and black light photograph was from green channel of RGB analysis.

2.5.2 UV-visible measurement

i) Selectivity

The PNA probe stock solution (100 μM , 1 μL) was mixed with the nucleic acid target (100 μM , 1.2 μL , 1.2 equiv) in 10 mM sodium phosphate buffer (pH 7.0, total volume = 10 μL) in a PCR tube and incubated for 15 minutes at room temperature. The mixture was transferred into a cuvette and mixed with solution of citrate-AuNPs (20 $\mu\text{g}/\text{mL}$) in 10 mM sodium phosphate buffer (pH 7.0, total volume = 990 μL) to obtain a solution having the final concentrations of PNA and nucleic acid target at 0.1 μM and 0.12 μM , respectively in a final volume of 1.0 mL. The mixture was incubated for 15 min before UV-visible spectra measurement.

ii) Sensitivity

The PNA probe-nucleic acid target-AuNP mixture was prepared as in 2.5.2 i) The UV-vis spectra were measured, and the calibration curve was prepared by plotting A_{520}/A_{650} or A/A_0 at 540 nm for 12 and 40 nm gold nanoparticles (AuNPs), respectively as a function of nucleic acid target concentration.

2.6 LAMP-amplification of *S. aureus* carrying staphylococcal enterotoxin A (SEA) gene

The DNA from Staphylococcal enterotoxin A (SEA)-producing *S. aureus* was amplified by using loop-mediated isothermal amplification (LAMP) technique. The experiments were performed by Ms. Ilada Choopara and Dr. Naraporn Somboonna, Department of Microbiology, Faculty of Science, Chulalongkorn University. First, 1.6 μM for each of the FIP, BIP, LF and LB primers, 0.2 μM for each of the F3 and B3 primers, 1.4 mM dNTPs, 0.3 M betaine, 6 mM MgSO_4 and *Bst* DNA polymerase (8 units) were introduced into the extracted DNA solution (~ 1 fg in Tris-HCl buffer (pH 7-9) 20 mM, $(\text{NH}_4)_2\text{SO}_4$ 10 mM, KCl 10 mM, MgSO_4 2 mM, and Triton X-100 0.1%, total volume = 15 μL). Subsequently, the mixture was incubated at 63 °C for 15 min and then the reaction was stopped by heating at 80 °C for 2 min. The sequence of the primers is summarized in **Table 2.2**

Table 2.2 Sequence of primers used for preparation of DNA samples by LAMP

Primer	Base sequence (5'→3')
Outer primer F3	TCTATTATTACAATGAAAA
Outer primer B3	ATTGATAACCATAATAAGCA
Inner primer FIP	CTGTAAAAAAGCCTTTAAACAATATTTTGCTAAAACTGAAAATAAA GAGAGTC
Inner primer BIP	GGTATAACGATTTATTAGTAGATTTTTTATACAAGTCTACTTTTTTC CCTT
Loop primer LF	TGCTAGTTAAAAATGTCGTATGAT
Loop primer BF	GATTCAAAGGATATTGTTGAT



CHAPTER III

RESULTS AND DISCUSSION

3.1 Synthesis and characterization of acpcPNA oligomers

The fluorescein-labeled acpcPNA oligomers primarily used in this research include **1)** 10mer random sequence PNA as a test sequence for reaction optimization, **2)** PNA21 designed for detection of miRNA21, and **3)** seaPNA designed for detection of staphylococcal enterotoxin A (SEA) gene which was amplified by LAMP technique (see the sequences in **Table 3.1**). Various L-amino acids were attached at the C-termini of the 10mer PNA test sequence to give PNA_{Lys}, PNA_{Lys}₃, PNA_{Lys}₅, and PNA_{Gl}. PNA21 and seaPNA were also modified with 5 lysine residues at the C-termini for the detection of miRNA21 and staphylococcal enterotoxin A (SEA) gene detection respectively. All PNA were obtained as C-terminal carboxamide.

All PNA were synthesized by Fmoc solid-phase peptide synthesis following the previously reported protocol⁴⁸ and were modified at the N-termini with 5(6)-carboxyfluorescein. After cleavage from the resin, the crude PNAs were purified by HPLC and characterized by MALDI-TOF mass spectrometry. All synthesized acpcPNA showed the expected mass and their purities were higher than 90% as confirmed by HPLC (**Figure 1-6A**). The concentrations were determined from absorbance at 260 nm monitored by UV-visible spectrophotometry using molecular extinction coefficient values calculated by an in-house web-based software developed by Prof. Dr. Tirayut Vilaivan at <http://www.chemistry.sc.chula.ac.th/pna>. The characterization data of all acpcPNA probes used in this study are shown in **Table 3.1**.

Table 3.1 Characterization data of fluorescein-labeled acpcPNAs

Name	PNA Sequence	t_R (min)	Yield (%)	Molecular weight (observed)	Molecular weight (calculated)
FAM-PNALys	FAM-GTAGATCACT-K-NH ₂	33.1	37%	3,875.9	3,875.1
FAM-PNALys ₃	FAM-GTAGATCACT-KKK-NH ₂	30.5	32%	4,129.0	4,131.5
FAM-PNALys ₅	FAM-GTAGATCACT-KKKKK-NH ₂	29.4	26%	4,387.8	4,387.8
FAM-PNAGlu	FAM-GTAGATCACT-E-NH ₂	33.2	23%	3,875.5	3,876.0
FAM-PNA21	FAM-AGTCTGATAAGC-KKKKK-NH ₂	30.3	17%	5,085.5	5,086.5
FAM-seaPNA	FAM-GCTTTTTTACA-KKKKK-NH ₂	30.3	29%	4,685.3	4,686.1

3.2 Synthesis and characterization of nanomaterials

3.2.1 Citrate-capped gold nanoparticles (citrate-AuNPs) (12 nm)

The 12 nm citrate-capped gold nanoparticles were synthesized following a literature procedure.^{66, 70} The obtained ruby-red solution of gold nanoparticles was characterized by transmission electron microscopy (TEM). As shown in **Figure 3.1A**, spherical particles were observed and with a mean diameter of 12.4 ± 2.3 nm. The UV-vis spectrum of the synthesized gold nanoparticles is presented in **Figure 3.1B**. It showed the maximum absorbance at 519 nm which is in good agreement with the literature value.⁶⁷

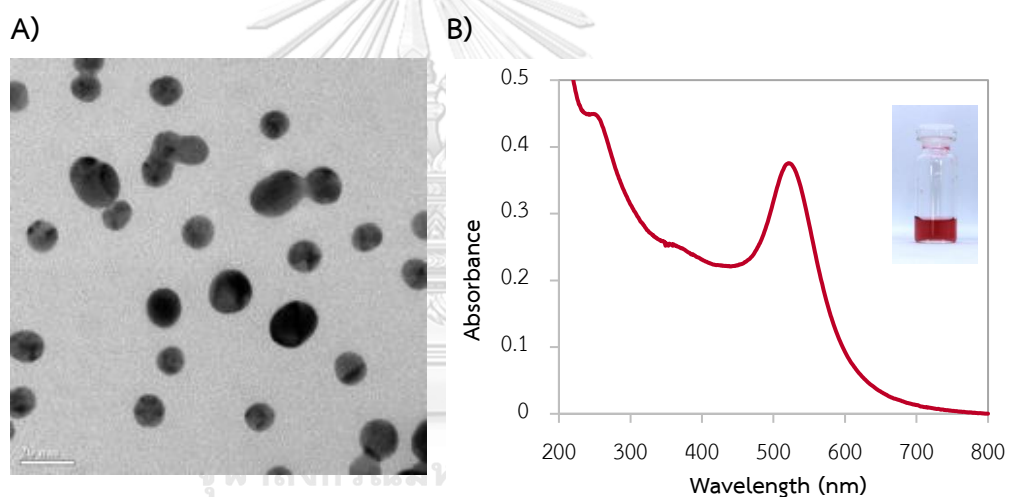


Figure 3.1 TEM-image (scale bar is 20 nm) (A) and UV-vis spectra of 12 nm citrate-coated gold nanoparticle (citrate-AuNPs) (B)

3.2.2 Citrate-capped gold nanoparticles (40 nm)

The 40 nm citrate-capped gold nanoparticles were synthesized following a literature procedure.⁶⁷ After the two-step synthesis using the 12 nm citrate-capped gold nanoparticles as seeds, the morphology and size were characterized by transmission electron microscope (TEM) (**Figure 3.2A**). Spherical particles were obtained with an average of diameter of 49 ± 9 nm. The color of the colloidal solution changed from ruby-red to purplish-red. A bathochromic shift of the absorption maxima in the UV-vis spectra from 519 to 540 nm (**Figure 3.2B**) is in accordance with the literature report.⁷¹

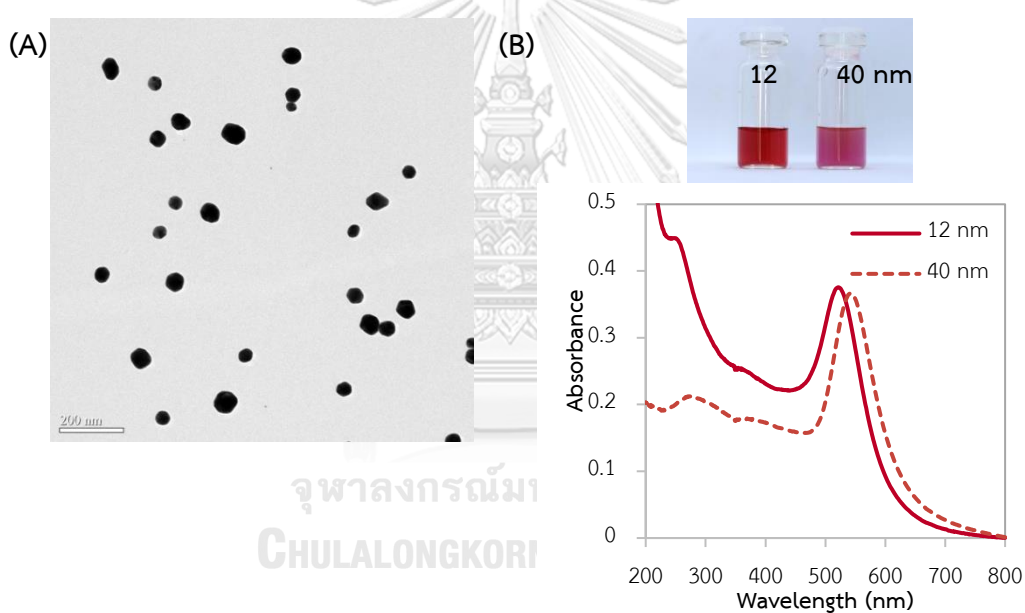


Figure 3.2 TEM image (scale bar 200 nm) (A) and comparison of UV-vis spectra of 12 and 40 nm gold nanoparticles (AuNPs) (B)

3.2.3 Silver nanoparticles (AgNPs)

The silver nanoparticles were synthesized following a literature procedure.⁶⁸ After heating of AgNO_3 and tri-sodium citrate, a yellow solution was obtained, and the particle size and morphology were confirmed by TEM. As shown in **Figure 3.3A**, roughly spherical particles were observed with mean particle size of 15.0 ± 1.8 nm. The UV-vis spectrum of the synthesized silver nanoparticles showed the maximum absorption at 419 nm which allowed with literature.⁶⁸

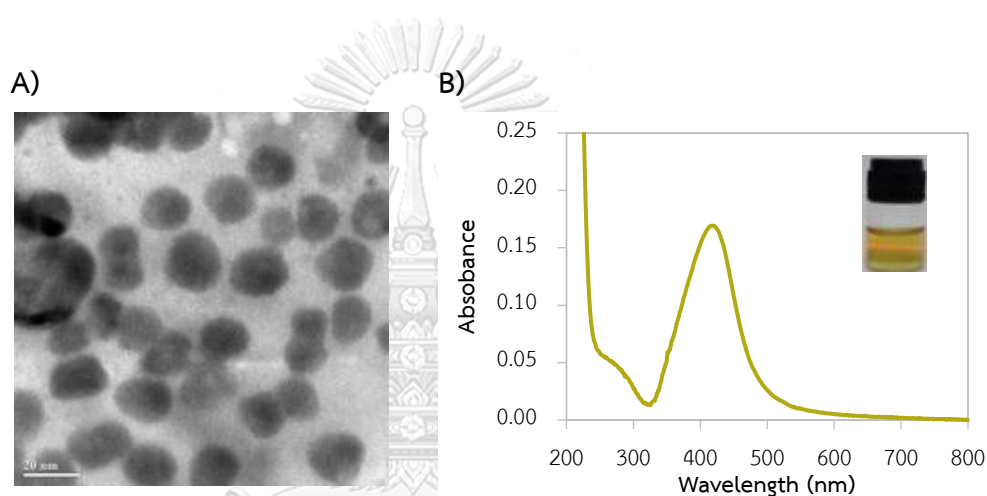


Figure 3.3 TEM-image (scale bar is 20 nm) (A) and UV-vis spectra of citrate-capped silver nanoparticle (citrate-AgNPs) (B)

3.2.4 Reduced graphene oxide (rGO)

The reduced graphene oxide (rGO) were synthesized following a literature procedure.⁶⁹ After hydrazine removal, the black pellets were re-dispersed in water to give a black colloidal solution. The ζ -potential of the rGO showed smaller negative value (-27.8 mV) than that of graphene oxide (-37.9 mV) indicating that the number of oxygen-containing negatively charged functional groups on the surface was decreased.

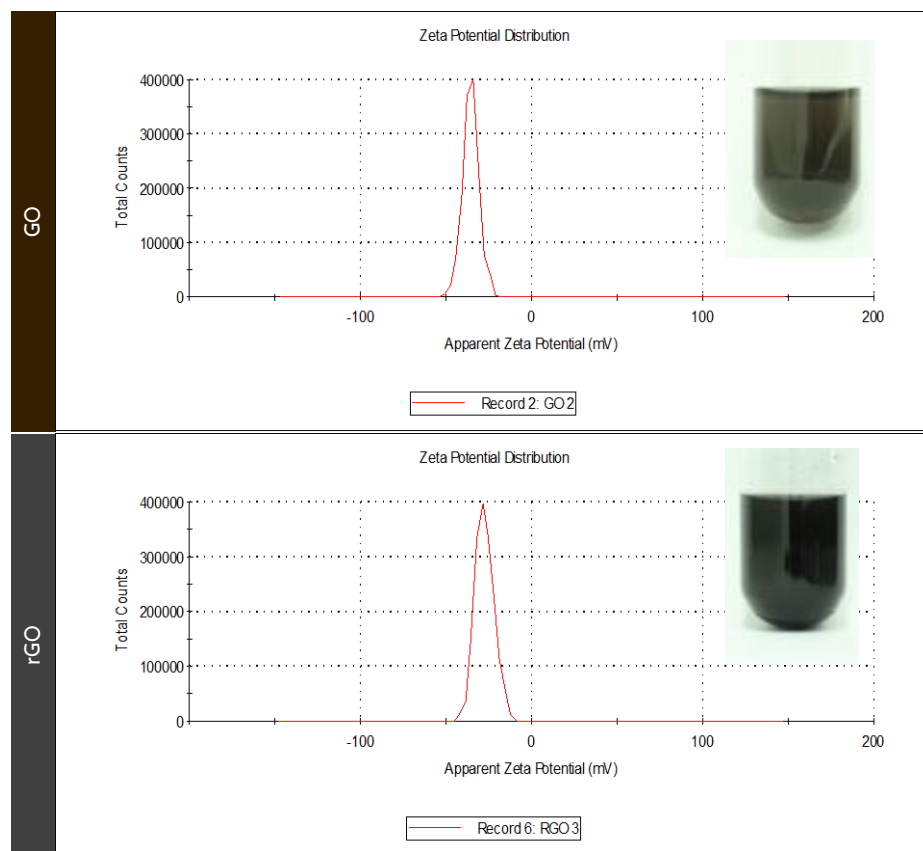


Figure 3.4 ζ -potential of graphene oxide (top) and reduced graphene oxide (bottom)

3.3 Fluorescence quenching efficiency

3.3.1 Type of quencher

Fluorescein-labeled oligonucleotides were widely used for nucleic acid detection by fluorescence assay.^{14, 24, 35} Our plan was to develop a new fluorescence detection of specific nucleic acid targets by combining the labeled acpcPNA probe and a suitable nanomaterial as an external quencher. It has been known for some times that DNA oligonucleotides could be adsorbed on surface of nanomaterials such as nanoscale carbon and metal nanoparticles by physical adsorption through π - π stacking and hydrogen bonding (H-bond) between nucleobase and the surface.^{57, 72, 73} This process is more efficient with single stranded DNA than double stranded DNA since in the former case the nucleobases were more readily accessible than the latter. However, these nanomaterials usually stabilized by

negatively charged surface modification (AuNPs or AgNPs) or surface functional groups (GO), their interactions with negatively-charged backbone of unmodified DNA oligonucleotide may not be optimal. In this work, the electrostatically neutral acpcPNA was employed in place of DNA oligonucleotide as a probe. The acpcPNA will be modified with charged modifiers with the aim to increase the adsorption affinity of the acpcPNA probe to the nanomaterial surface via enhanced electrostatic interaction. The stronger interaction between the PNA probe and the nanomaterial, as well as the high affinity and specificity towards DNA target of the PNA probe, were proposed to improve the performance of the nanomaterials-based nucleic acid detection further.

First, the quenching ability of PNA and DNA oligonucleotide probes by various nanomaterials known to adsorb DNA consisting of graphene oxide (GO),²⁴ reduced graphene oxide (rGO),⁷⁴ gold nanoparticles (AuNPs) and silver nanoparticles (AgNPs)⁷² were investigated. It has been known in the literature that labeled DNA oligonucleotides in single stranded form can readily adsorb onto nanomaterials such as gold nanoparticles and graphene oxide in a non-specific fashion. The contact quenching as well as fluorescence resonance energy transfer (FRET) from the labeled probe to the nanomaterial resulted in quenching of the fluorescence signal, which could be restored upon hybrid formation with the complementary nucleic acid target.^{21, 23, 34, 72, 73}

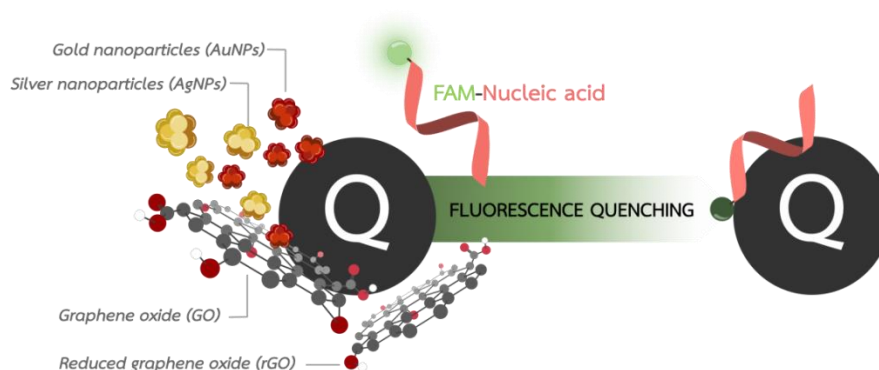


Figure 3.5 Fluorescence quenching of labeled oligonucleotides by nanomaterials

While it is known from the literature that the interaction between DNA oligonucleotides and gold nanoparticles¹² or graphene oxide^{73, 74} are primarily governed by the nucleobase, there are some other contributing factors as well. Since the surface potentials of the nanomaterials are generally charged, electrostatic interaction should play a supportive role to the association of the probe and the nanomaterials.⁷⁴ In this respect, the author proposed that PNA probes which are electrostatically neutral should be adsorbed more effectively to negatively-charged nanomaterials such as graphene oxide or citrate-capped gold nanoparticles than the traditionally used DNA oligonucleotide probes. There were few literature reports on using the classical aegPNA probes in combination with GO for development of DNA assays,⁵⁹ but the active role of the enhanced electrostatic interaction was not clarified. In this study, fluorescein-labeled 10mer acpcPNA probes carrying positively-charged (lysine) or negatively charged (glutamic acid) amino acids in varying number were synthesized and their interactions with various nanomaterials were studied in comparison with a fluorescein-labeled DNA probe bearing the same base sequence.

As shown in **Figure 3.6A**, only small quenching effect was observed with DNA probe with all types of nanomaterials including GO, rGO and 12 nm AuNPs. More efficient quenching was observed in the case of the FAM-PNALys probe carrying a single lysine residue at the C-terminus as shown in **Figure 3.6B**. Graphene oxide appeared to be the most effective quencher, although the maximum quenching efficiency observed was still only around 70% at 1 $\mu\text{g}/\text{mL}$ GO. Nevertheless, this clearly suggests that various nanomaterials can be used as external quencher and also demonstrated the superior performance of acpcPNA probe compared to the traditional DNA oligonucleotide probe.

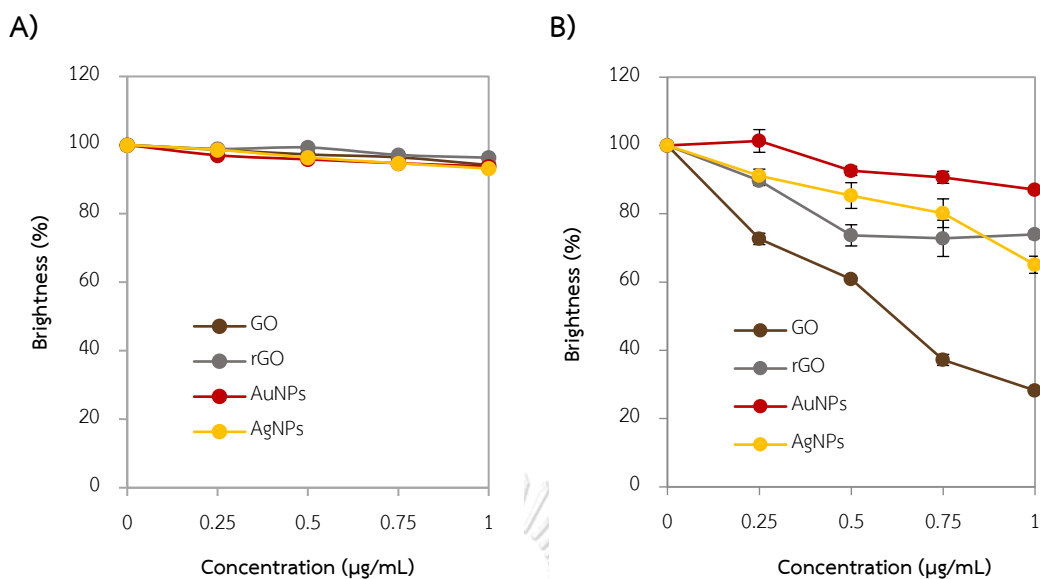


Figure 3.6 Fluorescence quenching of fluorescein-labeled DNA (A) and PNA-Lys (B) using various nanomaterials; graphene oxide (GO), reduced graphene oxide (rGO), gold nanoparticles (AuNPs), and silver nanoparticles (AgNPs). Conditions: 0.1 µM FAM-PNA/DNA in 10 mM Tris-HCl buffer (pH 7.4), fluorescence measurement; λ_{ex} 460 nm, PMT 940 V

3.3.2 Charge effect

To examine the effects of charge modifier on the PNA probe to the quenching efficiency, quenching studies of the labeled PNA probes carrying different number of lysine (Lys1, Lys3 and Lys5) and glutamic acid (Glu) residues which carry net charges of 1+, 3+, 5+ and 1-, respectively. The corresponding 10mer DNA probe would have 9- charge due to the presence of 9 phosphodiester groups.

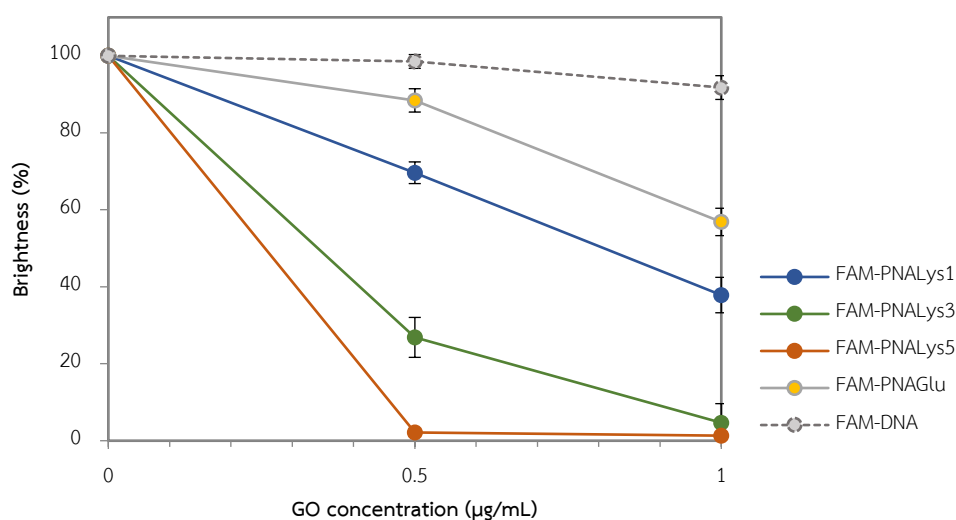


Figure 3.7 Fluorescence quenching of fluorescein-labeled acpcPNA and DNA probe by graphene oxide (GO). Conditions: 0.1 μM FAM-PNA/DNA in 10 mM Tris-HCl buffer (pH 7.4), fluorescence measurement; λ_{ex} 460 nm, PMT 940 V

In the presence of GO as a quencher, the data in **Figure 3.7** clearly show the difference in quenching efficiency among probes with different charges that is entirely consistent with the proposed role of electrostatic effects. When the number of lysine residues attached to the acpcPNA strand was increased from 1 to 5 in PNAlys, PNAlys₃ and PNAlys₅, it was clear that the fluorescence quenching efficiency became progressively more effective. While the quenching of PNAlys was only around 60-70%, the quenching of PNAlys₃ was over 95% and that of PNAlys₅ was almost 100% at 1 $\mu\text{g/mL}$ GO. In the case of PNAlys₅, this level of quenching was already achieved at 0.5 $\mu\text{g/mL}$ GO or even lower. On the other hand, DNA which are polyanionic due to the presence of multiple phosphate groups showed almost no quenching at all, and only around 10% quenching was observed at 1 $\mu\text{g/mL}$ GO. This might appear to be in contrast with the literature that reported a number of fluorescence-based DNA assays employing a combination of labeled oligonucleotide probe and GO.^{19, 23, 75} However, the present study was performed at low salt conditions (10 mM Tris-HCl buffer without added salt) while other studies were

performed at high salt conditions (up to 1000 mM). This will be explained in more details in topic **3.3.3**.

Surprisingly, even the PNA-Glu probe bearing a single negative charge showed appreciable quenching that was only slightly less efficient than the PNAlys probe bearing a single positive charge, as almost 40% quenching was observed at 1 $\mu\text{g/mL}$ GO, suggesting that other non-electrostatic effects such as π - π stacking and hydrogen bonding interaction might also get involved. Nevertheless, the experiments unequivocally demonstrated that PNA probes were more effectively quenched by GO than DNA probe with the same sequence under the same conditions, and that increasing the number of positive charges in the PNA probe could improve the quenching efficiency of the probes by GO. This can be explained by the fact that graphene oxide surface carried net negative charge due to the presence of numerous oxygen-containing functional groups.¹⁸ Consequently, positively-charged species should be more strongly adsorbed on to the GO surface via electrostatic interactions better than negatively-charged species.

Moreover, the kinetics of the quenching of PNAlys and PNAlys₅ was also studied in the presence of 0.5 $\mu\text{g/mL}$ of GO. As shown in **Figure 3.8**, the signal of both PNA probes declined rapidly within 10 minutes before remaining stable over the next 50 min period. Therefore, the quenching process was rapid and long incubation time was not necessary as previously reported in the case of DNA probes.^{24, 28}

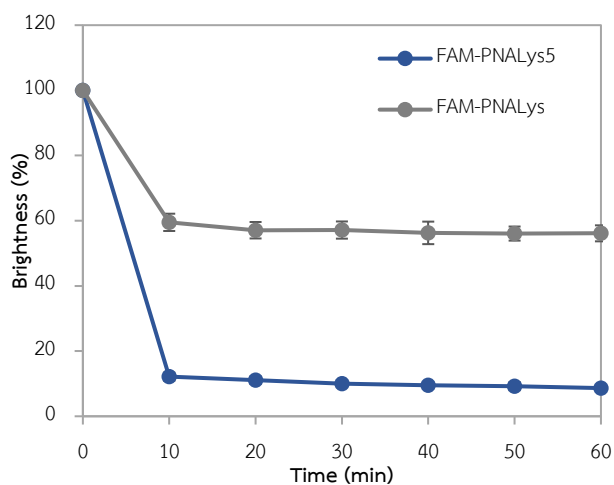


Figure 3.8 Kinetic profiles of fluorescence quenching of positively charged labeled acpcPNA with graphene oxide (GO). Conditions: 0.1 μM FAM-PNA, 0.5 $\mu\text{g}/\text{mL}$ of GO in 10 mM Tris-HCl buffer (pH 7.4), fluorescence measurement; λ_{ex} 460 nm, PMT 940 V

The quenching of the PNALys₅ probe was also explored with other types of nanomaterials. Gratifyingly, similar quenching effect was observed in all types of nanomaterials tested (**Figure 3.9**), suggesting the general applicability of the principle. To study the effect of particle size to the quenching process in the case of gold nanoparticles (AuNPs), the quenching effects by 12 and 40 nm gold nanoparticles (AuNPs) were compared. As shown in **Figure 3.9**, the quenching by 40 nm AuNPs was less efficient at low concentration than 12 nm AuNPs, although at 0.5 $\mu\text{g}/\text{mL}$, the quenching efficiencies were similar. This is because smaller particles may have higher surface area than large particles at the same concentration.

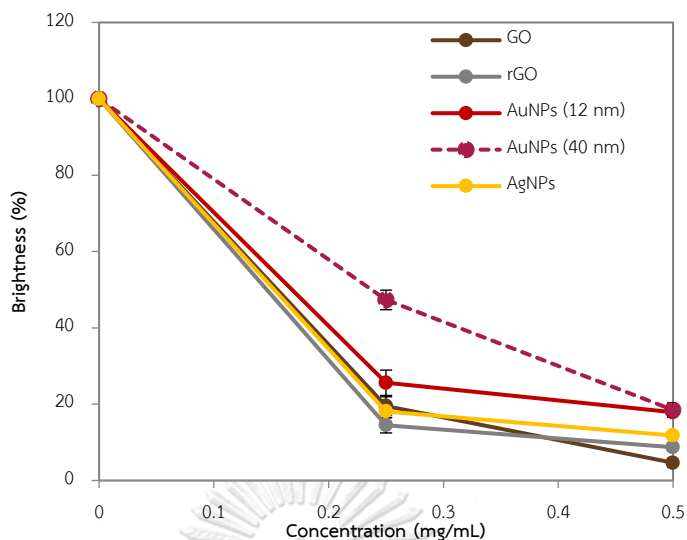


Figure 3.9 Fluorescence quenching of FAM-PNALys₅ using various nanomaterials: graphene oxide (GO), reduced graphene oxide (rGO), gold nanoparticles 12 and 40 nm (AuNPs), and silver nanoparticles (AgNPs). Conditions: 0.1 μ M FAM-PNALys₅ in 10 mM Tris-HCl buffer (pH 7.4), fluorescence measurement; λ_{ex} 460 nm, PMT 940 V

3.3.3 Salt effect

In order to gain further insights into the interactions between the PNA/DNA probes and nanomaterials, the fluorescein-labeled PNALys₅ and DNA were chosen as representative positively- and negatively-charged probes. Graphene oxide was first added to quench the signal from the probes. After that, the ionic strength of the solution was increased by addition of NaCl. In the case of DNA probe, the quenching efficiency was increased from 4% at 0 mM NaCl to around 40% at 1000 mM NaCl. This can be explained by attenuation of the repulsive electrostatic interaction between the negatively charged DNA backbone and the negatively charged GO surface in the presence of salt. This facilitates further interaction of the DNA base and GO by additional interactions such as π - π stacking and hydrogen bonding. As a result, the fluorescence quenching process was more favorable at high ionic strengths. On the other hands, quenching of PNALys₅ decreased from 97% to

90% over the same range of NaCl concentration (0-1000 mM). This can also be explained by the attenuation of the attractive electrostatic interaction between the positively charged PNALys₅ and the negatively charged GO surface. Nevertheless, even at high ionic strengths, the quenching of the PNALys₅ probe by GO was still much more effective than DNA probe.

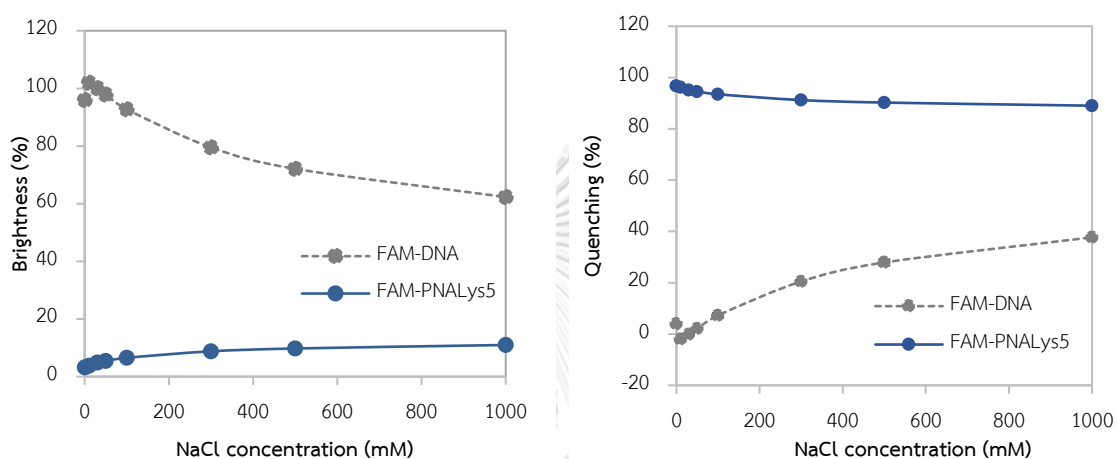


Figure 3.10 Quenching efficiencies of FAM-labeled DNA and PNALys₅ with graphene oxide (GO) at various of NaCl concentrations. Conditions: 0.1 μ M FAM-PNA/DNA, 1.0 μ g/mL of GO in 10 mM Tris-HCl buffer (pH 7.4), fluorescence measurement; λ_{ex} 460 nm, PMT 940 V

3.4 Fluorescence assay for DNA detection

3.4.1 Comparison of PNALys1 and PNALys5 probes

From the excellent quenching efficiency of lysine-labeled acpcPNA by GO, it was applied to use as a fluorogenic probe for determination of DNA sequences. In the case of DNA probes, the complementary DNA target competes with the GO in binding to the probe, resulting in displacement of the probe from the GO surface and therefore resulting in fluorescence increase.²⁰ The same effect was observed in aegPNA probes.⁵⁹ However, in this case it was not clear whether the hybridization between the probe and the DNA target would be sufficiently strong to overcome the enhanced electrostatic interaction between multiple-lysine-modified acpcPNA probes and the GO surface. To investigate the effects of positive charges on the PNA probe to the fluorescence restoration by DNA target, fluorescein-labeled PNALys and PNALys₅ probes (FAM-PNALys/Lys₅) were compared in the presence of GO as an external quencher. The PNA probes were separately incubated with complementary (comDNA) and single-base mismatch DNA (smDNA) to ensure that the probe was completely bound to the target DNA. Then, the GO quencher was added and the fluorescence signal was recorded. The comDNA-PNA duplexes displayed almost the same brightness as in the original PNA probe, i.e. no quenching, after adding GO indicating that the PNA-DNA duplexes were formed, and that the duplexes could not interact with the GO similar to DNA-DNA duplexes. In the case of smDNA, the fluorescence signals decreased. But the signal from the PNALys probe was higher than that of PNALys₅ probe, indicating that the PNALys₅ probe can better discriminate between complementary and single-base mismatched DNA target than the PNALys probe. This might be explained by the lower background signal of the PNALys₅ probe. As a result, PNALys₅ was chosen as the probe for DNA sequence determination in the next experiments.

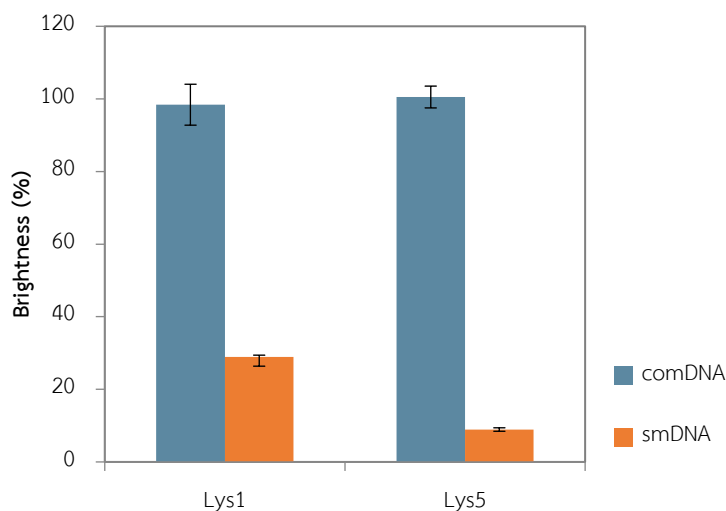


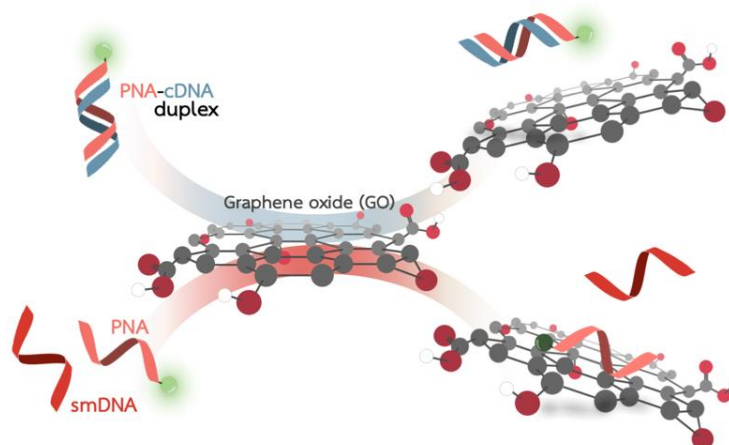
Figure 3.11 Distinguishing fluorescent signal for DNA detection using FAM-labeled PNALys and PNALys₅ probes with graphene oxide (GO). Conditions: 0.1 μM FAM-PNA, 0.12 μM DNA (1.2 equiv), 0.5 $\mu\text{g/mL}$ of GO in 10 mM Tris-HCl buffer (pH 7.4), fluorescence measurement; λ_{ex} 460 nm, PMT 940 V

3.4.2 Comparison of target mixing order

The previous experiment (3.4.1) showed that the preformed PNA-DNA duplexes could not be absorbed by GO, which suggests that it is feasible to develop and assay to distinguish between the free and hybridized PNA probes. However, the feasibility of the displacement of the GO-bound PNA probe by the complementary DNA target is still unknown. In this part, the target mixing order was studied using FAM-labeled PNALys₅ as a probe. The mixing order PNA-DNA-quencher where by the DNA was added to the probe, followed by the GO quencher as shown in **Figure 3.12A** gave the results shown in **Figure 3.13(i)**. ComDNA gave over 100% of brightness while smDNA gave under 5%, which was similar to the free probe in the absence of DNA target. Relative fluorescence (F/F_0) was calculated from the fluorescence intensities after (F) and before (F_0) the addition of DNA. The relative fluorescence of comDNA was 17 times higher than that of smDNA, indicating a good discrimination between complementary and mismatched DNA targets. Next, the

signal restoration was also studied by changing the mixing sequence to PNA-quencher-DNA (Figure 3.12B). From the results in Figure 3.13(ii), single strand PNA probe in the absence of DNA target 8% brightness of the original value. After adding the smDNA, the signal remained the same as in the absence of target, while the comDNA restored the signal to almost 60% of the original value of the free probe. Comparison of relative fluorescence values, comDNA gave 6 times larger F/F_0 than smDNA. Even though the signal restoration was not as complete as in the case of PNA-DNA-quencher addition sequence, this method was still acceptable for signal discrimination and could be useful under circumstances that the PNA-DNA duplexes could not be formed first such as intracellular nucleic acid detection. It can therefore be concluded that both PNA-DNA-quencher and PNA-quencher-DNA addition sequences were applicable with PNAlys₅ probe, although the PNA-DNA-quencher method gave better performance in term of completeness of signal restoration and specificity.

(A)



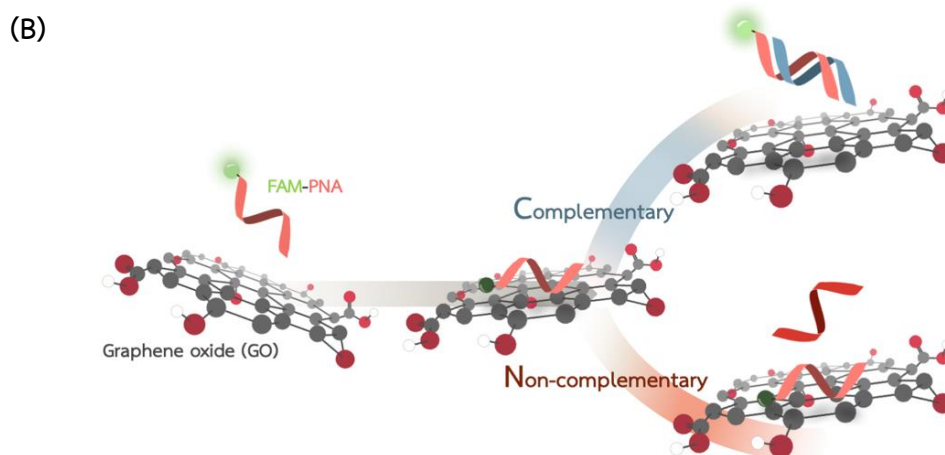


Figure 3.12 Fluorogenic assays for DNA detection with different mixing recognition, PNA+DNA+GO (A), and PNA+GO+DNA (B)

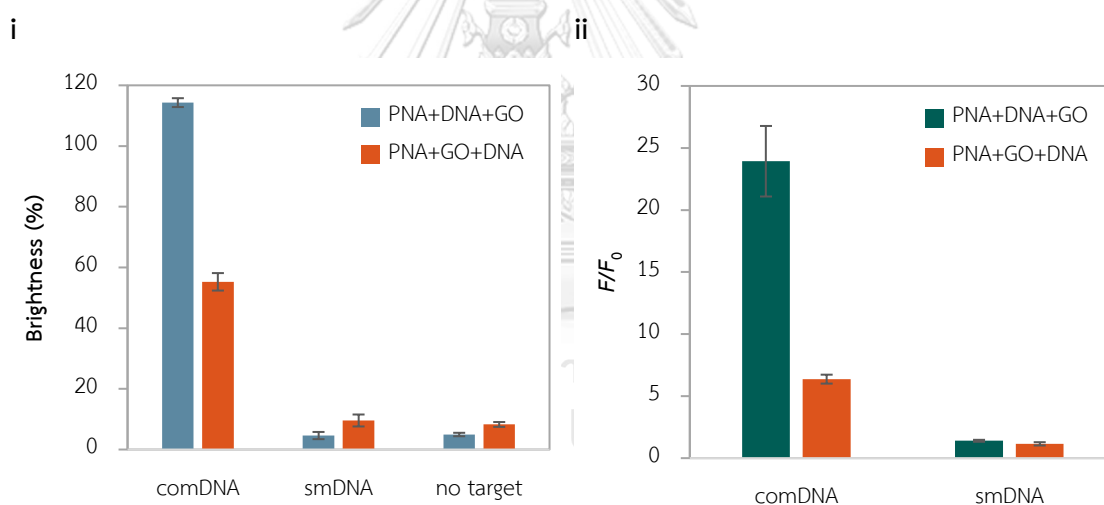


Figure 3.13 Brightness (i) and F/F_0 (ii) obtained from different order of mixing of PNA (FAM-PNALys₅), DNA and quencher (GO). Conditions: 0.1 μ M FAM-PNA, 0.12 μ M DNA (1.2 equiv), 0.5 μ g/mL of GO in 10 mM Tris-HCl buffer (pH 7.4), fluorescence measurement; λ_{ex} 460 nm, PMT 940 V

3.4.3 Kinetics of the signal restoration of PNA probes

In this part, synthetic DNA target was introduced into the GO-quenched FAM-PNALys/PNALys₅ probes, and the fluorescence was observed as function of time. To begin with, the FAM-PNALys probe after quenching with 0.5 µg/mL graphene oxide (GO) gave a signal at 52% of the original probe. This was restored to 90% after adding complementary target (comDNA) within 10 minutes and then the signal remained stable over the next several ten minutes. In contrast, the single-base mismatched DNA target (smDNA) did not change the signal of the quenched probe over the same period of time. However, the background fluorescence was still rather high. When the amount of the GO quencher was increased to 1.0 µg/mL GO, the PNALys probe was quenched to 30% of the original probe. The signal increased gradually within 10 minutes when comDNA was added, and no change was observed with smDNA. However, when the concentration of GO was increased, the signal in the case of comDNA was restored less efficiently, and only 60% value of the original probe was obtained. For the relative fluorescence (F/F_0), comDNA showed 1.6-fold and 2-fold larger than smDNA at GO concentrations of 0.5 and 1.0 µg/mL, respectively. The kinetics studies hereby suggest that the signal restoration reached its maximum within 10 minutes and good discrimination between complementary and mismatched DNA targets could be achieved, although the efficiency was better at high quencher concentration.

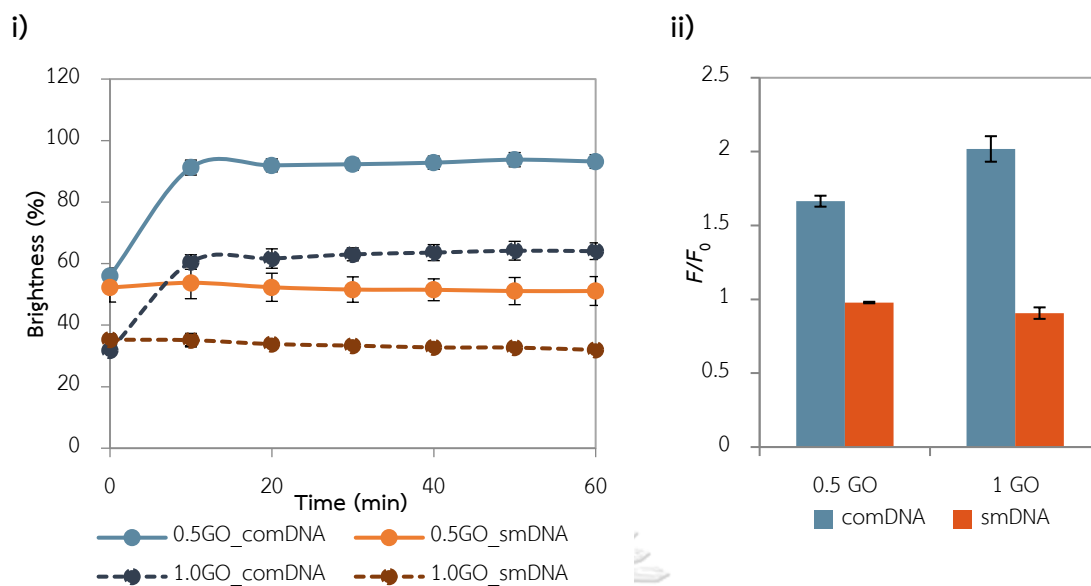


Figure 3.14 Kinetic profiles of fluorescence recovery (i) and relative fluorescence signal (F/F_0) (ii) using FAM-PNALys with graphene oxide (GO). Conditions: 0.1 μM FAM-PNALys, 0.12 μM DNA (1.2 equiv) in 10 mM Tris-HCl buffer (pH 7.4), fluorescence measurement; λ_{ex} 460 nm, PMT 940 V

When FAM-labeled PNALys₅ was used as a probe as shown in **Figure 3.15**, the background was much lower (10% of the original signal of the probe) even at 0.5 $\mu\text{g/mL}$ of graphene oxide (GO). When the DNA was added, the brightness was restored to 55% of the original signal of the probe over a period of 1 h. Even after 1 h, the signal was still gradually increased, indicating the slow kinetics of the displacement of the probe from the GO surface. Again, no signal change was observed over the same period in the case of smDNA. Thus, DNA sequence discrimination could be noticed clearly using just 0.5 $\mu\text{g/mL}$ of graphene oxide (GO) for PNALys₅ probe. This leads to the conclusion that the increased number of positive charges negatively affect the kinetics of the probe displacement by the target and fluorescence restoration. This is not unexpected considering the increased strength of the electrostatic interaction between the probe and the GO surface.

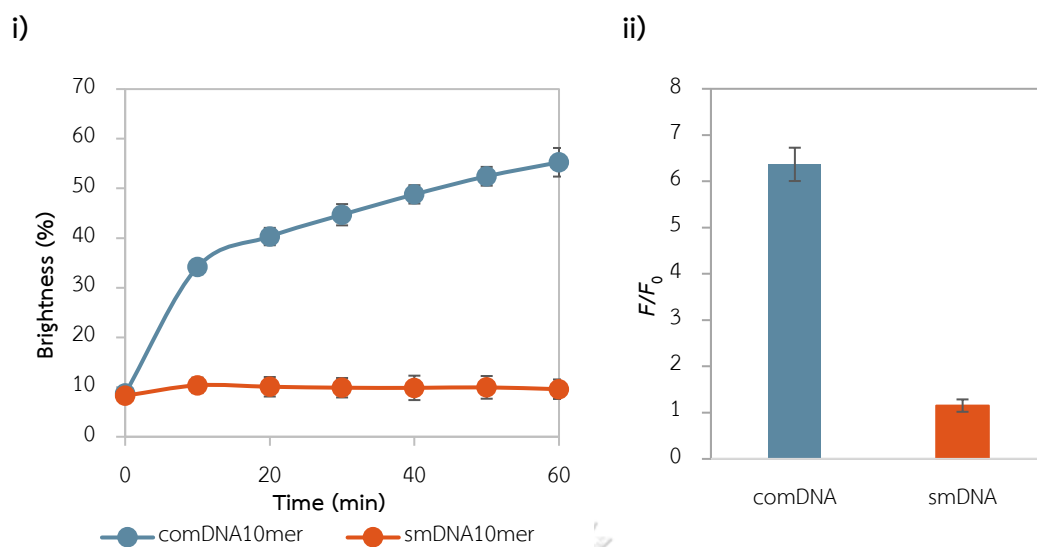
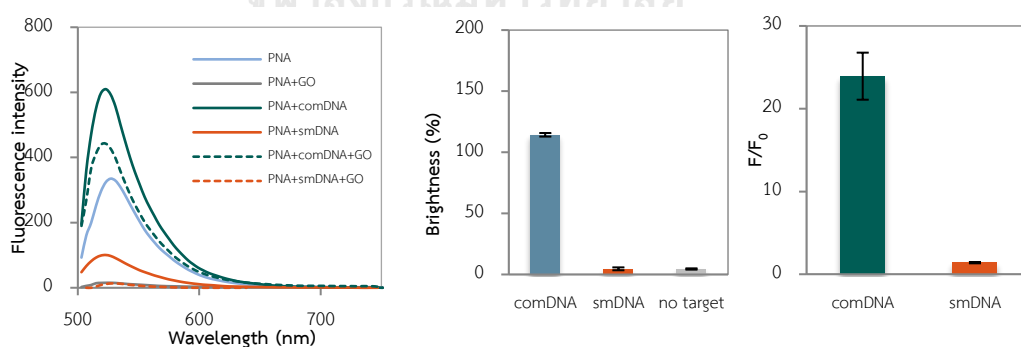


Figure 3.15 Kinetic profiles of fluorescence recovery (i) and relative fluorescence signal (F/F_0) (ii) using FAM-PNALys₅ with graphene oxide (GO). Conditions: 0.1 μ M FAM-PNALys₅, 0.12 μ M DNA (1.2 equiv), 0.5 μ g/mL of GO in 10 mM Tris-HCl buffer (pH 7.4), fluorescence measurement; λ_{ex} 460 nm, PMT 940 V

3.4.4 Application to various quenchers

A) GO



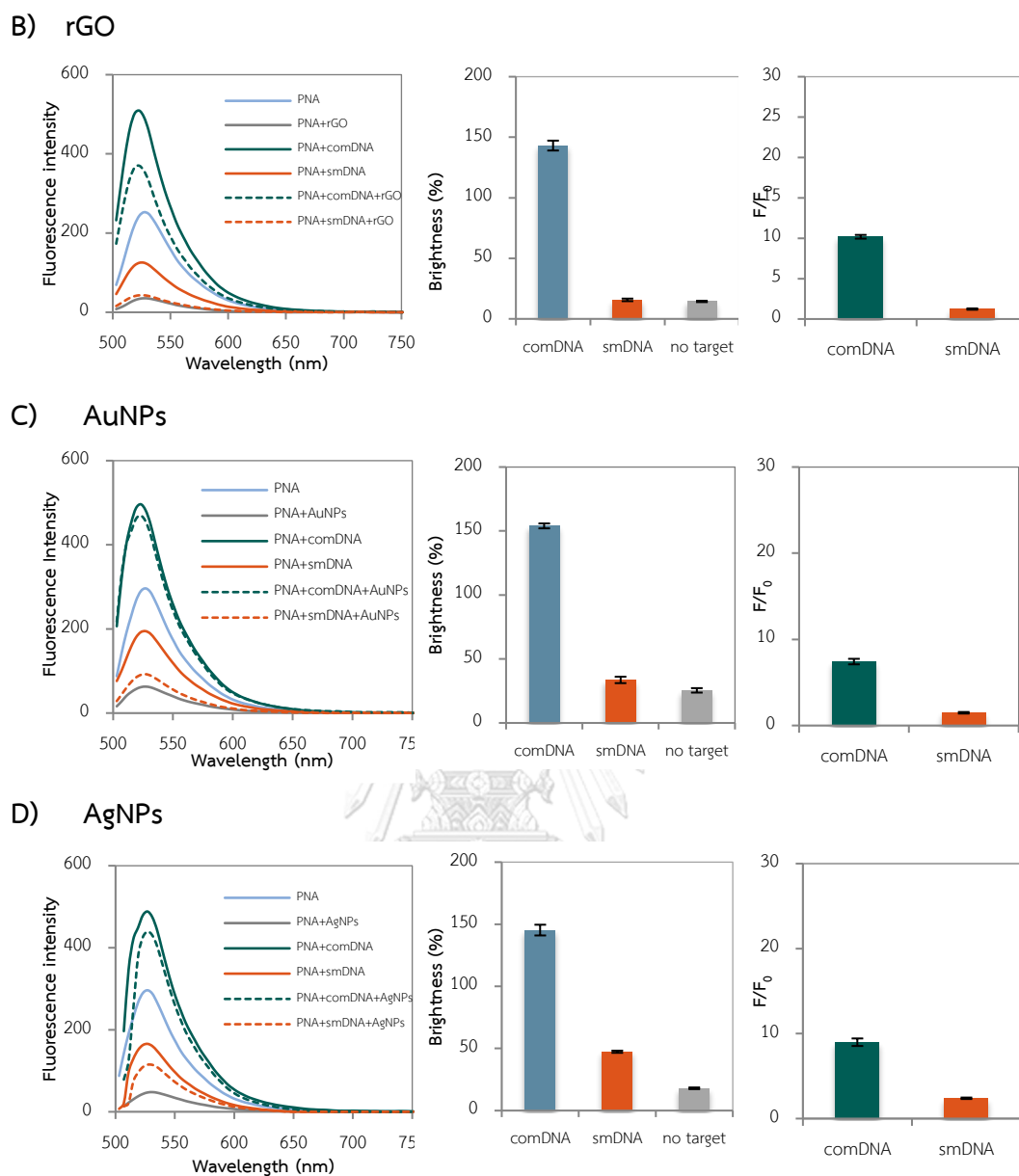


Figure 3.16 Fluorescence discrimination for DNA sequence detection using FAM-PNALys₅ using various nanomaterials as quencher: graphene oxide (A), reduced graphene oxide (B), gold nanoparticles (C), and silver nanoparticles (D) Conditions: 0.1 μM FAM-PNA, 0.12 μM DNA (1.2 equiv), 0.5 $\mu\text{g/mL}$ of nanomaterial in 10 mM Tris-HCl buffer (pH 7.4), fluorescence measurement; λ_{ex} 460 nm, PMT 940 V

From previous encouraging results, the PNA-DNA-quencher addition sequence was also applied with PNALys₅ probe and other nanomaterial quenchers including reduced graphene oxide (rGO), citrate-capped gold nanoparticles (AuNPs) and silver nanoparticles (AgNPs). In all cases, the signal restoration was considerably larger with comDNA than smDNA. The signal restoration from smDNA target was generally similar to without DNA target, with the exception of AgNPs, whereby the signal of smDNA was more than twice of the absence of DNA. In term of signal restoration and specificity, GO appeared to be the best quencher to be used in combination with PNALys₅ probe followed by rGO and AuNPs.

3.4.5 Sensitivity

The fluorescence response of quenched PNALys and PNALys₅ probes at various concentrations of comDNA was examined using 0.5 µg/mL of graphene oxide (GO) or gold nanoparticles (AuNPs) as the quencher. A linear correlation between the fluorescence signal and the DNA target concentration over a range of 5-25 nM and the limit of detection (LOD) was calculated from $3\sigma/S$, where σ was obtained from fluorescence signal of PNA+quencher (baseline) and S was obtained from the slope of the linear calibration curve. Comparison of sensitivity between FAM-PNALys and PNALys₅ probe using GO as quencher was shown in **Figure 3.17** revealed sub-nanomolar detection limits for DNA target. The LOD of FAM-PNALys₅ probe was 0.12 ± 0.03 nM which were six times lower than that of FAM-PNALys (0.7 ± 0.02 nM). According to literature reports, DNA-GO and aegPNA-GO platforms exhibited LOD around 1 nM²⁴ and 10 nM,⁵⁹ respectively. Therefore, acpcPNA presented higher sensitivity as shown by the lower limit of DNA detection over traditional DNA and aegPNA probes by 10- and 100-fold, respectively.

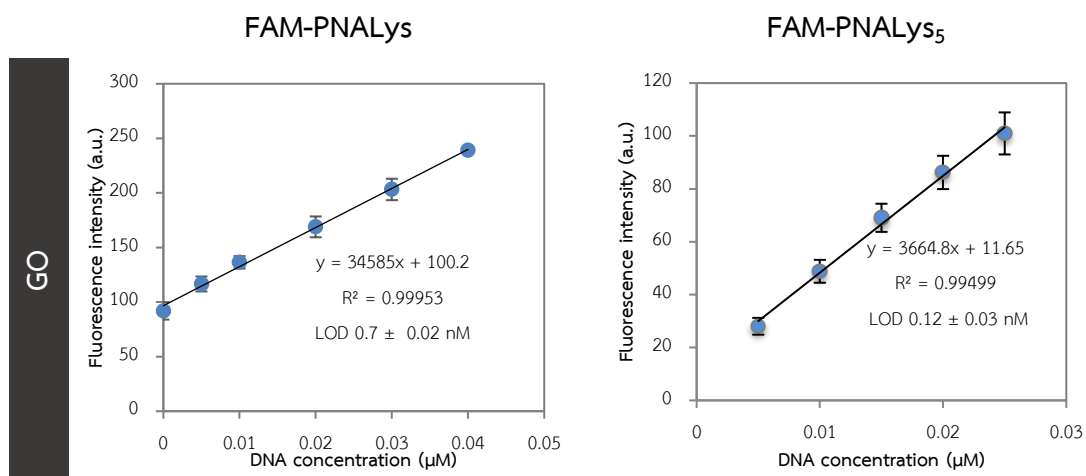


Figure 3.17 Calibration curves for DNA detection by FAM-PNALys and FAM-PNALys₅ using graphene oxide (GO) (PNA+GO+DNA). Conditions: 0.1 μM FAM-PNA, 0.5 μg/mL of GO in 10 mM Tris-HCl buffer (pH 7.4), fluorescence measurement; λ_{ex} 460 nm, PMT 940 V

Not only the graphene oxide, but gold nanoparticles (12 and 40 nm) were taken into comparison. The limits of detections were summarized in **Figure 3.18**. AuNPs with small particle size (12 nm) showed LOD of 0.20 ± 0.02 nM which was 3-time lower than the larger particle (40 nm) and almost close to GO. Thus, FAM-PNALys₅ probe can be used with various nanomaterials quenchers for DNA sequence detection.

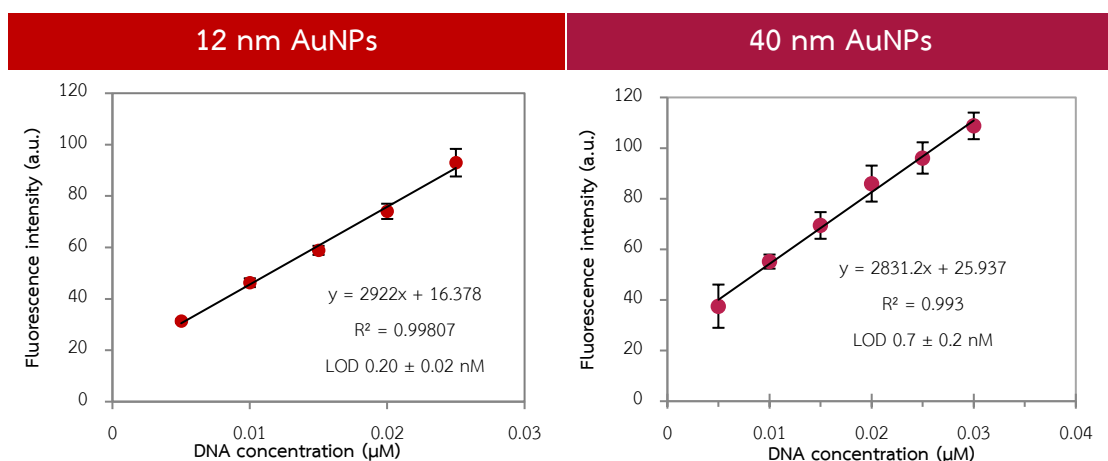


Figure 3.18 Calibration curves of DNA detection by FAM-PNALys₅ using citrate-capped gold nanoparticles (12 and 40 nm AuNPs) (PNA+AuNPs+DNA). Conditions: 0.1 μM FAM-PNALys₅, 0.5 μg/mL of AuNPs in 10 mM Tris-HCl buffer (pH 7.4), fluorescence measurement; λ_{ex} 460 nm, PMT 940 V

3.4.6 Application for the detection of real DNA samples

To challenge the developed DNA sequence detection method, it was applied for the detection of real DNA samples obtained from LAMP (loop-mediated isothermal amplification) which was a simple DNA amplification method that can be performed at a fixed temperature and therefore does not require a thermal cycler. Due to the fact that natural DNAs are in double-strand forms with very long chain, it is the most important to include DNA denaturation step prior to the PNA binding. In our preliminary data employing the probe FAM-seaPNA and GO, the mixing step also played an important role for the performance of the detection. First, the PNA+quencher+DNA mixing order was adopted and no difference in signals could be observed between complementary and non-complementary DNA targets. This is because there was competition between quenched PNA-DNA, free PNA-DNA and DNA-DNA binding rate over the period of incubation time. However, when the mixing order was changed to PNA+DNA+quencher (**Figure 3.19**), the fluorescence signals in SEA-producing *S. aureus* positive and negative samples (no DNA or *E. coli* DNA) could

be readily distinguished as shown by the larger fluorescence in the case of positive samples. The largest discrimination was observed at 0.5 $\mu\text{g/mL}$ GO. Smaller but still appreciable fluorescence differences were also observed with 12 nm AuNPs as quencher as shown in **Figure 3.20**.

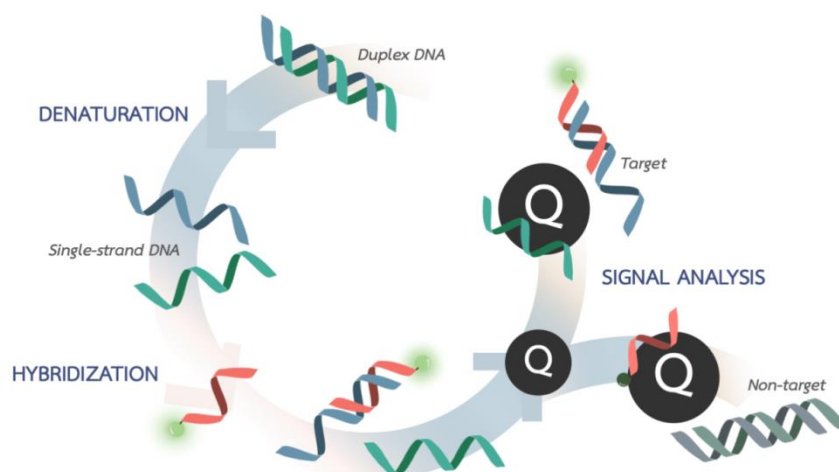


Figure 3.19 Detection process for DNA real sample

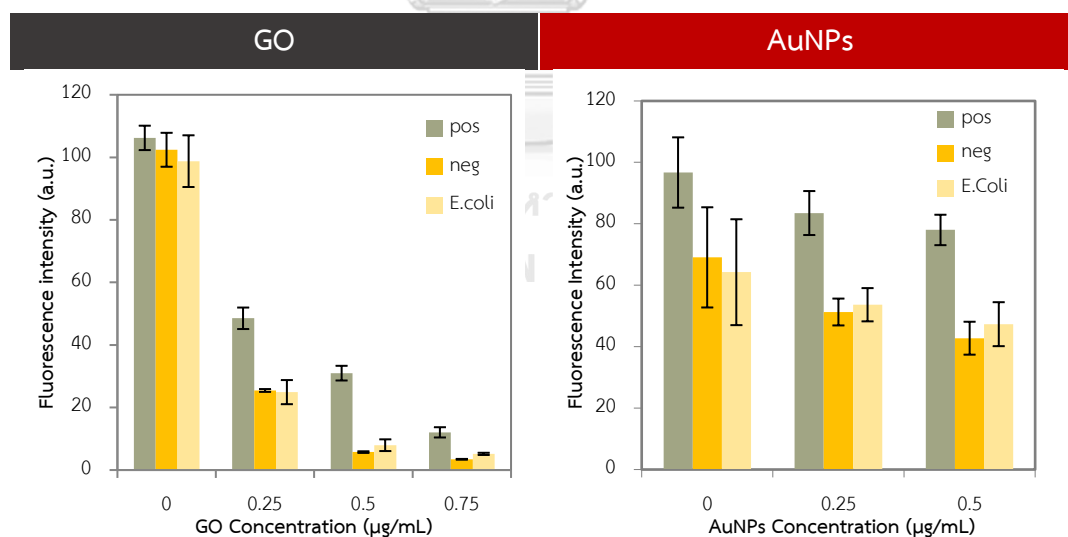


Figure 3.20 Fluorescence assay of LAMP-amplified DNA from real samples using graphene oxide (GO) (A) and 12 nm gold nanoparticles (AuNPs) (B). Conditions: 0.1 μM FAM-seaPNA in 10 mM Tris-HCl buffer (pH 7.4), fluorescence measurement; λ_{ex} 460 nm, PMT 940 V

3.4.7 Effect of non-specific DNA from (poly-adenine)

In this part, the effect of non-specific displacement of the adsorbed PNA and DNA probes were compared. The poly-adenine DNA homopolymer (poly-dA) was used as a model competitor DNA since there are literature reports that at the individual nucleobase level, purines are adsorbed on carbon-based nanomaterials more tightly than pyrimidines.^{25, 26} The rate of signal recovery between pre-adsorbed DNA probe and target was also very slow and slower than non-specific displacement induced by poly-A DNA.²⁴ Thus, in this study, the resistance to non-specific displacement from GO surface by DNA (dA₁₂) was compared between tradition DNA and acpcPNA probes. The results clearly show that the undesirable nonspecific displacement could occur only in the case of DNA probe. In other words, PNA probes are more resistant to non-specific displacement by non-target DNA and should therefore be less prone to give false positive results than DNA probes.

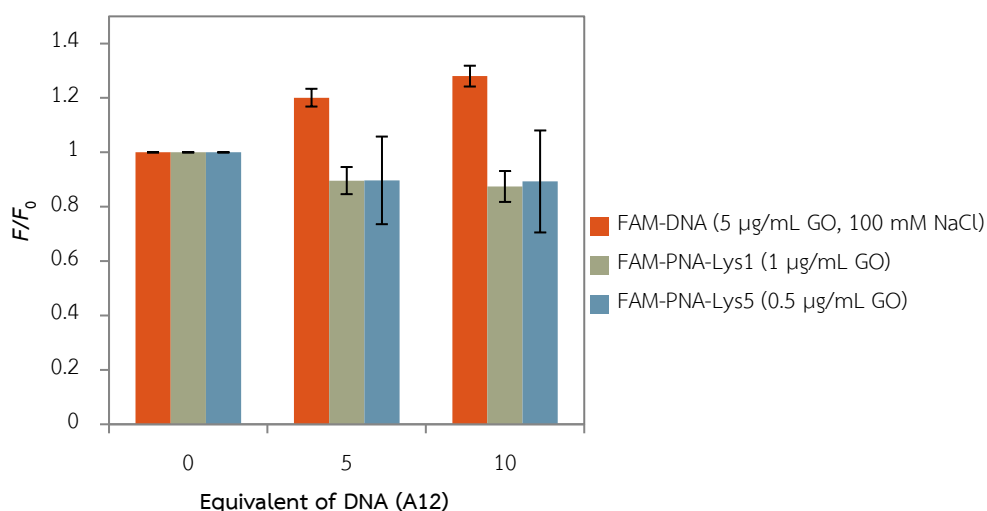


Figure 3.21 Non-specific fluorescence increase of nucleic acid probe in presence of poly-dA as a non-specific competitor. Conditions: 0.1 µM FAM-PNALys₅ in 10 mM Tris-HCl buffer (pH 7.4), fluorescence measurement; λ_{ex} 460 nm, PMT 940 V

3.4.8 Comparison with aegPNA probe

There are some literature reports on the use of fluorescein labeled-aegPNA probe in combination with GO as external quencher for fluorescence turn-on nucleic acid sensing.⁵⁸⁻⁶⁰ The detection method offered simple, selective and sensitive biosensor due to low background signal. The DNA detection using of non-immobilized PNA-GO platform was recently developed by Zhang and co-workers.⁵⁹ They demonstrated that PNA could interact on GO-sheet much more strongly than DNA at the same amount of GO (1.0 $\mu\text{g}/\text{mL}$ in 25 mM HEPES buffer (pH 7.4), 100 mM NaCl) because of its net neutral charge backbone. However, they reported that although the quenching was found to be rather fast, the restoration was slow and required almost 40 min at elevated temperature (45 °C) even in the presence of large excess of DNA targets. For positively-charged modified acpcPNA probe employed in this work, low background signal was obtained at lower concentration of GO (0.5 $\mu\text{g}/\text{mL}$) in the absence of salt, and the restoration rate was faster than aegPNA. It can even take place at ambient temperature and near stoichiometric amounts of DNA target. In term of specificity, single-base mismatch DNA could be readily distinguished by both aegPNA and acpcPNA probes, but the signal difference between complementary and mismatched targets is larger for acpcPNA probes.⁵⁹ In addition, the limit of DNA detection was reported as 10 nM while the use of FAM-PNALys₅ probe developed here exhibited 100 times lower LOD. Thus, the positively charged modified acpcPNA in this work is more efficient as a probe for highly sensitive and selective DNA sensor under simple experimental conditions (salt and heat is not required).

3.5 Fluorescence assay for detection of MicroRNA21

3.5.1 Kinetics

In addition to the detection of DNA targets, microRNA21 (miRNA21) which is a short (22 bases) RNA that and regularly expressed in cancer cells⁷⁶ was selected as another target. The optimal condition based on graphene oxide (GO) and gold nanoparticles (citrate-AuNPs) was utilized as quencher representatively. Consistent with previous experiments, at the same concentration of quenchers, graphene oxide (GO) could quench FAM-PNA21 more efficiently than gold nanoparticles (12 nm AuNPs) as shown at the starting point in the **Figure 3.22**. After addition of miRNA21, the brightness from both systems was increased before becoming steady during a 30 minutes period. Signal generated due to the addition of miRNA21 when using graphene oxide (GO) quencher increased moderately, while the use of gold nanoparticles (12 nm AuNPs) resulted in smaller increase from starting point. This is because numerous FAM-PNALys₅ could be adsorbed on graphene oxide (GO) surface higher than gold nanoparticles (AuNPs) and lead to lower brightness. When miRNA21 was introduced, miRNA21 could perfectly bind with adsorbed PNA on graphene oxide surface. Subsequently, kinetic of fluorescence recovery in presence of AuNPs was faster than GO. In case of ncRNA, the signal was same at starting point in present of graphene oxide (GO). Interestingly, the brightness percentage was slightly decreased after ncRNA addition in the case of AuNPs. No satisfactory explanation can be provided based on presently available data. Nevertheless, it can be concluded that the combination of acpcPNA probe and either GO or AuNPs is also suitable for the detection of RNA targets offering rapid response time and high specificity.

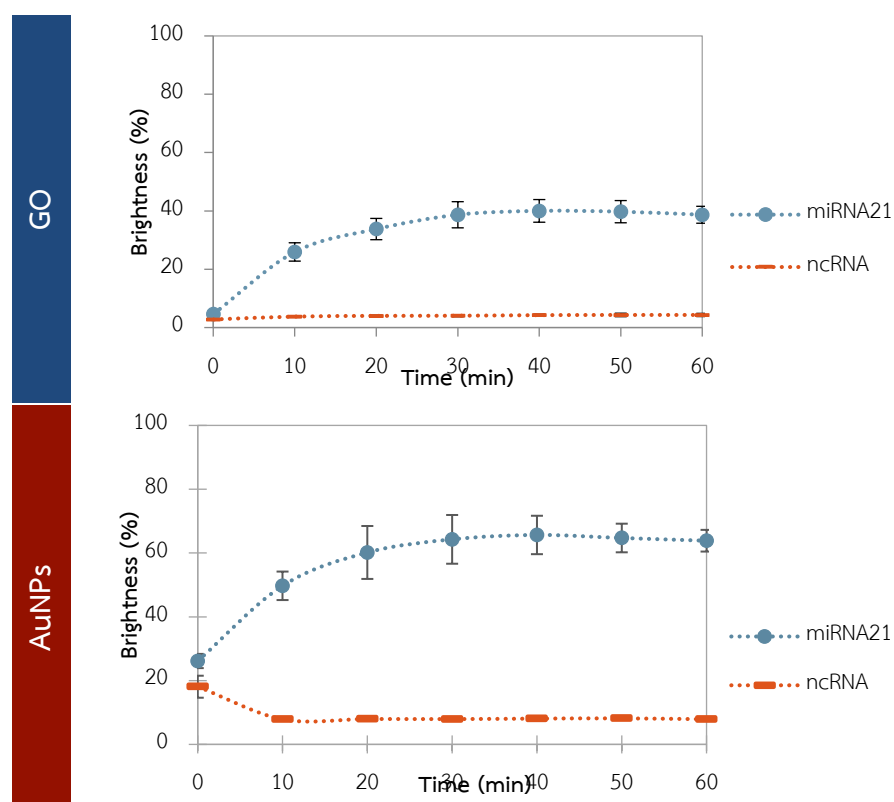


Figure 3.22 Kinetic profiles of fluorescence recovery for miRNA21 detection (PNA+quencher+miRNA21). Conditions: 0.1 μM FAM-PNA21, 1.2 equiv miRNA21, 0.5 $\mu\text{g/mL}$ of quencher in 10 mM Tris-HCl buffer (pH 7.4), fluorescence measurement; λ_{ex} 460 nm, PMT 940 V

3.5.2 Variation of detection matrices

3.5.2.1 Effect of protein matrix (BSA)

Bovine serum albumin (BSA) has been reported to improve the efficiency of a similar PNA-GO-based DNA sensor. In this experiment, only comDNA was collated and the fluorescence was restored faster and more completely in the presence BSA. Therefore, the presence of BSA was the one factor which could promote fluorescence recovery in the RNA detection experiment. Especially in AuNPs system, presence of 0.01% BSA supported restoration of fluorescence signal as shown in **Figure 3.23**.

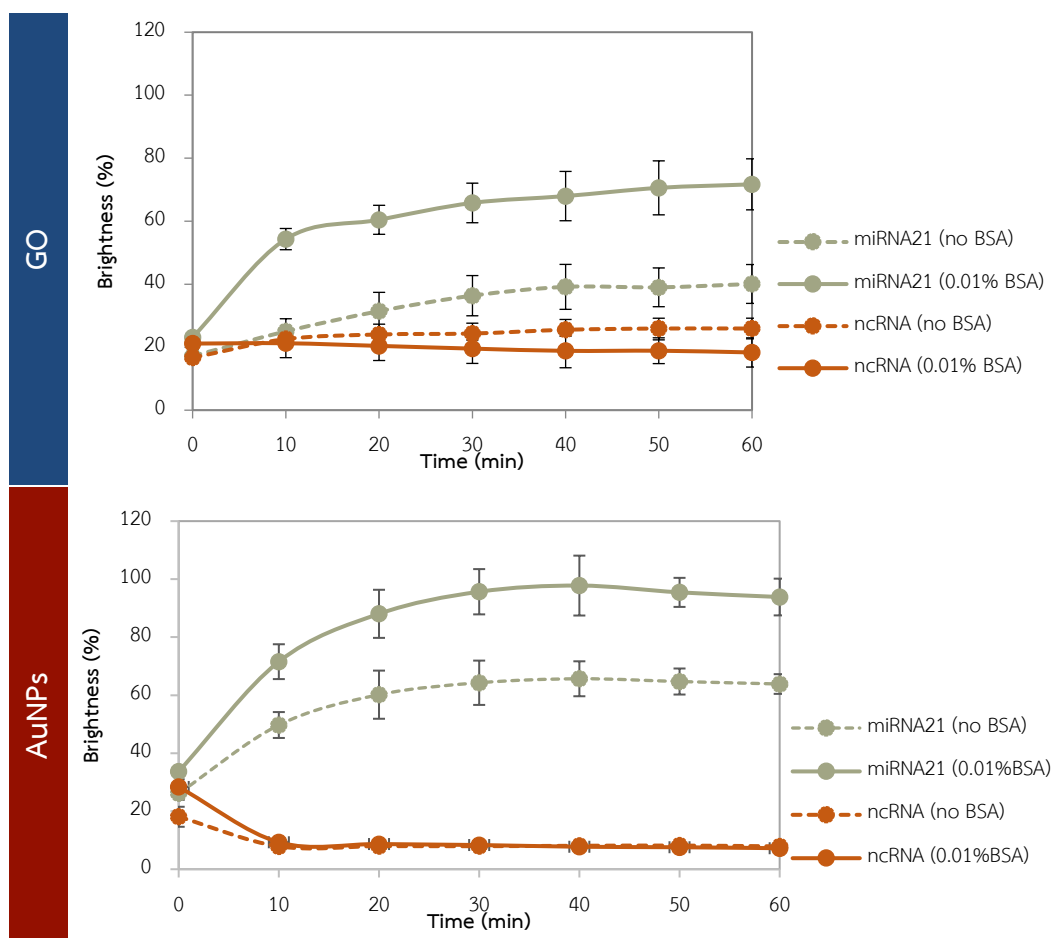


Figure 3.23 Kinetic profiles of fluorescence recovery for miRNA21 detection in 0.01% BSA solution. Conditions: 0.1 μ M FAM-PNA21, 1.2 equiv miRNA21 in 10 mM Tris-HCl buffer (pH 7.4), fluorescence measurement; λ_{ex} 460 nm, PMT 940 V

3.5.2.2 Effect of salt

Salt concentration is another factor which should be considered due to the potential effects on the electrostatic interaction between the probe and the quencher. As shown in data from graphene oxide (GO) quencher (**Figure 3.24a**), not only the signal from miRNA21 target but also from ncRNA increased significantly at higher salt concentrations. At 100 mM NaCl, the signal was almost similar to miRNA21. Smaller fluorescence increase in the presence of ncRNA was observed in

the case of gold nanoparticles (AuNPs) system. It is therefore important to control the salt concentration to maximize the difference between complementary and non-complementary RNA targets.

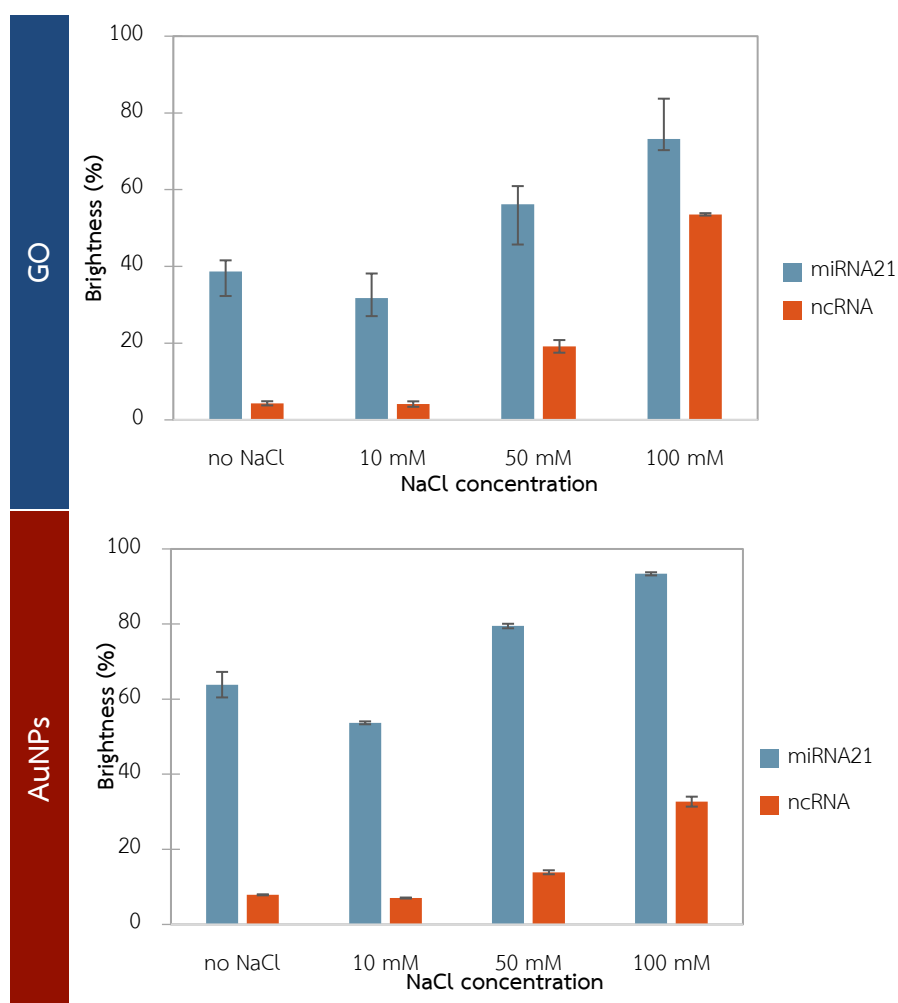


Figure 3.24 Fluorescence recovery for miRNA21 detection in various NaCl solutions. Conditions: 0.1 μ M FAM-PNA21, 1.2 equiv miRNA21 in 10 mM Tris-HCl buffer (pH 7.4), fluorescence measurement; λ_{ex} 460 nm, PMT 940 V

3.5.3 Limit of RNA detection

The sensitivity of RNA detection was also studied using miRNA21 as target and 0.5 $\mu\text{g/mL}$ of graphene oxide (GO) and gold nanoparticles (AuNPs) as external quencher. The linear curves were presented in **Figure 3.25**. The detection limit (LOD) was calculated from $3\sigma/S$, where σ was obtained from fluorescence signal of PNA-quencher and S was obtained from the slope of the curve. The two types of quencher exhibited similar LODs for miRNA21 detection at 0.8 nM. Compared with DNA, the acpcPNA-nanomaterial sensor developed in this work was more sensitive to DNA than RNA due to the preference for binding of acpcPNA to DNA over RNA. However, the LOD of the RNA detection was still in the sub-nanomolar range.

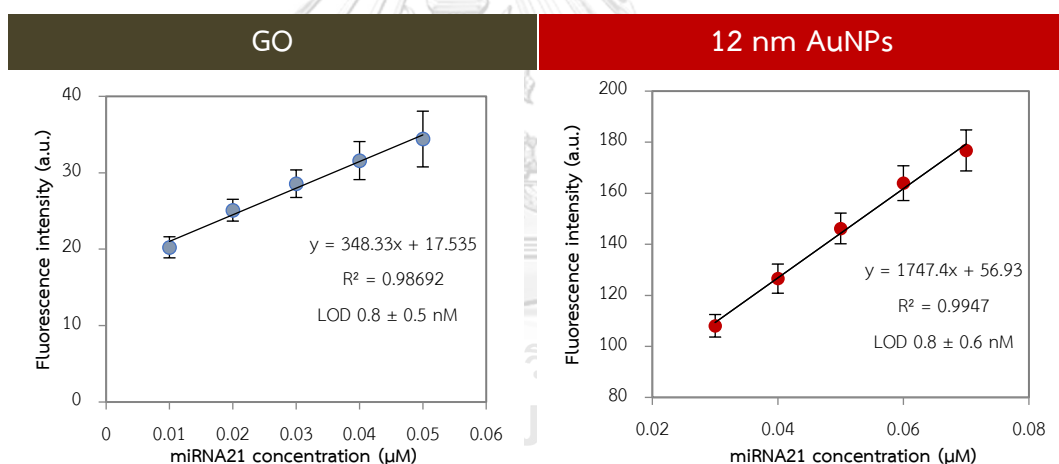


Figure 3.25 Calibration curves of miRNA21 detection by FAM-PNA21 using GO and AuNPs as quencher (PNA+quencher+DNA). Conditions: 0.1 μM FAM-PNA21, 0.5 $\mu\text{g/mL}$ of quencher in 10 mM Tris-HCl buffer (pH 7.4), fluorescence measurement; λ_{ex} 460 nm, PMT 940 V

3.5.4 Comparison to other probe/nanomaterial platforms

i) DNA sensing on graphene oxide

In this work, acpcPNA-graphene oxide combination was employed as turn-on fluorescence DNA and RNA sensor. The presence of multiple lysine-attachment on the acpcPNA probe increases the number of positive charges, which improves the adsorption of the fluorescein-label probe by the nanomaterials. The advantages of this PNA-based probes were low background signal and high responsiveness to DNA/RNA targets under low salt conditions at room temperature. A comparison with similar works is shown in **Table 3.2** in terms of specificity, sensitivity and limitation. Graphene oxide based biosensor for *in vitro* detection using fluorescein-label DNA probe by Liu²⁴ and aegPNA by Guo⁵⁹ were chosen as comparators. PNAs exhibited higher specificity than traditional DNA probe due to binding affinity and charge properties on their backbone, while single-base mismatched discrimination was not easily distinguished by DNA probes. For sensitivity, this work presented higher sensitivity for DNA detection than both aegPNA and DNA probes (**Table 3.2**). Other nucleic acid probes were limited by high background signal, resulting in poor sensitivity. In addition, the present work required no salt and heat for detection. The present acpcPNA probe method may be improved for more advanced applications such as *in vivo* detection of nucleic acids.

Table 3.2 Comparison with other nucleic acid probes in term of specificity, sensitivity and limitation

	Fluorescein-label probe		
	DNA probe ²⁴	aegPNA probe ⁵⁹	acpcPNA probe (<i>this work</i>)
Specificity	Non-complementary discrimination	Single-base mismatches discrimination	Single-base mismatches discrimination
Sensitivity	1 nM	10 nM	0.1 nM
Limitation	<ul style="list-style-type: none"> i) Multiple steps required (DNA adsorption, DNA-GO removing and washing, DNA desorption) ii) Long-time experimental process (overnight for incubation time) iii) High salt environment (100 mM NaCl, 2 mM MgCl₂) iv) Non-specific displacement by non-target DNA 	<ul style="list-style-type: none"> i) Excess DNA target and heating required (45 °C) ii) Slow restoration time (>30 min) iii) High salt environment (100 mM NaCl) 	<ul style="list-style-type: none"> i) Non-specific displacement by long-chain of non-target DNA

ii) DNA sensing on gold nanoparticles

In addition to graphene oxide (GO), gold nanoparticles (AuNPs) is another popular nanomaterial quencher frequently adopted for biosensor works. In general, DNA-functionalized AuNPs have been utilized for DNA/RNA detection such as the Nanoflare system.⁷⁷ While some PNA-AuNPs platforms for colorimetric detection are known,^{63, 64, 78} the corresponding platforms for fluorescence detection has still limited. In this research, immobilization of the PNA probe on the gold surface is avoided. For DNA detection, Ma and co-workers⁷⁹ reported that FAM-DNA was used as a probe to detect single- and double-strand DNA. In this method, fluorescently-labelled was quenched by unmodified-gold nanoparticles and the signal could be restored selectively for target DNA, which single-base mismatch and random DNA sequence were compared. In term of sensitivity, around 0.3 nM of detection limit was reported which close to the value obtained from this study. However, their method was performed in 10 mM of NaCl and required 7.5 mM of spermine as additive. AcpcPNA could be used without additives required, thus, the lysine modified acpcPNA probes in this work presented a novel platform which required no immobilization and offered simple, sensitive and selective detection.

3.6 Colorimetric assay for nucleic acid detection employing gold nanoparticles

Due to the surface plasmon resonance (SPR) phenomenon, the absorbance of metal nanoparticles may vary according to their shape and size. This effect could be employed for visual detection of biomolecules⁸⁰ such as nucleic acids.⁸¹ Interactions between nucleobase and gold nanoparticles was demonstrated from literature works.^{73, 82} In general, the particles surface is shielded due to the DNA adsorption and the aggregation was prevented under high salt concentration environment. On the other hand, the electrostatically neutral PNA should promote aggregation of gold nanoparticles upon adsorption on gold nanoparticles surface. In this study, the detection principle was designed by using L-lysine-modified acpcPNA which could be adsorbed on gold surface. It was proposed that positive charges on the modified-PNA could promote adsorption and particle aggregation as shown in **Figure 3.26**.

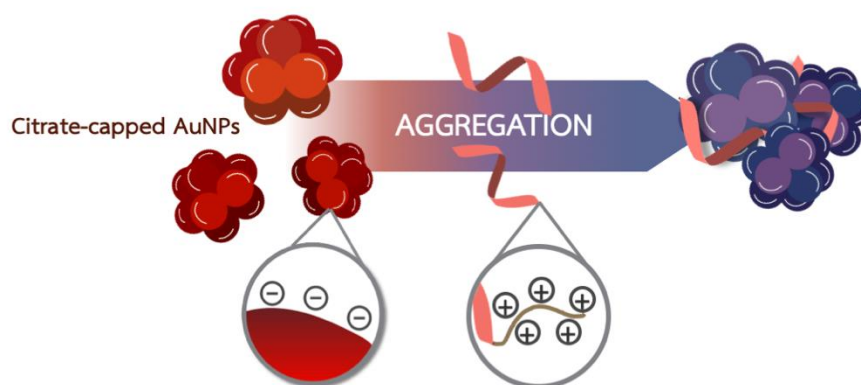


Figure 3.26 Induced-aggregation of citrate-coated gold nanoparticles by positively charged modified acpcPNA

The main objective of this part of the research focused on the development of a DNA sensing platform based on visual detection using acpcPNA probes. The detection principle could be explained in **Figure 3.27**. Free acpcPNA could be adsorbed onto the surface of gold nanoparticles leading to color change from red to purple due to aggregation while PNA-DNA duplex could not. Therefore, the two forms of acpcPNA, i.e. single-strand and PNA-DNA duplex forms, could be

distinguished by color change of gold nanoparticles. Although the principle was already demonstrated sometimes ago with aegPNA,⁶² it was proposed that the performance of the PNA-based colorimetric sensing platform could be improved with the use of acpcPNA modified with multiple positively-charged lysine residues.

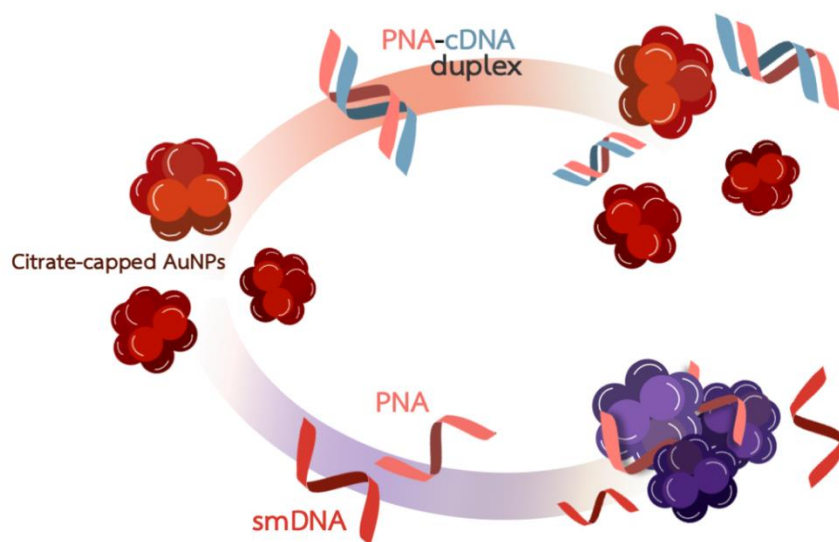


Figure 3.27 Colorimetry of DNA detection using citrate-coated gold nanoparticles

3.6.1 Buffer variation

Since aggregation of gold nanoparticles is known to be accelerated in the presence of salts,^{41, 62} it is important to find the right buffer that does not prematurely induce aggregation. In a preliminary experiment, the ability of two commonly used buffers for nucleic acid studies to induce aggregation of citrate-coated gold nanoparticles (citrate-AuNPs) was studied. At 10 mM concentration of buffer, the gold nanoparticles solution remained red in phosphate buffer (pH 7.0) indicating the absence of aggregation. However, the solution turned blue in Tris-HCl buffer (pH 7.4) at the same buffer concentration. Therefore, phosphate buffer (pH 7.0) was chosen as the buffer for the next experiments.

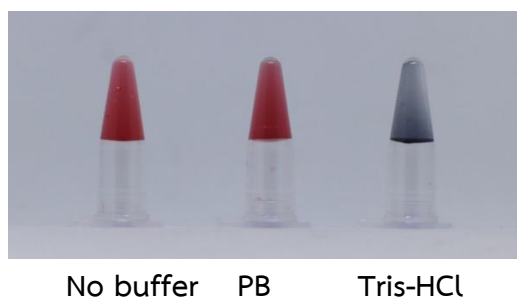


Figure 3.28 Aggregation of citrate gold nanoparticles in various buffer systems
 Conditions: 200 $\mu\text{g}/\text{mL}$ of citrate-gold nanoparticles (AuNPs (12 nm)) in 10 mM of phosphate buffer (pH 7.0)

3.6.2 Effect of charge on the acpcPNA probe

Next, the ability of charge-modified acpcPNA to induce aggregation of the gold nanoparticles was studied. The effect of different type (L-lysine and L-glutamic acid) and number of amino acids used as charge modifier on the acpcPNA was studied. As shown in **Figure 3.29**, the red color of gold nanoparticles changed to purple when FAM-PNALys was added. The same phenomenon was not observed in the presence of various concentrations of FAM-PNAGlu. This suggested that the positive charge of L-lysine was important in inducing aggregation by promoting adsorption of the acpcPNA on the negatively-charged surface of the citrate-AuNPs (**Figure 3.26**). On the other hand, negative charge repulsion between L-glutamic acid and gold surface prevented the adsorption and hence no particle aggregation. This explanation was confirmed by the stronger effect of acpcPNA bearing multiple positive charges (FAM-PNALys₅), whereby the color change from red to dark-blue was clearly visible at lower PNA concentration than FAM-PNALys. Complete precipitation was observed when FAM-PNALys₅ was sufficiently high (1 μM).

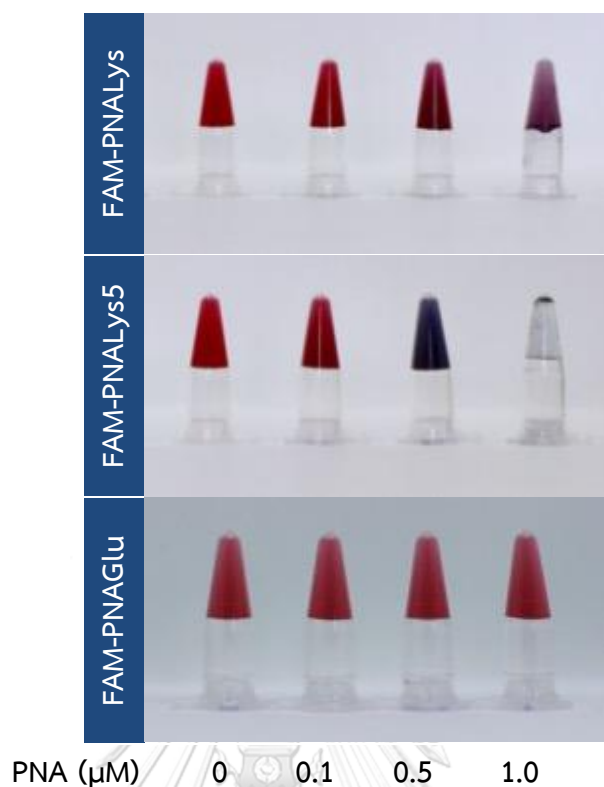


Figure 3.29 Aggregation of citrate gold nanoparticles in various concentrations of labeled-acpcPNAs. Conditions: 200 μg/mL of citrate-gold nanoparticles (AuNPs (12 nm)) in 10 mM of phosphate buffer (pH 7.0)

Next, the effects of other additives such as salt were studied. In subsequent experiments, the range of salt concentration was optimized. In these experiments, the concentration of the gold nanoparticles was reduced from 200 to 50 μg/mL whereby the color change could still be clearly observed. This is to avoid the problem of aggregation at too high concentration of gold nanoparticles even in the presence of only small amount of salt. The concentration of FAM-PNALys₅ was therefore re-optimized, and it revealed that distinct color change was observed at 0.5 μM of FAM-PNALys₅ or higher as shown in **Figure 3.30**.

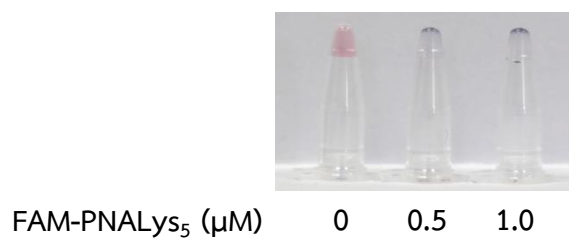


Figure 3.30 Optimization of FAM-PNALys₅ concentration in gold nanoparticles. Conditions: 50 mg/mL of citrate-gold nanoparticles (AuNPs (12 nm)) in 10 mM of phosphate buffer (pH 7.0)

In addition, the effect of salt concentration was investigated by addition of NaCl to the gold nanoparticles solution in the absence of the PNA probe. According to **Figure 3.31**, no aggregation was observed as shown by the red color until at least 50 mM NaCl was added, and complete precipitation was observed at 100 mM. Therefore 50 mM NaCl was chosen for the next experiments.



Figure 3.31 Optimization of NaCl concentration that does not precipitate 50 μg/mL of gold nanoparticles (AuNPs (12 nm))

3.6.3 Colorimetric detection of nucleic acids

i) Short DNA oligonucleotide target

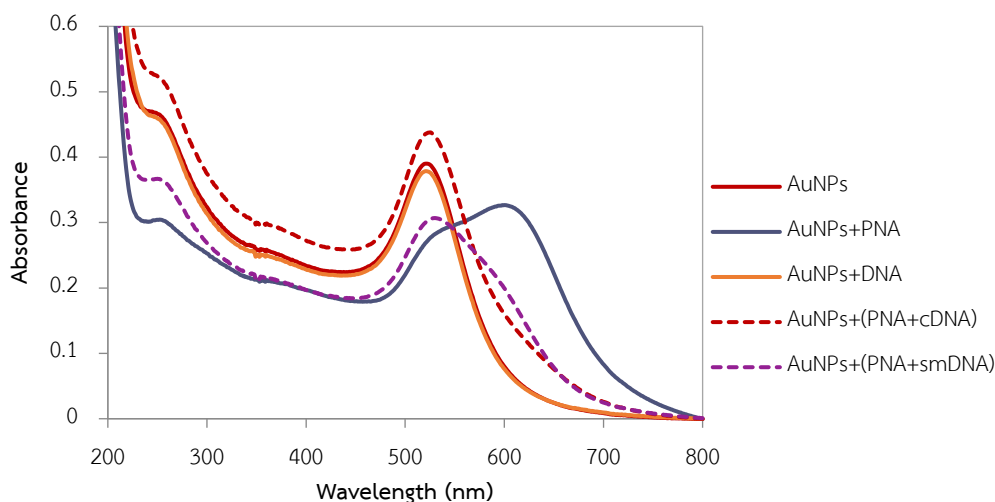


Figure 3.32 UV-visible spectra of colorimetric DNA detection using PNALys₅ and gold nanoparticles (AuNPs (12 nm)). Conditions: 0.1 μ M of FAM-PNALys₅, 0.12 μ M (1.2 equiv) DNA, 50 μ g/mL of citrate-gold nanoparticles (AuNPs) in 10 mM of phosphate buffer (pH 7.0)

Firstly, the proof-of-principle experiment was carried out by mixing gold nanoparticles, DNA and PNA probes together and the color change was monitored by UV-visible spectrophotometry. As shown in **Figure 3.32**, the results were in good agreement with the naked eyes experiments whereby aggregation was induced by single-stranded acpcPNA probe FAM-PNALys₅ (ssPNA) as shown by a bathochromic shift of the absorption maxima of the UV-vis spectrum. No such shift was observed in the presence of PNA probe together with a single-stranded DNA target with a sequence complementary to the PNA probe. This suggests that the complementary DNA and PNA strands interact to form a hybrid with net negative charge that could not effectively induce aggregation of the gold nanoparticles as the case of single stranded PNA probe. Besides, the single-base mismatch DNA oligonucleotide (smDNA) also promoted distinct color change, although not as strong as in the absence of DNA. This is because some non-specific binding of

the PNA probe and the mismatched DNA target may occur, and this reduced the availability of the unbound PNA probe that cause partial aggregation without salt. No aggregation was observed in the absence of PNA probe in all cases.

The color change was subsequently confirmed by naked eyes detection experiments. Single-stranded acpcPNA probe induced the color change from red to purple, while single-base mismatch DNA (smDNA) caused some visible color change but much less distinctive than the single stranded PNA probe. The experiments were therefore repeated in the presence of 50 mM NaCl to further promote aggregation of the gold nanoparticles. To our delight, a clear color change from red to purple with some precipitation was observed with both ssPNA and ssPNA+smDNA without any effects on the ssPNA+cDNA as shown in **Figure 3.33**. The observed results confirmed that NaCl could be used as accelerator for gold nanoparticles aggregation induced by positively charged PNA probe. Importantly, the addition of NaCl substantially improved discrimination between complementary and single-base mismatched DNA oligonucleotide targets.

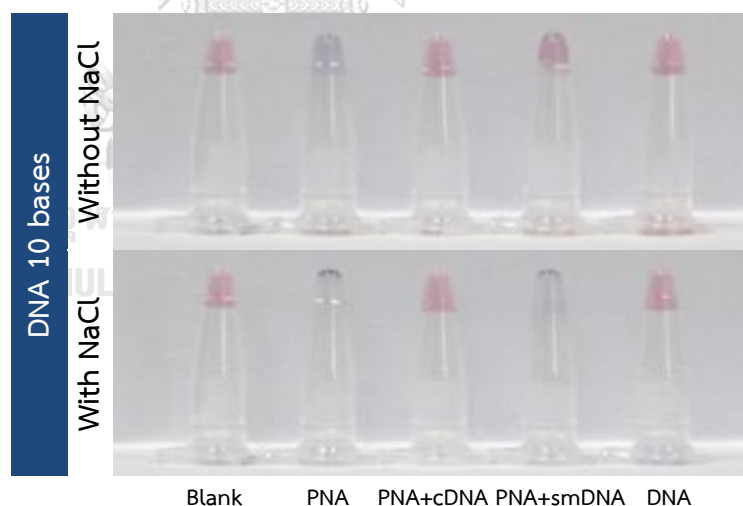


Figure 3.33 Comparison of colorimetric detection of short-chain-DNA using FAM-PNALys₅ with and without addition of NaCl. Conditions: 0.1 μM of FAM-PNALys₅, 0.12 μM (1.2 equiv) DNA, 50 $\mu\text{g}/\text{mL}$ of citrate-gold nanoparticles (AuNPs (12 nm)), 50 mM NaCl in 10 mM of phosphate buffer (pH 7.0)

In previous experiments, 12 nm citrate-capped gold nanoparticles were used as a model study. To investigate the effect of the size of the gold nanoparticles, another set of experiments was performed with 40 nm citrate-capped gold nanoparticles for comparison. From UV-visible spectra, the free 40 nm citrate-capped gold nanoparticles showed a surface plasmon band at 540 nm, which is more red-shifted than the 20 nm in accordance with theory.⁷¹ Reduction of the magnitude of this original plasmon band was observed together with broadening and appearance of a new red-shifted band at 760 nm in the presence of single-stranded PNA probe and PNA-smDNA mixture in absence of NaCl. For naked-eye detection, the expected color change pattern was observed, i.e. light-red in the presence of complementary and purple to blue with single-base mismatched DNA target. It should be noted that the color change in the case of 40 nm gold nanoparticles was more distinctive than 12 nm without the need for NaCl addition.

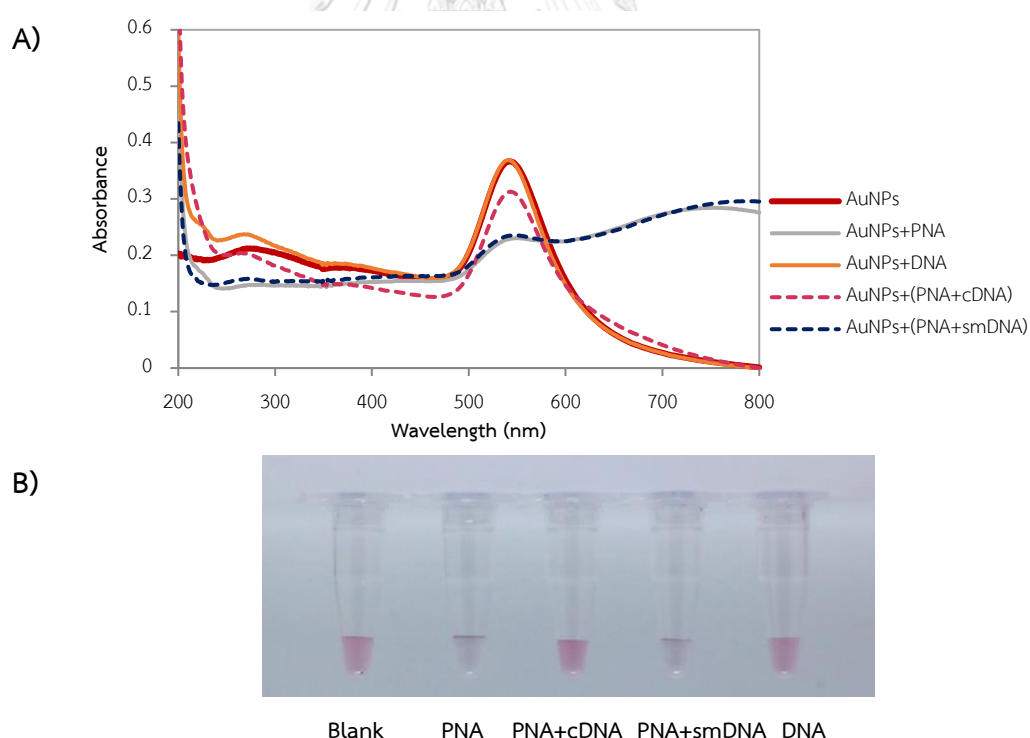


Figure 3.34 UV-visible spectrum (A) and naked-eyes colorimetric detection (B) of short-chain-DNA using FAM-PNALys₅ with gold nanoparticles (40 nm). Conditions: 0.1 μ M of FAM-PNALys₅, 0.12 μ M (1.2 equiv) DNA, 50 μ g/mL of citrate-gold nanoparticles (AuNPs (40 nm)) in 10 mM of phosphate buffer (pH 7.0)

ii) Long-chain DNA target

The experiments carried out so far used short oligonucleotides that possessed exactly the same length as the PNA probe as the target. In real DNA samples, the target DNA to be detected is expected to be much longer than the probe. To further evaluate the performance of the gold nanoparticles-PNA probe platform for colorimetric detection of DNA targets that are longer than the PNA probe, the naked eye detection experiments were carried out on 30nt DNA oligonucleotide targets using the same 10mer acpcPNA probe. When the regular procedure employing 12 nm gold nanoparticles without addition of NaCl was used, the color change was observed in the case of ssPNA only. No color change was observed in the case of PNA+smDNA mixture, indicating the inability to distinguish mismatched target with long sequence probably due to increased affinity between PNA and the long DNA target. Nevertheless, the aggregation was clearly observed for both of ssPNA and PNA-ncDNA if NaCl was added. This experiment confirmed that the developed platform is applicable to both short and long DNA targets and also confirmed the beneficial effect of adding NaCl in promoting the color change in the case of mismatched DNA target, therefore improving the specificity of the detection.

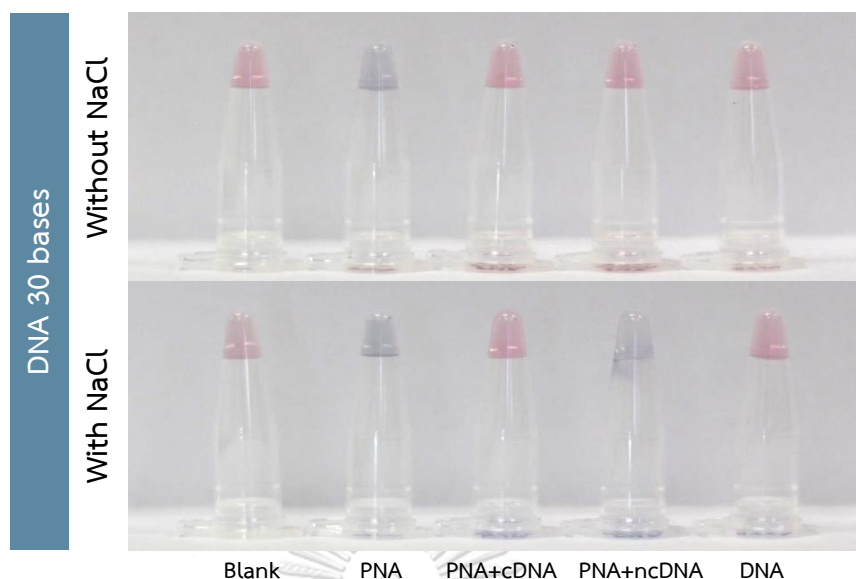


Figure 3.35 Comparison of colorimetric detection of long-chain-DNA using FAM-PNALys₅ between with and without addition of NaCl. Conditions: 0.1 μM of FAM-PNALys₅, 0.12 μM (1.2 equiv) DNA, 50 $\mu\text{g}/\text{mL}$ of citrate-gold nanoparticles (AuNPs (12 nm)), 50 mM NaCl in 10 mM of phosphate buffer (pH 7.0)

iii) Detection of real DNA sample

Next, the colorimetric detection of gold nanoparticles was adapted to detect real DNA samples which were produced by LAMP amplification of DNA from *S. aureus* - a bacterial human pathogen that causes a wide variety of clinical demonstration. As shown in the first row of **Figure 3.36**, several shades of gold solution were observed. The color change was observed in all samples when the PNA probe was added, while PNA+SA positive sample was red-purple and others were more bluish in color. It was proposed that the concentration of the PNA probe might be too high therefore the remaining excess PNA probe could induce aggregation of the gold nanoparticles. Following this, FAM-seaPNA concentration was reduced from 0.25 to 0.01 μM and the results were similar to the use of 0.25 μM of FAM-seaPNA. Although the color of PNA+complementary DNA was not as distinctive as in synthetic DNA, the different shade could be readily distinguished from other non-complementary DNA cases.

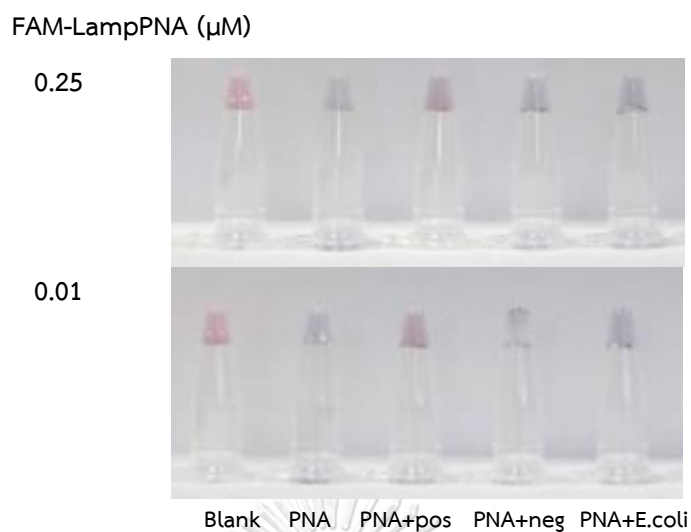


Figure 3.36 Colorimetric assay for detection of DNA real sample at different FAM-seaPNA concentrations. Conditions: 50 $\mu\text{g}/\text{mL}$ of citrate-gold nanoparticles (AuNPs (12 nm)), in 10 mM of phosphate buffer (pH 7.0)

iv) MicroRNA21 target

To further demonstrate the applicability of the developed colorimetric DNA sensing platform for RNA targets, the colorimetric detection of microRNA21, a short RNA that is known to be over expressed in cancer cells,⁷⁶ was chosen as a test case using another FAM-labeled PNA probe (FAM-PNA21) with a sequence AGT CTG ATA AGC corresponding to partial sequence of microRNA21. When the optimal conditions used for DNA targets were employed, the RNA targets could be readily detected in a sequence-specific fashion as shown in **Figure 3.37**. Again, the distinctive color change from red to blue was observed in the presence of non-complementary RNA target, which is in accordance with the results with DNA targets. The data therefore confirm that RNA could be acceptable target as well as DNA.

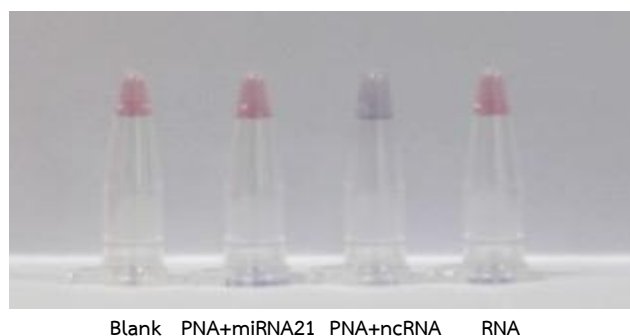


Figure 3.37 Colorimetric detection of for miRNA21 using FAM-PNA21 and 12 nm gold nanoparticles. Conditions: 0.1 μM of FAM-PNA21, 0.12 μM (1.2 equiv) miRNA21, 0.25 mM of citrate-gold nanoparticles (AuNPs (12 nm)) in 10 mM phosphate buffer (pH 7.0)

3.6.4 Sensitivity of the colorimetric assay

To determine the limit of detection of nucleic acid targets of the developed colorimetric assay, 0.1 μM of FAM-PNALys₅ were incubated with various concentrations of nucleic acid targets followed by addition of gold nanoparticles solution and the absorbance change was measured by UV-vis spectrophotometry. The ratios of the absorbance at 520 and 650 nm (A_{520}/A_{650}) were plotted against nucleic acid concentrations. Linear calibration curves were obtained and the limits of detection (LOD) were calculated from $3\sigma/S$ where σ was obtained from relative absorption of PNA+AuNPs (background) and S was obtained from the slope of the curve. The results revealed that the developed method was sensitive enough to detect sub-nanomolar quantities of nucleic acid targets, i.e. 0.13 ± 0.03 nM for DNA detection and 0.21 ± 0.04 nM for RNA detection, using 12 nm of citrate-gold nanoparticles.

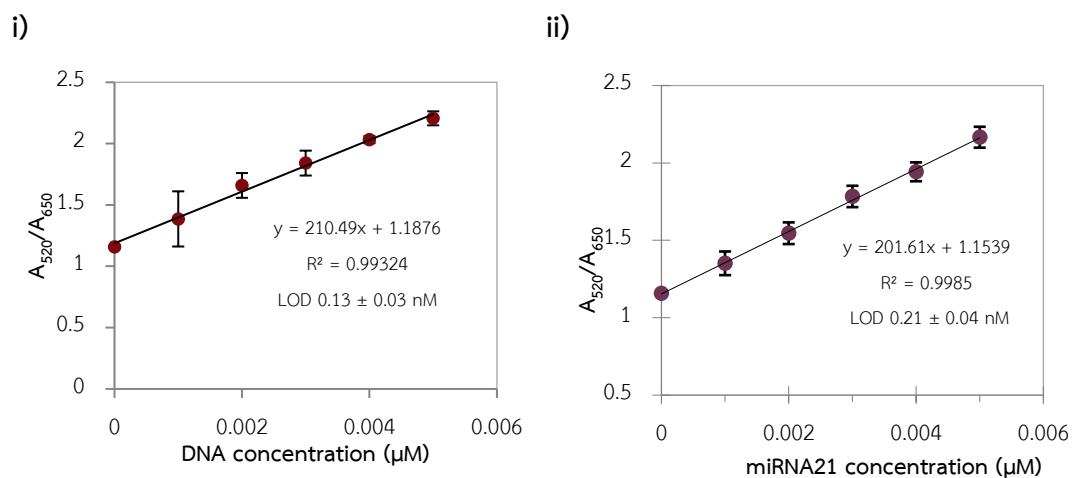


Figure 3.38 Calibration curves for colorimetric DNA detection (i), and RNA detection (ii) using 12 nm gold nanoparticles and FAM-PNALys₅ as a probe. Conditions: 0.1 μM of FAM-PNALys₅, 20 $\mu\text{g}/\text{mL}$ of citrate-gold nanoparticles (AuNPs (12 nm)) in 10 mM of phosphate buffer (pH 7.0)

For the 40 nm gold nanoparticles, the plot of A_{50}/A_{650} and concentration did not give linear relationship because of some precipitation of the gold nanoparticles. Therefore, the ratio of the absorbance at 540 nm before and after mixing (A/A_0) was employed instead of A_{520}/A_{650} . The calibration curve exhibited a good linear response over the concentration range between 2 and 6 nM as shown in **Figure 3.39**. The limit of DNA detection for DNA detection by 40 nm gold nanoparticles was 0.55 ± 0.06 nM, which was somewhat higher than that of 12 nm gold nanoparticles, but was still in sub-nanomolar range.

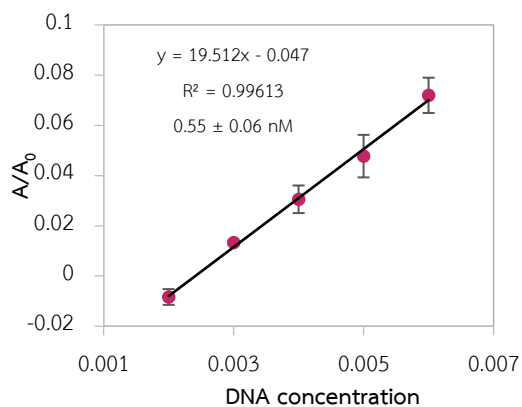


Figure 3.39 Calibration curve for colorimetric DNA detection using 40 nm gold nanoparticles and FAM-PNALys5 as a probe. Conditions: 0.1 μ M of FAM-PNALys5, 20 μ g/mL of citrate-gold nanoparticles (AuNPs (12 nm)) in 10 mM of phosphate buffer (pH 7.0)



3.6.5 Dual-mode detection

One of the most attractive properties of gold nanoparticles (AuNPs) is that they can not only change color according to the degree of aggregation but can also act as an efficient quencher. The possibilities for developing a dual-mode colorimetric and fluorescence detection of nucleic acid targets employing labeled acpcPNA probes and gold nanoparticles were explored. The principle of the detection is shown in **Figure 3.40**.

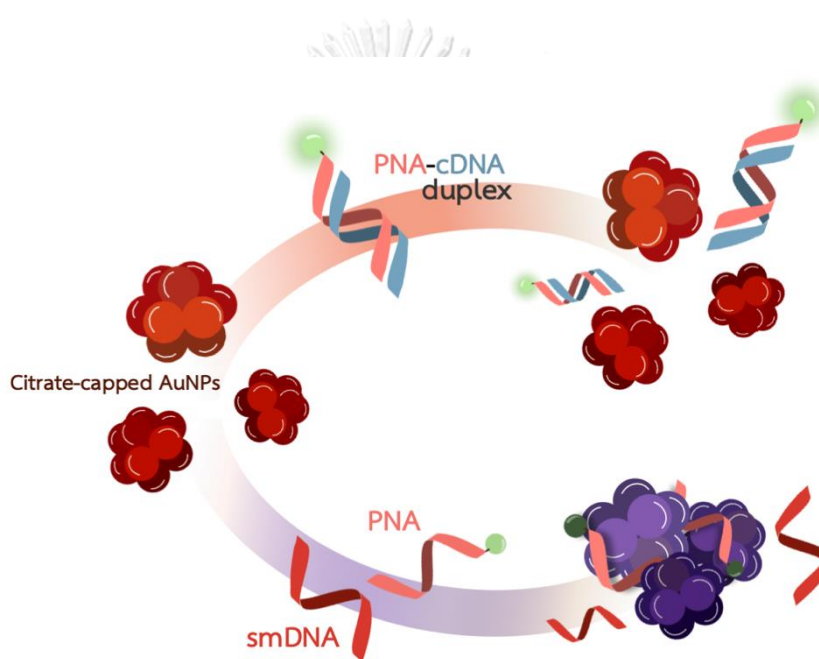
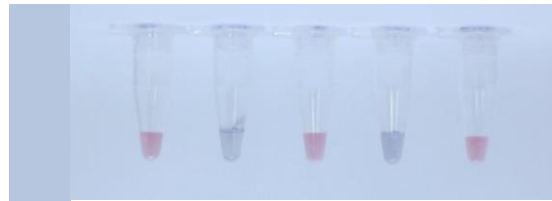


Figure 3.40 The principle of dual-mode detection using citrate-coated gold nanoparticles

A)



Day-light

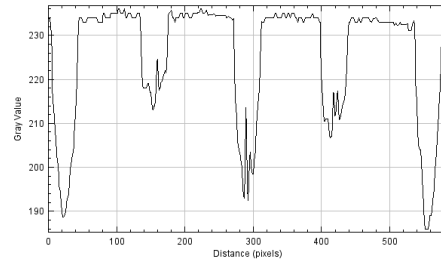
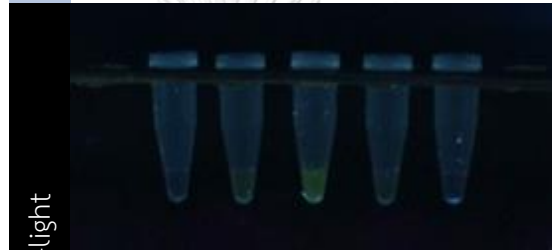


Image analysis from gray-scale



Black-light

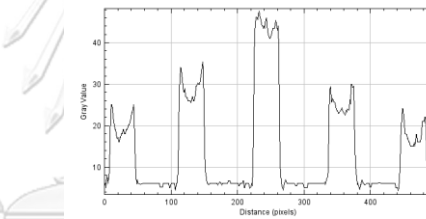


Image analysis from RGB (green channel)

Blank PNA PNA+comDNA PNA+smDNA DNA

จุฬาลงกรณ์มหาวิทยาลัย
CHULALONGKORN UNIVERSITY

B)



Day-light

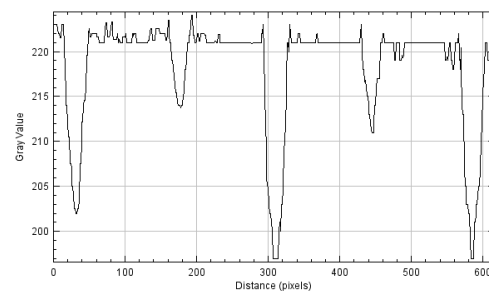


Image analysis from gray-scale

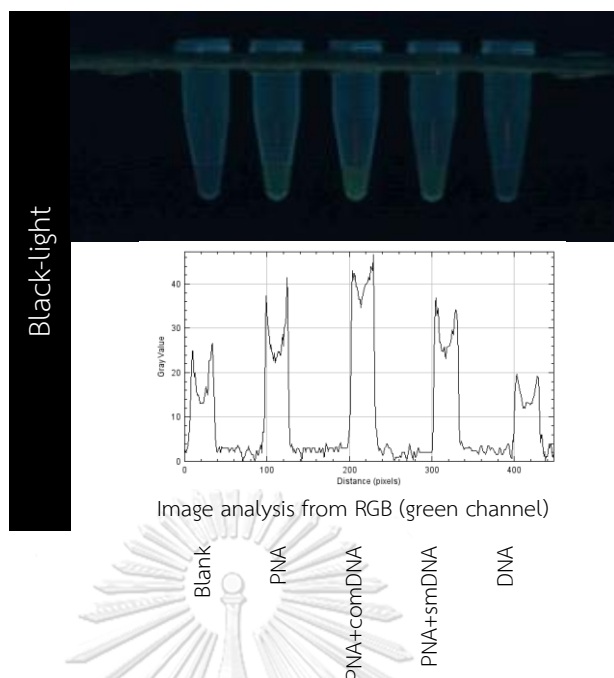


Figure 3.41 Dual-mode detection of DNA using FAM-PNALys₅ and citrate-gold nanoparticles (AuNPs) with 12 nm (A) and 40 nm (B). Conditions: 1 μ M of FAM-PNALys₅, 1.2 μ M (1.2 equiv) DNA, 50 μ g/mL of citrate-gold nanoparticles (AuNPs (12 nm)) in 10 mM of phosphate buffer (pH 7.0)

From the colorimetric detection results with a model DNA target (10 bases) at high concentration of FAM-PNA-Lys₅ probe (from 0.1 μ M to 1 μ M) to ensure that fluorescence emission would be clearly observed by naked eyes, blue color was observed only in the case of single-strand FAM-PNALys₅ and mismatched DNA (smDNA) systems without the addition of NaCl because of the excess of FAM-PNA-Lys₅. When these blue solutions were observed under black-light (365 nm), no fluorescence was observed, indicating effective quenching of the FAM-labeled PNA probe due to the strong electrostatic adsorption by the gold nanoparticles. On the other hand, the red solution of PNA probe+complementary DNA target showed a clearly visible green fluorescence as shown in **Figure 3.41**. The same effect was also observed with 40 nm gold nanoparticles. From image analysis by ImageJ software, the results were consistent with naked-eyes detection. In colorimetric mode, the grayscale images were used and the plot profiles revealed higher signal intensity for the red than the blue solutions. In fluorescence mode, each image was split into RGB

channels and only green channel was used. The plot profiles showed that the highest intensity of green color was observed in the case of PNA-complementary DNA duplex.

3.6.6 Comparison to other colorimetric DNA detection employing gold nanoparticles

In this work, lysine-modified acpcPNA was performed as colorimetric assay for DNA sequence discrimination using citrate-coated gold nanoparticles without covalent immobilization of the probe. Colorimetric detection served as a convenience way of detection without the need of sophisticated instruments. In general, colorimetric DNA detection using traditional DNA probe need DNA immobilization step.⁸³ In general, in the absence of salt DNA could not induce AuNPs aggregation. In contrast, PNA could serve as the aggregator of AuNPs by itself and therefore surface functionalization or addition of salt was not necessary.^{62, 63} In term of selectivity, single-base mismatched target could be readily distinguished by PNA probe, while the same level of specificity was not demonstrated in DNA probe, whereby only discrimination between target and random DNA sequence was demonstrated. For sensitivity, the present acpcPNA-AuNPs based colorimetric detection exhibited low limit of detection of DNA at 0.13 nM (DNA/PNA ratio 0.001) which was lower than other similar works reported by Kanjanawarut (ratio 0.1)⁶², Rho (ratio 0.5)⁸⁴ and Li (ratio 0.2)⁴¹. Hence, in this study revealed higher sensitivity compared with previously published works.

CHAPTER IV

CONCLUSION

In this work, nucleic acid sensing platforms based on a combination of combining with pyrrolidinyl peptide nucleic acid (acpcPNA) probes and selected nanomaterials including graphene oxide (GO), reduced graphene oxide (rGO), gold nanoparticles (AuNPs), and silver nanoparticles (AgNPs) were developed. The important finding is that the presence of multiple positive charges on the acpcPNAs (in the form of lysine attachment at the C-termini) enhanced the PNA adsorption by the negatively-charged GO, resulting in improvement of quenching efficiency of the fluorescent-labeled acpcPNA probe by GO. Addition of complementary DNA/RNA target in near-stoichiometric amounts resulted in efficient desorption of the PNA probe from GO in absence of salt and heat as often required for DNA or other PNA probes. This combination of fluorescent-labeled acpcPNA probe and GO as external quencher could readily distinguish between complementary and single-base-mismatched DNA targets at room temperature. The detection limit both DNA and RNA detection were in sub-nanomolar range, which were lower than traditional DNA and aegPNA probes. Two methods of nucleic acids detection with different order of mixing (PNA-quencher-DNA and PNA-DNA-quencher) were proven to be applicable, although the kinetics and completeness of the fluorescence restoration was superior for the latter case. The detection principle is general for all nanomaterials tested, although GO appeared to give the best performance. For gold nanoparticles, adsorption of acpcPNA not only resulted in fluorescence quenching, but also caused a red-to-purple color change due to the aggregation of the gold nanoparticles as a result of charge neutralization. PNA-DNA and PNA-RNA hybrids failed to induce such aggregation and therefore the presence or absence of complementary DNA or RNA targets can be verified by colorimetric assay. The limits of detection for the AuNPs-based assay were also in sub-nanomolar range for both DNA and RNA targets. Using one fluorescence-labeled PNA probe in combination with gold nanoparticles,

a dual-sensing platform (fluorescence and colorimetric) for visual detection of DNA/RNA was achieved.

This study provides a robust platform for nucleic acid detection that is simple, rapid, sensitive, selective and cost-effective without requiring sophisticated instrument. The sensing platforms could be adapted to detect real DNA samples obtained by LAMP amplification.



REFERENCES

1. Comstock, M. J., Fluorescent Chemosensors for Ion and Molecule Recognition, Copyright, 1993 Advisory Board, Foreword. *ACS Symp. Ser.* **1993**, 538, 1-6.
2. Pan, T.-M.; And, T.-W.; Shih, T.-W., *Detection of genetically modified soybeans in miso by polymerase chain reaction and nested polymerase chain reaction.* 2003; Vol. 11, p 154-158.
3. Akane, A.; Seki, S.; Shiono, H.; Nakamura, H.; Hasegawa, M.; Kagawa, M.; Matsubara, K.; Nakahori, Y.; Nagafuchi, S.; Nakagome, Y., Sex determination of forensic samples by dual PCR amplification of an X-Y homologous gene. *Forensic Sci. Int.* **1992**, 52 (2), 143-148.
4. Li, Y.; Liu, S.; Ling, L., Sensitive Fluorescent Sensor for Recognition of HIV-1 dsDNA by Using Glucose Oxidase and Triplex DNA. *J. Anal. Methods. Chem.* **2018**, 2018, 8298365.
5. Joshi, V. G.; Chindera, K.; Singh, A. K.; Sahoo, A. P.; Dighe, V. D.; Thakuria, D.; Tiwari, A. K.; Kumar, S., Rapid label-free visual assay for the detection and quantification of viral RNA using peptide nucleic acid (PNA) and gold nanoparticles (AuNPs). *Anal. Chim. Acta* **2013**, 795, 1-7.
6. Wang, J.; Xu, D.; Kawde, A.-N.; Polsky, R., Metal Nanoparticle-Based Electrochemical Stripping Potentiometric Detection of DNA Hybridization. *Anal. Chem.* **2001**, 73 (22), 5576-5581.
7. Zhao, C.; Wu, L.; Ren, J.; Qu, X., A label-free fluorescent turn-on enzymatic amplification assay for DNA detection using ligand-responsive G-quadruplex formation. *Chem. Commun.* **2011**, 47 (19), 5461-5463.
8. Chinen, A. B.; Guan, C. M.; Ferrer, J. R.; Barnaby, S. N.; Merkel, T. J.; Mirkin, C. A., Nanoparticle Probes for the Detection of Cancer Biomarkers, Cells, and Tissues by Fluorescence. *Chem. Rev.* **2015**, 115 (19), 10530-10574.
9. Liu, Z.; Liu, B.; Ding, J.; Liu, J., Fluorescent sensors using DNA-functionalized graphene oxide. *Anal. Bioanal. Chem.* **2014**, 406 (27), 6885-6902.

10. Valentini, P.; Pompa, P. P., Gold nanoparticles for naked-eye DNA detection: smart designs for sensitive assays. *RSC Advances* **2013**, *3* (42), 19181-19190.
11. Ho, N. R. Y.; Lim, G. S.; Sundah, N. R.; Lim, D.; Loh, T. P.; Shao, H., Visual and modular detection of pathogen nucleic acids with enzyme–DNA molecular complexes. *Nat. Commun.* **2018**, *9* (1), 3238.
12. Wang, Y.; Li, Z.; Wang, J.; Li, J.; Lin, Y., Graphene and graphene oxide: biofunctionalization and applications in biotechnology. *Trends Biotechnol.* **2011**, *29* (5), 205-212.
13. Saha, K.; Agasti, S. S.; Kim, C.; Li, X.; Rotello, V. M., Gold Nanoparticles in Chemical and Biological Sensing. *Chem. Rev.* **2012**, *112* (5), 2739-2779.
14. Tyagi, S.; Kramer, F. R., Molecular Beacons: Probes that Fluoresce upon Hybridization. *Nat. Biotechnol.* **1996**, *14* (3), 303-308.
15. Tan, W.; Wang, K.; Drake, T. J., Molecular beacons. *Curr. Opin. Chem. Biol.* **2004**, *8* (5), 547-553.
16. Jayagopal, A.; Halfpenny, K. C.; Perez, J. W.; Wright, D. W., Hairpin DNA-Functionalized Gold Colloids for the Imaging of mRNA in Live Cells. *J. Am. Chem. Soc.* **2010**, *132* (28), 9789-9796.
17. Jackson, S. R.; Wong, A. C.; Travis, A. R.; Catrina, I. E.; Bratu, D. P.; Wright, D. W.; Jayagopal, A., Chapter Four - Applications of Hairpin DNA-Functionalized Gold Nanoparticles for Imaging mRNA in Living Cells. In *Methods in Enzymology*, Filonov, G. S.; Jaffrey, S. R., Eds. Academic Press: 2016; Vol. 572, pp 87-103.
18. Luo, J.; Cote, L. J.; Tung, V. C.; Tan, A. T. L.; Goins, P. E.; Wu, J.; Huang, J., Graphene Oxide Nanocolloids. *J. Am. Chem. Soc.* **2010**, *132* (50), 17667-17669.
19. He, S.; Song, B.; Li, D.; Zhu, C.; Qi, W.; Wen, Y.; Wang, L.; Song, S.; Fang, H.; Fan, C., A Graphene Nanoprobe for Rapid, Sensitive, and Multicolor Fluorescent DNA Analysis. *Adv. Funct. Mater.* **2010**, *20* (3), 453-459.
20. Lu, C.-H.; Yang, H.-H.; Zhu, C.-L.; Chen, X.; Chen, G.-N., A Graphene Platform for Sensing Biomolecules. *Angew. Chem. Int. Ed.* **2009**, *48* (26), 4785-4787.
21. Paul, T.; Bera, S. C.; Agnihotri, N.; Mishra, P. P., Single-Molecule FRET Studies

- of the Hybridization Mechanism during Noncovalent Adsorption and Desorption of DNA on Graphene Oxide. *J. Phys. Chem. B* **2016**, *120* (45), 11628-11636.
22. Jhaveri, S. D.; Kirby, R.; Conrad, R.; Maglott, E. J.; Bowser, M.; Kennedy, R. T.; Glick, G.; Ellington, A. D., Designed Signaling Aptamers that Transduce Molecular Recognition to Changes in Fluorescence Intensity. *J. Am. Chem. Soc.* **2000**, *122* (11), 2469-2473.
23. Wu, M.; Kempaiah, R.; Huang, P.-J. J.; Maheshwari, V.; Liu, J., Adsorption and Desorption of DNA on Graphene Oxide Studied by Fluorescently Labeled Oligonucleotides. *Langmuir* **2011**, *27* (6), 2731-2738.
24. Liu, B.; Sun, Z.; Zhang, X.; Liu, J., Mechanisms of DNA Sensing on Graphene Oxide. *Anal. Chem.* **2013**, *85* (16), 7987-7993.
25. Varghese, N.; Mogera, U.; Govindaraj, A.; Das, A.; Maiti, P. K.; Sood, A. K.; Rao, C. N. R., Binding of DNA Nucleobases and Nucleosides with Graphene. *ChemPhysChem* **2009**, *10* (1), 206-210.
26. Antony, J.; Grimme, S., Structures and interaction energies of stacked graphene-nucleobase complexes. *PCCP* **2008**, *10* (19), 2722-2729.
27. Hwang, D. W.; Choi, Y.; Kim, D.; Park, H. Y.; Kim, K. W.; Kim, M. Y.; Park, C.-K.; Lee, D. S., Graphene oxide-quenching-based fluorescence in situ hybridization (G-FISH) to detect RNA in tissue: Simple and fast tissue RNA diagnostics. *Nanomed. Nanotechnol. Biol. Med.* **2019**, *16*, 162-172.
28. Huang, P.-J. J.; Liu, J., DNA-Length-Dependent Fluorescence Signaling on Graphene Oxide Surface. *Small* **2012**, *8* (7), 977-983.
29. Huang, P.-J. J.; Liu, J., Molecular Beacon Lighting up on Graphene Oxide. *Anal. Chem.* **2012**, *84* (9), 4192-4198.
30. Lin, Y.-W.; Liu, C.-W.; Chang, H.-T., DNA functionalized gold nanoparticles for bioanalysis. *Analytical Methods* **2009**, *1* (1), 14-24.
31. Jamdagni, P.; Khatri, P.; Rana, J. S., Nanoparticles based DNA conjugates for detection of pathogenic microorganisms. *Int. Nano. Lett.* **2016**, *6* (3), 139-146.
32. Zhao, W.; Lin, L.; Hsing, I. M., Rapid Synthesis of DNA-Functionalized Gold Nanoparticles in Salt Solution Using Mononucleotide-Mediated Conjugation.

- Bioconjugate Chem.* **2009**, *20* (6), 1218-1222.
33. Heuer-Jungemann, A.; Harimech, P. K.; Brown, T.; Kanaras, A. G., Gold nanoparticles and fluorescently-labelled DNA as a platform for biological sensing. *Nanoscale* **2013**, *5* (20), 9503-9510.
 34. Zhang, H.; Wang, L.; Jiang, W., Label free DNA detection based on gold nanoparticles quenching fluorescence of Rhodamine B. *Talanta* **2011**, *85* (1), 725-729.
 35. Dubertret, B.; Calame, M.; Libchaber, A. J., Single-mismatch detection using gold-quenched fluorescent oligonucleotides. *Nat. Biotechnol.* **2001**, *19*, 365.
 36. Maxwell, D. J.; Taylor, J. R.; Nie, S., Self-Assembled Nanoparticle Probes for Recognition and Detection of Biomolecules. *J. Am. Chem. Soc.* **2002**, *124* (32), 9606-9612.
 37. Rycenga, M.; Cobley, C. M.; Zeng, J.; Li, W.; Moran, C. H.; Zhang, Q.; Qin, D.; Xia, Y., Controlling the Synthesis and Assembly of Silver Nanostructures for Plasmonic Applications. *Chem. Rev.* **2011**, *111* (6), 3669-3712.
 38. Elghanian, R.; Storhoff, J. J.; Mucic, R. C.; Letsinger, R. L.; Mirkin, C. A., Selective Colorimetric Detection of Polynucleotides Based on the Distance-Dependent Optical Properties of Gold Nanoparticles. *Science* **1997**, *277* (5329), 1078.
 39. Chen, X.-J.; Sanchez-Gaytan, B. L.; Qian, Z.; Park, S.-J., *Noble metal nanoparticles in DNA detection and delivery*. John Wiley & Sons, Ltd: 2012; Vol. 4, p 273-290.
 40. Mancuso, M.; Jiang, L.; Cesarman, E.; Erickson, D., Multiplexed colorimetric detection of Kaposi's sarcoma associated herpesvirus and Bartonella DNA using gold and silver nanoparticles. *Nanoscale* **2013**, *5* (4), 1678-1686.
 41. Li, H.; Rothberg, L., Colorimetric detection of DNA sequences based on electrostatic interactions with unmodified gold nanoparticles. *Proceedings of the National Academy of Sciences of the United States of America* **2004**, *101* (39), 14036.
 42. He, H.; Dai, J.; Duan, Z.; Zheng, B.; Meng, Y.; Guo, Y.; Dan, X., Unusual sequence length-dependent gold nanoparticles aggregation of the ssDNA

- sticky end and its application for enzyme-free and signal amplified colorimetric DNA detection. *Sci Rep.* **2016**, *6*, 30878.
43. Liu, P.; Yang, X.; Sun, S.; Wang, Q.; Wang, K.; Huang, J.; Liu, J.; He, L., Enzyme-Free Colorimetric Detection of DNA by Using Gold Nanoparticles and Hybridization Chain Reaction Amplification. *Anal. Chem.* **2013**, *85* (16), 7689-7695.
44. Nielsen, P. E., Peptide nucleic acid: a versatile tool in genetic diagnostics and molecular biology. *Curr. Opin. Biotechnol.* **2001**, *12* (1), 16-20.
45. Nielsen, P. E.; Haaima, G., Peptide nucleic acid (PNA). A DNA mimic with a pseudopeptide backbone. *Chem. Soc. Rev.* **1997**, *26* (2), 73-78.
46. Vilaivan, T., Pyrrolidinyl PNA with α/β -Dipeptide Backbone: From Development to Applications. *Acc. Chem. Res.* **2015**, *48* (6), 1645-1656.
47. Vilaivan, T.; Lowe, G., A Novel Pyrrolidinyl PNA Showing High Sequence Specificity and Preferential Binding to DNA over RNA. *J. Am. Chem. Soc.* **2002**, *124* (32), 9326-9327.
48. Vilaivan, T.; Srisuwannaket, C., Hybridization of Pyrrolidinyl Peptide Nucleic Acids and DNA: Selectivity, Base-Pairing Specificity, and Direction of Binding. *Org. Lett.* **2006**, *8* (9), 1897-1900.
49. Vilaivan, T.; Suparpprom, C.; Harnyuttanakorn, P.; Lowe, G., Synthesis and Properties of Novel Pyrrolodinyl PNA Carrying β -amino Acid Spacers. *Tetrahedron Lett.* **2001**, *42*, 5533-5536.
50. Vilaivan, T., Fluorogenic PNA probes. *Beilstein J. Org. Chem.* **2018**, *14*, 253-281.
51. McNeer, N. A.; Chin, J. Y.; Schleifman, E. B.; Fields, R. J.; Glazer, P. M.; Saltzman, W. M., Nanoparticles Deliver Triplex-forming PNAs for Site-specific Genomic Recombination in CD34+ Human Hematopoietic Progenitors. *Mol. Ther.* **2011**, *19* (1), 172-180.
52. Ma, X.; Devi, G.; Qu, Q.; Toh, D.-F. K.; Chen, G.; Zhao, Y., Intracellular Delivery of Antisense Peptide Nucleic Acid by Fluorescent Mesoporous Silica Nanoparticles. *Bioconjugate Chem.* **2014**, *25* (8), 1412-1420.

53. Bertucci, A.; Lülfi, H.; Septiadi, D.; Manicardi, A.; Corradini, R.; De Cola, L., Intracellular Delivery of Peptide Nucleic Acid and Organic Molecules Using Zeolite-L Nanocrystals. *Adv. Healthc. Mater.* **2014**, *3* (11), 1812-1817.
54. Pita, M.; Abad, J. M.; Vaz-Dominguez, C.; Briones, C.; Mateo-Martí, E.; Martín-Gago, J. A.; del Puerto Morales, M.; Fernández, V. M., Synthesis of cobalt ferrite core/metallic shell nanoparticles for the development of a specific PNA/DNA biosensor. *J. Colloid Interface Sci.* **2008**, *321* (2), 484-492.
55. Fang, H.; Zhang, K.; Shen, G.; Wooley, K. L.; Taylor, J.-S. A., Cationic Shell-Cross-Linked Knedel-like (cSCK) Nanoparticles for Highly Efficient PNA Delivery. *Mol. Pharm.* **2009**, *6* (2), 615-626.
56. Wang, Z.; Zhang, K.; Shen, Y.; Smith, J.; Bloch, S.; Achilefu, S.; Wooley, K. L.; Taylor, J.-S., Imaging mRNA expression levels in living cells with PNA-DNA binary FRET probes delivered by cationic shell-crosslinked nanoparticles. *Org. Biomol. Chem.* **2013**, *11* (19), 3159-3167.
57. Park, J. S.; Goo, N.-I.; Kim, D.-E., Mechanism of DNA Adsorption and Desorption on Graphene Oxide. *Langmuir* **2014**, *30* (42), 12587-12595.
58. Kotikam, V.; Fernandes, M.; Kumar, V. A., Comparing the interactions of DNA, polyamide (PNA) and polycarbamate nucleic acid (PCNA) oligomers with graphene oxide (GO). *PCCP* **2012**, *14* (43), 15003-15006.
59. Guo, S.; Du, D.; Tang, L.; Ning, Y.; Yao, Q.; Zhang, G.-J., PNA-assembled graphene oxide for sensitive and selective detection of DNA. *Analyst* **2013**, *138* (11), 3216-3220.
60. Ryoo, S.-R.; Lee, J.; Yeo, J.; Na, H.-K.; Kim, Y.-K.; Jang, H.; Lee, J. H.; Han, S. W.; Lee, Y.; Kim, V. N.; Min, D.-H., Quantitative and Multiplexed MicroRNA Sensing in Living Cells Based on Peptide Nucleic Acid and Nano Graphene Oxide (PANGO). *ACS Nano* **2013**, *7* (7), 5882-5891.
61. Tu, Y.; Wu, P.; Zhang, H.; Cai, C., Fluorescence quenching of gold nanoparticles integrating with a conformation-switched hairpin oligonucleotide probe for microRNA detection. *Chem. Commun.* **2012**, *48* (87), 10718-10720.
62. Kanjanawarut, R.; Su, X., Colorimetric Detection of DNA Using Unmodified

- Metallic Nanoparticles and Peptide Nucleic Acid Probes. *Anal. Chem.* **2009**, *81* (15), 6122-6129.
63. Su, X.; Kanjanawarut, R., Control of Metal Nanoparticles Aggregation and Dispersion by PNA and PNA–DNA Complexes, and Its Application for Colorimetric DNA Detection. *ACS Nano* **2009**, *3* (9), 2751-2759.
64. Askaravi, M.; Rezaatofghi, S. E.; Rastegarzadeh, S.; Seifi Abad Shapouri, M. R., Development of a new method based on unmodified gold nanoparticles and peptide nucleic acids for detecting bovine viral diarrhea virus-RNA. *AMB Express* **2017**, *7* (1), 137.
65. Suparpprom, C.; Srisuwannaket, C.; Sangvanich, P.; Vilaivan, T., Synthesis and oligodeoxynucleotide binding properties of pyrrolidinyl peptide nucleic acids bearing prolyl-2-aminocyclopentanecarboxylic acid (ACPC) backbones. *Tetrahedron Lett.* **2005**, *46* (16), 2833-2837.
66. Turkevich, J.; Stevenson, P. C.; Hillier, J., A Study of the nucleation and growth processes in the synthesis of colloidal gold. *Discuss. Faraday Soc.* **1951**, *11*, 55-75.
67. Geitner, N. K.; Marinakos, S. M.; Guo, C.; O'Brien, N.; Wiesner, M. R., Nanoparticle Surface Affinity as a Predictor of Trophic Transfer. *Environ. Sci. Technol.* **2016**, *50* (13), 6663-6669.
68. Pillai, Z. S.; Kamat, P. V., What Factors Control the Size and Shape of Silver Nanoparticles in the Citrate Ion Reduction Method? *J. Phys. Chem. B* **2004**, *108* (3), 945-951.
69. Cao, N.; Zhang, Y., Study of reduced graphene oxide preparation by Hummer's method and related characterization. *J Nanomater.* **2015**, *2015*, 5.
70. Li, C.; Li, D.; Wan, G.; Xu, J.; Hou, W., Facile synthesis of concentrated gold nanoparticles with low size-distribution in water: temperature and pH controls. *Nanoscale Res. Lett.* **2011**, *6* (1), 440-440.
71. Schürmann, R.; Bald, I., Effect of adsorption kinetics on dissociation of DNA-nucleobases on gold nanoparticles under pulsed laser illumination. *PCCP* **2017**, *19* (17), 10796-10803.
72. Farkhari, N.; Abbasian, S.; Moshaii, A.; Nikkhah, M., Mechanism of adsorption

- of single and double stranded DNA on gold and silver nanoparticles: Investigating some important parameters in bio-sensing applications. *Colloids Surf. B. Biointerfaces* **2016**, *148*, 657-664.
73. Liu, J., Adsorption of DNA onto gold nanoparticles and graphene oxide: surface science and applications. *Phys. Chem. Chem. Phys.* **2012**, *14* (30), 10485-96.
74. Lu, C.; Huang, P.-J. J.; Liu, B.; Ying, Y.; Liu, J., Comparison of Graphene Oxide and Reduced Graphene Oxide for DNA Adsorption and Sensing. *Langmuir* **2016**, *32* (41), 10776-10783.
75. Yi, J. W.; Park, J.; Singh, N. J.; Lee, I. J.; Kim, K. S.; Kim, B. H., Quencher-free molecular beacon: Enhancement of the signal-to-background ratio with graphene oxide. *Bioorg. Med. Chem. Lett.* **2011**, *21* (2), 704-6.
76. Kumarswamy, R.; Volkmann, I.; Thum, T., Regulation and function of miRNA-21 in health and disease. *RNA Biology* **2011**, *8* (5), 706-713.
77. Seferos, D. S.; Giljohann, D. A.; Hill, H. D.; Prigodich, A. E.; Mirkin, C. A., Nano-Flares: Probes for Transfection and mRNA Detection in Living Cells. *J. Am. Chem. Soc.* **2007**, *129* (50), 15477-15479.
78. Abdul Rahman, S.; Saadun, R.; Azmi, N. E.; Ariffin, N.; Abdullah, J.; Yusof, N. A.; Sidek, H.; Hajian, R., Label-Free Dengue Detection Utilizing PNA/DNA Hybridization Based on the Aggregation Process of Unmodified Gold Nanoparticles. *J Nanomater.* **2014**, *2014*, 1-5.
79. Ma, H.; Li, Z.; Xue, N.; Cheng, Z.; Miao, X., A gold nanoparticle based fluorescent probe for simultaneous recognition of single-stranded DNA and double-stranded DNA. *Microchimica Acta* **2018**, *185* (2), 93.
80. Elahi, N.; Kamali, M.; Baghersad, M. H., Recent biomedical applications of gold nanoparticles: A review. *Talanta* **2018**, *184*, 537-556.
81. Ma, X.-M.; Sun, M.; Lin, Y.; Liu, Y.-J.; Luo, F.; Guo, L.-H.; Qiu, B.; Lin, Z.-Y.; Chen, G.-N., Progress of Visual Biosensor Based on Gold Nanoparticles. *Chin. J. Anal. Chem.* **2018**, *46* (1), 1-10.
82. Nelson, E. M.; Rothberg, L. J., Kinetics and Mechanism of Single-Stranded DNA

- Adsorption onto Citrate-Stabilized Gold Nanoparticles in Colloidal Solution. *Langmuir* **2011**, *27* (5), 1770-1777.
83. Nourisaeid, E.; Mousavi, A.; Arpanaei, A., Colorimetric DNA detection of transgenic plants using gold nanoparticles functionalized with L-shaped DNA probes. *Physica E: Low-dimensional Systems and Nanostructures* **2016**, *75*, 188-195.
84. Rho, S.; Kim, S. J.; Lee, S. C.; Chang, J. H.; Kang, H.-G.; Choi, J., Colorimetric detection of ssDNA in a solution. *Curr. Appl. Phys.* **2009**, *9* (2), 534-537.





APPENDIX

จุฬาลงกรณ์มหาวิทยาลัย
CHULALONGKORN UNIVERSITY

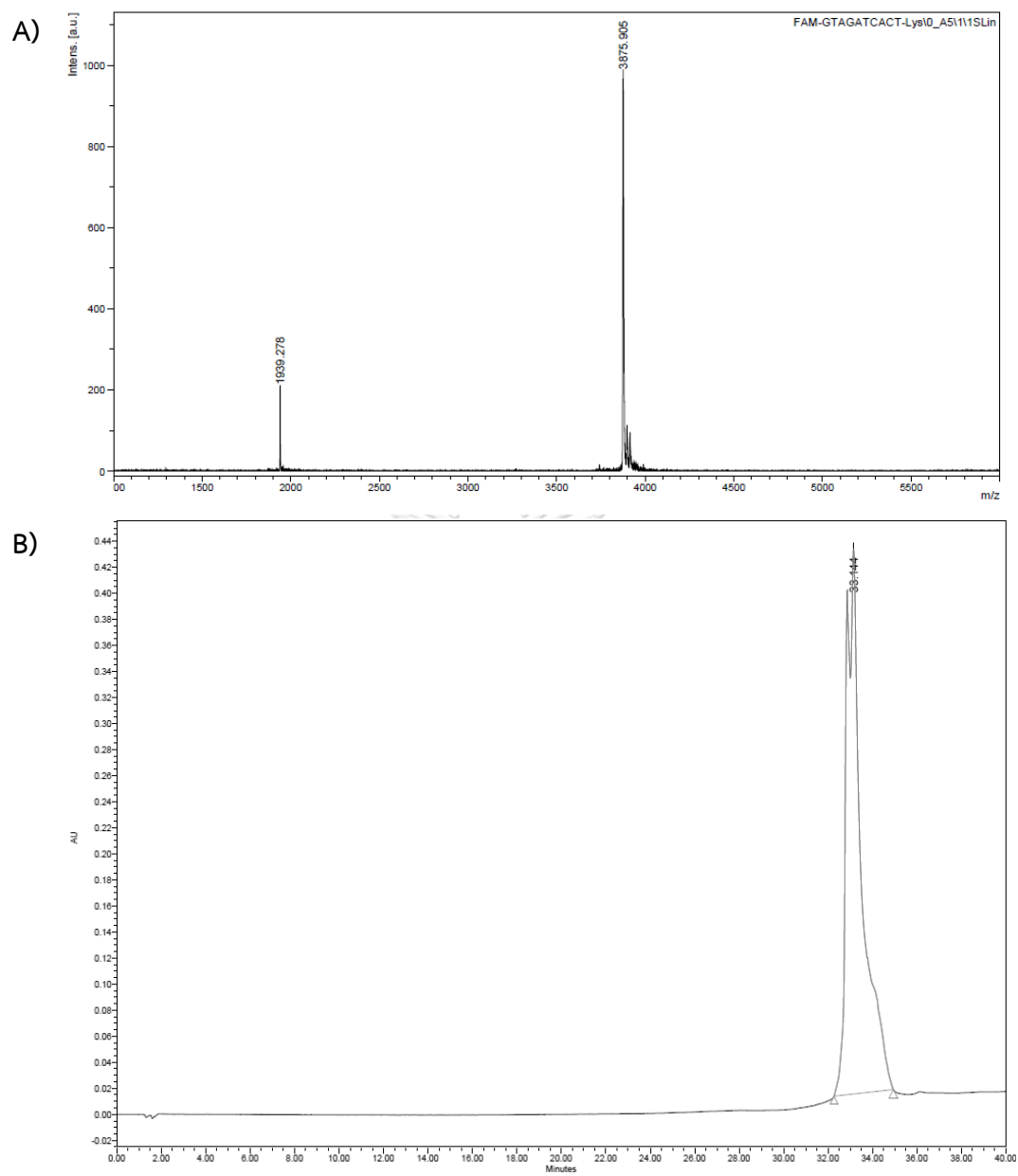


Figure A1 Mass spectrum (A) and chromatogram (B) of FAM-PNALys

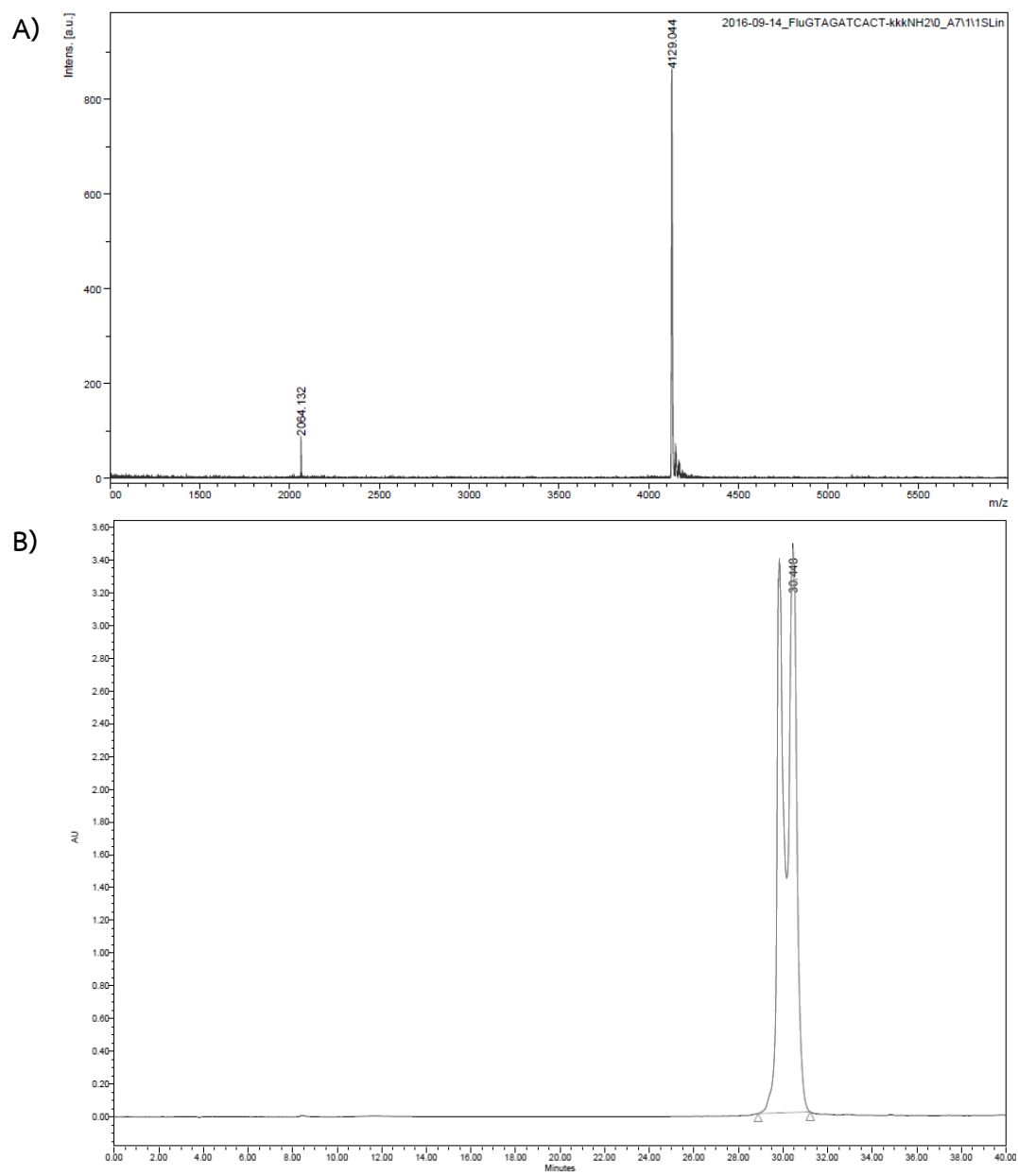


Figure A2 Mass spectrum (A) and chromatogram (B) of FAM-PNALys₃

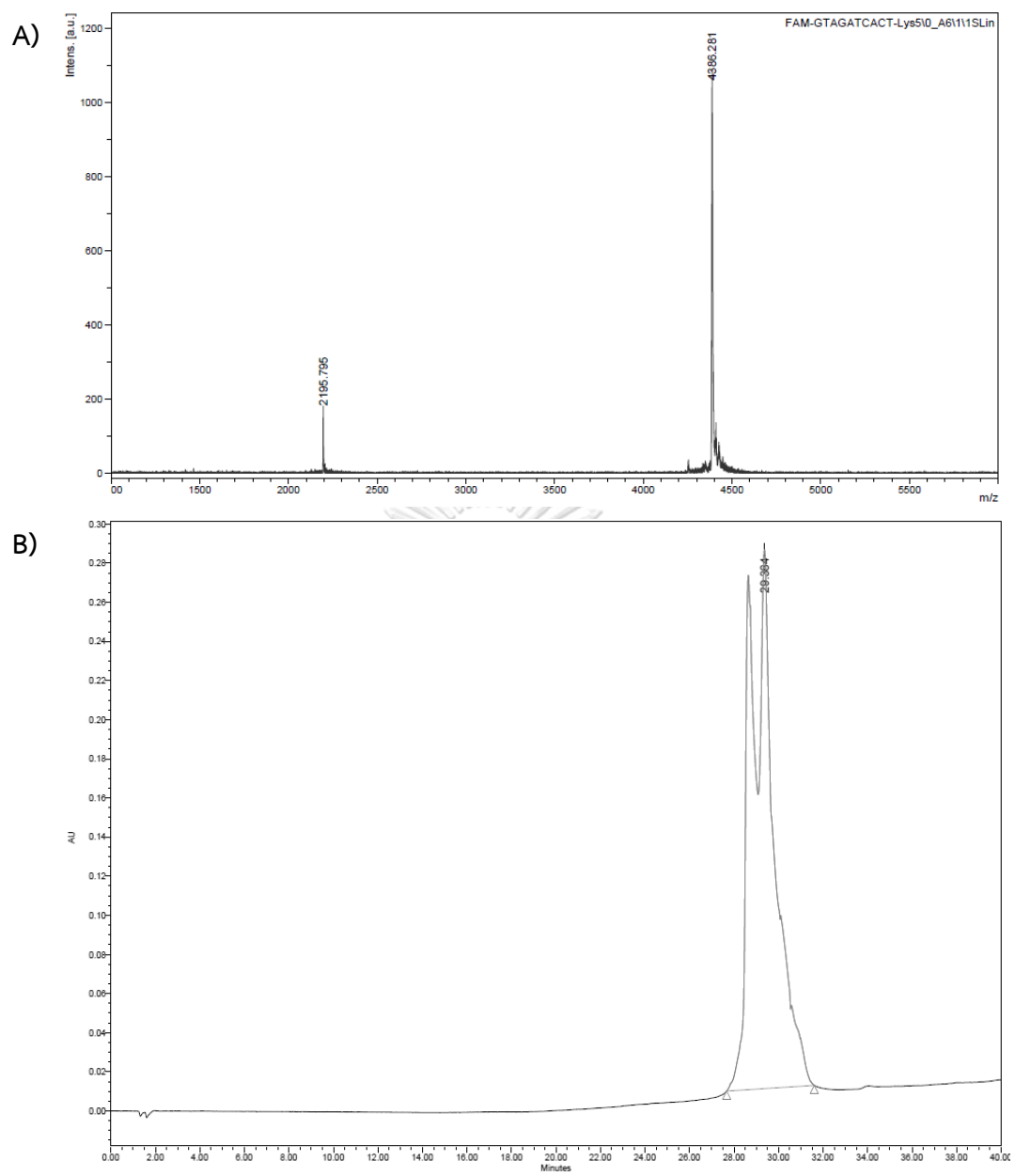


Figure A3 Mass spectrum (A) and chromatogram (B) of FAM-PNALys₅

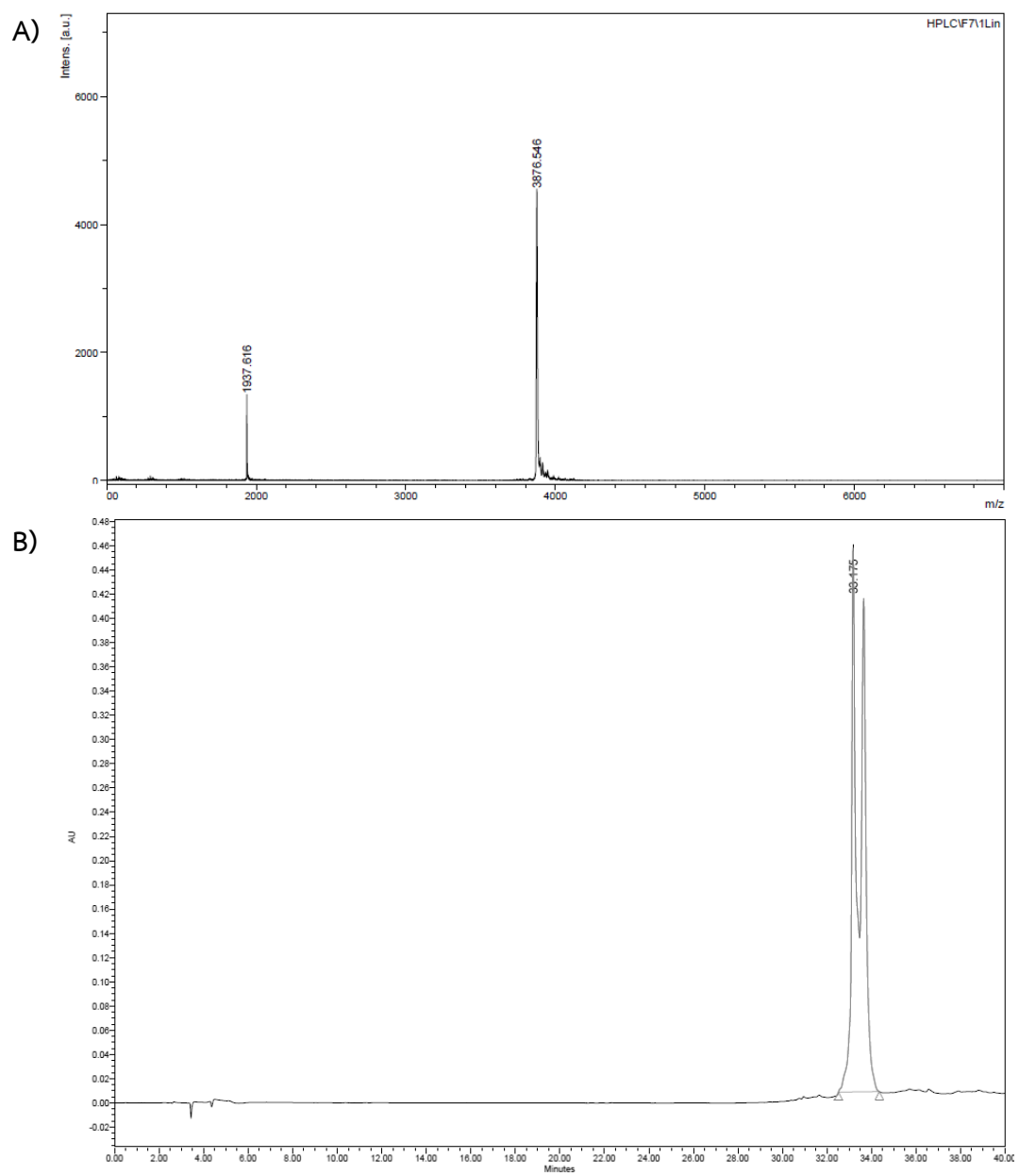


Figure A4 Mass spectrum (A) and chromatogram (B) of FAM-PNAGlu

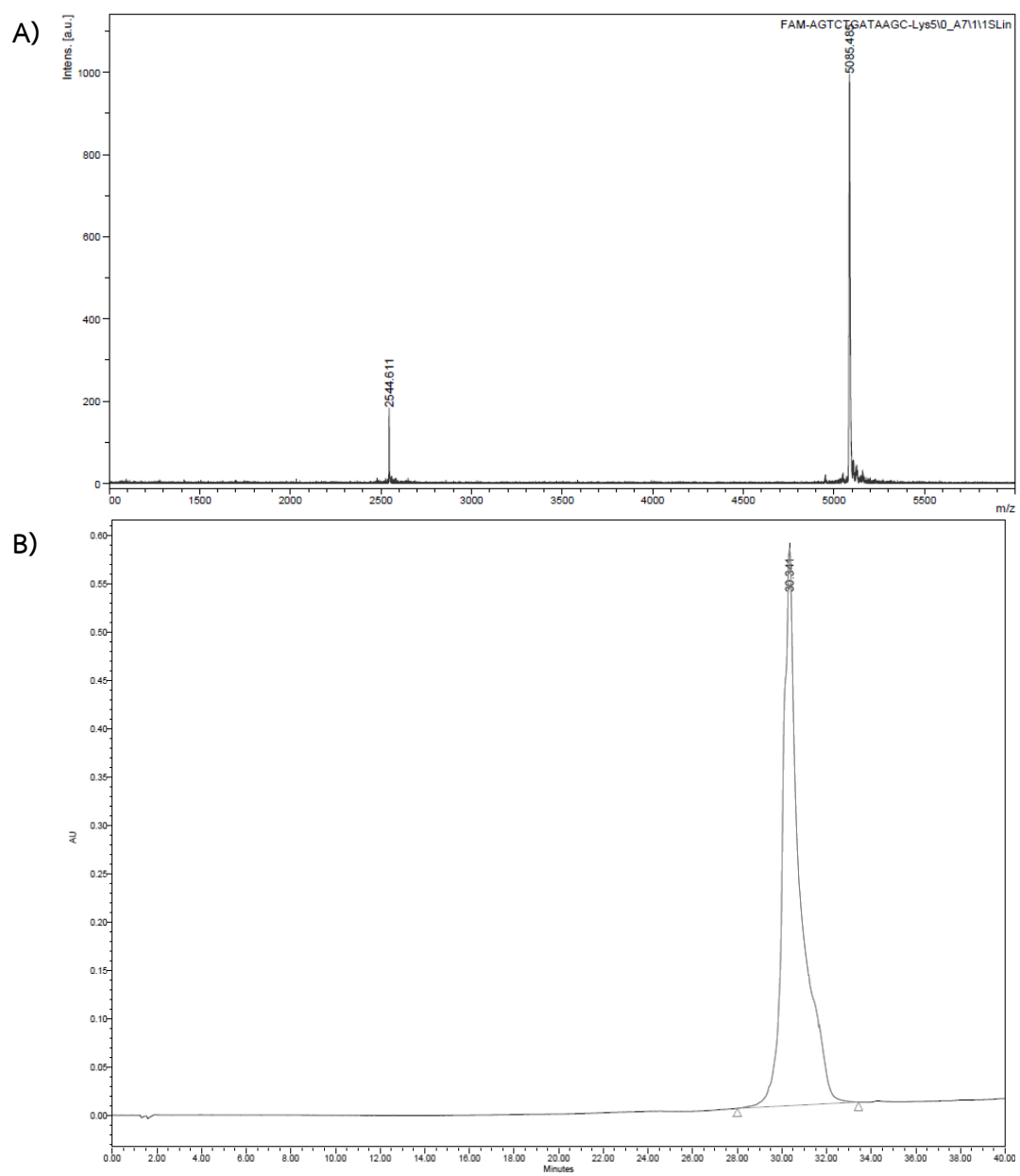


Figure A5 Mass spectrum (A) and chromatogram (B) of FAM-PNA21

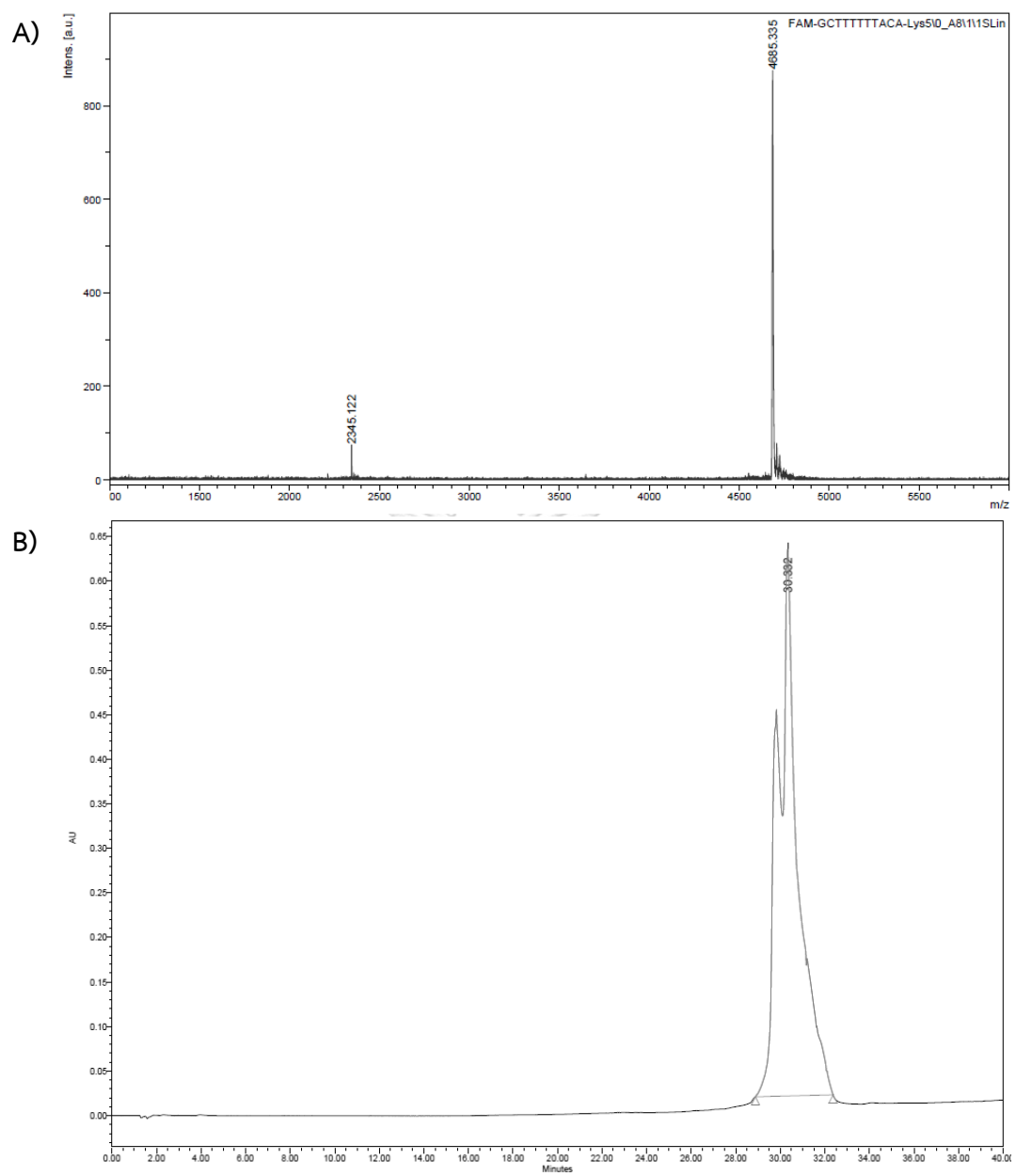


Figure A6 Mass spectrum (A) and chromatogram (B) of FAM-seaPNA

VITA

NAME Kriangsak Faikhruea

DATE OF BIRTH 27 November 1992

PLACE OF BIRTH Samutsongkhram, Thailand

INSTITUTIONS ATTENDED B.Sc. (Chemistry), Department of Chemistry, Faculty of Science, Chulalongkorn University

HOME ADDRESS Rayong, Thailand

